Comparative Characterization of Electronic Packaging Materials through Steady State Thermal Conductivity Measurements

by

John Franklin Maddox, Jr.

A thesis submitted to the Graduate Faculty of
Auburn University
in partial fulfillment of the
requirements for the Degree of
Master of Science

Auburn, Alabama
August 9, 2010

Keywords: thermal conductivity, thermal resistance, delamination, thermal adhesive, pressure sensitive adhesive, epoxy, alumina granules

Approved by

Roy W. Knight, Co-Chair, Assistant Professor of Mechanical Engineering
Sushil H. Bhavnani, Co-Chair, Professor of Mechanical Engineering
Jeyhoon M. Khodadadi, Professor of Mechanical Engineering

Abstract

The decreasing feature size and increasing power generation of modern electronic devices have created a need for increasingly effective and efficient thermal management solutions to remove the high heat fluxes being generated. The complexity of these devices makes it difficult to model the effects of changing a single component on the system as a whole and often necessitates the use of experimental measurements when comparing alternative solutions.

In harsh environments, including high shock and vibration, magnetic devices such as transformer coils are potted to enhance thermal performance and provide mechanical protection. One potting compound frequently used is epoxy containing alumina particles. A nominally isotropic and uniform potting compound consisting of approximately 70 to 80% by volume 14-28 mesh (0.6 to 1.2 mm across) alumina granules in low viscosity epoxy was tested to determine its thermal properties. Examination by optical microscopy revealed significant variation in volume fraction of alumina particles by location. The specific heat and thermal conductivity of the compound were measured using a Differential Scanning Calorimeter and a comparative cut bar apparatus based on ASTM D 5470. The thermal properties were found to vary with time, location, and temperature; with the specific heat ranging from $1.00\,\mathrm{J/g\cdot K}\pm 14\%$ at 25°C to $1.22\,\mathrm{J/g\cdot K}\pm 12\%$ at 125°C and an apparent thermal conductivity of $2.56\,\mathrm{W/m\cdot K}\pm 23\%$. Users of such compounds should be aware that the thermal properties are not necessarily constant in time or uniform, and assuming that they are could lead to significant errors when modeling their performance.

Steady state thermal conductivity measurements were used to compare printed circuit boards (PCB) manufactured from the same design by different vendors and the effect of vias filled with an epoxy versus unfilled vias on the thermal resistance of a PCB. It was found

that the thermal resistance of the PCBs varied as much as 30% between vendors and that the PCBs with the unfilled vias performed slightly better than those with the filled vias.

A non-destructive method was used to determine the effects of thermal cycling on the thermal performance of a PCB attached to an aluminum substrate with a thermal adhesive. This method allows for a comparison of the thermal performance of various thermal interface materials (TIM) in an industrial application. Testing was done on FR4 and Flex boards, both with and without overmolding, attached using pressure sensitive adhesive and an alternative proprietary adhesive. Baseline measurements were taken, then the boards were cycled from -40 to 125°C on a 90-minute cycle with 15-minute dwells at the target temperatures. It was found that both adhesives showed an increase in thermal conductivity, possibly due to curing, and delamination occurred at 17 out of 35 locations with the alternative adhesive within the first 1500 cycles while no delamination occurred with the PSA.

Table of Contents

List of Abbreviations

Acronyms

ALT   alternative adhesive

CTE   coefficient of thermal expansion

DSC   differential scanning calorimeter

FR4   flame retardant 4

NTC   negative thermal coefficient

PBGA plastic ball grid array

PCB   printed circuit board

PDF   probability density function

PIL   Python Imaging Library

PSA   pressure sensitive adhesive

RGB   red, green, and blue color model

RTD   resistance temperature detector

TIM   thermal interface material

English letter symbols

a radius of filler particle, m

c_p specific heat, kJ/kg $\cdot$ K

I	electrical current, A
k	thermal conductivity, $W/m \cdot K$
L	length, m
n	number of measurements
P	power dissipated, W
Q	energy, J
q	heat, W
R	thermal resistance, K/W
R_e	electrial resistance, Ω
$t_{1/2}$	time corresponding to $T_{max}/2$, s
T	temperature, K
t	time, s
V	voltage, V

Greek letter symbols

α	thermal diffusivity, m^2/s
β	skin constant, $W/m^2 \cdot K$
δ_i	uncertainty of i, has the same units as i
ΔT	temperature difference, K
λ	apparent thermal conductivity, $W/m \cdot K$
ω	dimensionless time (scaled Fourier number), $\pi^2 \alpha t/L^2$

Φ volume fraction of filler particle, %

ρ density, kg/m^3

Θ dimensionless temperature, $T(L,t)/T_{max}$

Superscripts

$''$ per unit area, m^{-2}

$'''$ per unit volume, m^{-3}

Subscripts

bot   bottom metering block

cal   calibration curve

cond   conduction

cont   contact

conv   convection

f   filler particle

FM   flux meter

j   junction

jx   junction to reference point

lower   lower bound

m   matrix material

max   maximum

mb   metering bar

meas   measured value

s   sample

top   top metering block

upper   upper bound

x   reference point

Chapter 1

Introduction

The removal of heat from electronic components has become an increasingly important aspect of electronics packaging in recent years. As electronic devices have become smaller and more powerful, they have also started to generate more heat in a smaller area. Because of this trend, thermal management solutions are having to become increasingly more efficient and effective in order to handle the escalating heat flux being generated.

If the heat is not effectively removed from a device, it will cause the temperature of the device to rise excessively, which negatively impacts the performance and reliability of the device. At higher temperatures, processors operate less efficiently and require more power. This causes a decrease in computational speed as well as a decrease in battery life for mobile devices. Additionally, large temperature gradients create stresses which can decrease the life of the device.

The difference in the coefficient of thermal expansion (CTE) between dissimilar materials causes shear stresses to be generated during normal operation of an electronic device. The cyclic nature of these stresses causes fatigue at the joints, which leads to cracking and ultimately failure. Minimizing the temperature change experienced by a device will diminish the effects of CTE stresses and thus lead to improved reliability.

The heat generated in an electronic device must eventually be rejected to the environment. This process is enhanced in a number of ways, usually with a heat sink being attached to the heat producing components in a device. However, the thermal resistance from the components to the heat sink can become a bottleneck if measures are not taken to decrease the contact resistance between the two. While the contact resistance could be decreased by pressing one surface against the other with sufficient force, this is not optimal from a

reliability or manufacturing point of view. Additionally, the irregular shapes of some electronic components make it difficult to attach a heat sink. One solution to these problems is to incorporate an intermediate medium which helps to transfer the heat from the electrical component to the heat sink that interacts with the environment.

1.1 Potting Compounds

Electronic components with irregular form factors and components exposed to harsh environments are often encapsulated in a potting compound. The encapsulant is usually made out of a thermally conductive dielectric material. Some such materials which are being increasingly used as potting compounds are ceramic oxide filled polymers. The motivation for this is that the composite retains the electrical and thermal properties of the ceramic while keeping the mechanical properties of the polymer, which allows the compound to be easily incorporated into the manufacturing processes used to package electronics. One common polymer that is used is epoxy, the properties of which can be adjusted by altering the components and curing agents used.

Epoxy containing alumina granules is frequently used to encapsulate magnetic devices since it has a relatively high dielectric constant and thermal conductivity while still being conformal enough, prior to curing, to be easily applied during assembly. The higher thermal conductivity of the potting compound helps to remove the heat generated by the device, while the mechanical support supplied by the hardened resin helps to protect the device, especially in harsh environments with high shock and vibration.

In order to properly model the performance of a device encapsulated in a potting compound, it it necessary to have accurate values for the thermophysical properties of the composite. However, these properties can be difficult to predict, especially when the filler particles are packed closely enough to interact with one another. This study will experimentally

determine the properties of one such composite consisting of Stycast W-19 epoxy impregnated with T64 tabular alumina which is used to encapsulate a power transformer attached to a liquid cooled heat sink.

1.2   Printed Circuit Boards

Many modern electronic devices are assembled on printed circuit boards (PCB), which provide signal connection, electrical isolation, radiation insulation, and mechanical support. Most PCBs consist of multiple copper layers separated by layers of insulation. The copper layers can be signal layers, which route the signals between the components, or ground/power planes, which are used to supply a common ground and reference voltage the components in the assembly. The insulation between the copper layers is usually provided by alternating layers of pre-impregnated, or pre-preg, woven glass fiber with uncured epoxy, and core, woven glass fiber with cured epoxy and copper foil bonded to each side. The term stack-up is used to refer to the number, order, and thickness of the layers. The stack-up will usually be vertically symmetric so as to avoid warping due to CTE effects. A diagram of a six layer stack up is shown in Figure 1.1.

The different layers in a PCB are connected through plated holes called vias. These vias can be designed to transmit signals, power, and/or heat. There are three main type
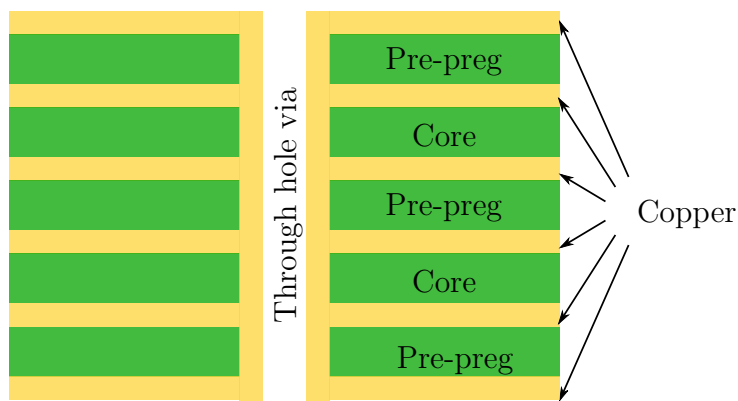
Figure 1.1: Diagram of a printed circuit board with 6 layers of copper separated by alternating layers of pre-preg and core with a through hole via.

of vias: through hole vias, blind vias, and buried vias. A through hole via is one that goes from the top of a PCB to the bottom through all the layers. A blind via is one that starts at either the top or the bottom and goes through one or more layers but does not go all the way through. A buried via is one that goes through one or more interior layers but does not extend through either the top of the bottom layer of the PCB. This study will look at the effects of filling through hole copper plated vias with an epoxy on the thermal resistance of a PCB.

It is common for an electronics manufacturer to send a PCB design to a third party vendor for fabrication. However, the decisions made and the equipment used by the vendor can have significant effects on the final properties and performance of the PCB. This study will measure at the difference in the thermal properties of PCBs fabricated from three vendors using the same PCB design.

1.3   Thermal Interface Materials

When attaching a heat sink to an electronic component with a planar surface it is common to use a thermal interface material (TIM) to decrease the interfacial thermal resistance. Some TIMs in use today are soft metals, thermal greases, epoxy resins, pressure sensitive adhesive tapes (PSA), phase change materials, and elastomer pads [1, 2]. The properties of these materials are often enhanced by the addition of judiciously selected particles to increase the bulk thermal conductivity of the material.

The use of a thermal adhesive as a TIM gives the added benefit of securing the two surfaces together without the need for external clamping. This reduces the complexity of a device by reducing the number of components; simplifies the manufacturing, as adhesives are relatively easy to apply when compared to the alternatives; and increases the reliability of the device by absorbing thermally induced stresses. Adhesives, both electrically conductive and thermally conductive, are used in the assembly of many automotive electronics [3].

When used as a TIM in these applications, it is necessary that the adhesive exhibit reliable performance both mechanically and thermally.

The effects of aging [4] and thermal cycling [5–9] on the mechanical strength of various adhesives have been well documented in the literature. However, there is less information about the effects of aging and thermal cycling on the thermal performance of these adhesives. Since degradation in thermal performance can ultimately lead to electrical failure, it is important to understand how the properties of a TIM will change during the life cycle of a product. This study will look at how the thermal performance of two competing thermal adhesives are effected by accelerated aging through the use of thermal cycling.

Background

2.1 Conduction

The molecules within a medium, be it solid, liquid, gas, or plasma, are constantly interacting with one another. As this occurs, the molecules transfer kinetic energy, or heat, back and forth between themselves. Since the motion of the molecules is random, there is no directional preference to the energy transfer, but rather the net flow of energy is from regions of high energy to regions of low energy, by a process called conduction. Temperature is a measure of the average kinetic energy of the particles within a medium, with higher temperatures corresponding to higher concentrations of energy. With this definition of temperature, conduction is a diffusive transfer of heat driven by a temperature gradient, governed by the equation

$$\rho c_p \frac{\partial T}{\partial t} + \nabla \cdot \boldsymbol{q}'' - q''' = 0 \tag{2.1}$$

where ρ is the density, c_p is the specific heat, T is the temperature, t is the time, $\boldsymbol{q}''$ is the heat flux vector, and q''' is the heat generation.

2.1.1 Thermal Conductivity

Conduction within a medium can be described by the Fourier's law,

$$\boldsymbol{q}'' = -k\nabla T, \tag{2.2}$$

which relates the heat flux to the temperature gradient through the use of a proportionality constant, k, called thermal conductivity. The thermal conductivity is a material property

which can vary with temperature and is usually, but not necessarily, isotropic. Thermal conductivity typically increases with temperature for gases and decreases with temperature for solids and liquids. For a one dimensional case, the Fourier's law reduces to

$$q'' = -k\frac{dT}{dx}.$$

(2.3)

2.1.2 Thermal Resistance

It is often convenient to view the flow of heat as being analogous to the flow of electricity. In an electrical circuit, the flow of electrons is driven by a voltage potential, V, and the rate of flow, I, is limited by the electrical resistance, R_e, as governed by the equation

$$R_e = \frac{V}{I}.$$

(2.4)

In this sense, the temperature gradient is analogous to the voltage potential and the flow of heat is analogous to the current. At this point, a term called thermal resistance can be introduced to be analogous to the electrical resistance, where thermal resistance is the ability of a material to resist the flow of heat. Following the analogy, the thermal resistance, R, can be related to the temperature and heat flow as

$$R = \frac{\Delta T}{q}$$

(2.5)

where ΔT is the temperature difference between two points which drives the flow of heat, q.

Conduction Resistance

For the case of one dimensional steady state conduction, i.e. a plane wall, the thermal conductive resistance, R_{cond}, is defined by rearranging Eq. (2.3) to be of the from of Eq. (2.5),

$$R_{cond} = \frac{\Delta T}{q} = \frac{L}{kA}$$

(2.6)

7

or, in terms of heat flux,

$$R_{cond}A = \frac{\Delta T}{q''} = \frac{L}{k} \tag{2.7}$$

where L is the distance between the temperatures of ΔT and A is the cross-sectional area normal to the heat flow.

The circuit analogy is particularly useful when analyzing composite systems in which an equivalent thermal circuit can be used to model heat flowing through multiple mediums in either series or parallel. For example, one dimensional conduction through three consecutive plane walls with differing properties can be modeled as three thermal resistances in series, as shown in Figure 2.1.
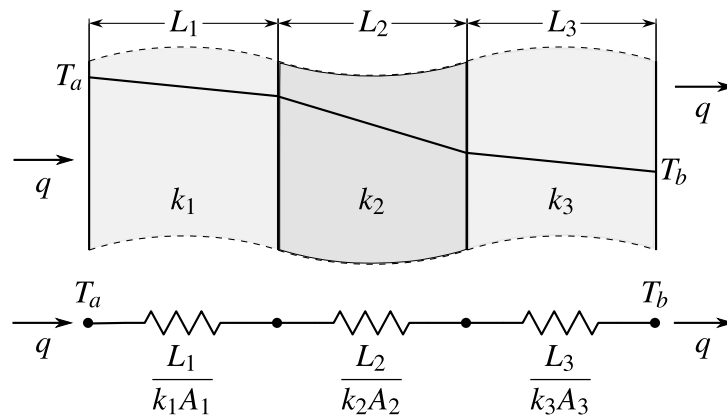
Figure 2.1: One dimensional conduction through a layered medium modeled with an equivalent thermal circuit.

Contact Resistance

An additional thermal resistance, called thermal contact resistance, exists at the interface between two solids and is primarily due to roughnesses effects at the contacting surfaces. All real surfaces have asperities which cause them to have a roughness. This being the case, when two materials are in contact with one another, the contact is not uniform across the surfaces but rather it occurs only at discrete locations. This results in gaps being interspersed between contact points along the interface. These gaps are usually filled with air, although they could also be filled with another fluid or evacuated.

The heat being transfered across the interface can take one of two paths. The first path is through the contact areas in which the conductive flow is primarily governed by the thermal conductivities of the two materials. The second path is across the gaps. Since it is usually the case that the gaps are too small for bulk fluid motion to take place, the modes for heat transfer across the gaps are limited to conduction through the fluid and radiation. The two paths can be viewed as parallel thermal resistances with a combined equivalent thermal resistance, R_{cont}. Since the conductivity of the fluid is usually lower than that of the contacting materials, more of the heat will tend to flow through the contact areas than across the gaps, as illustrated in Figure 2.2.
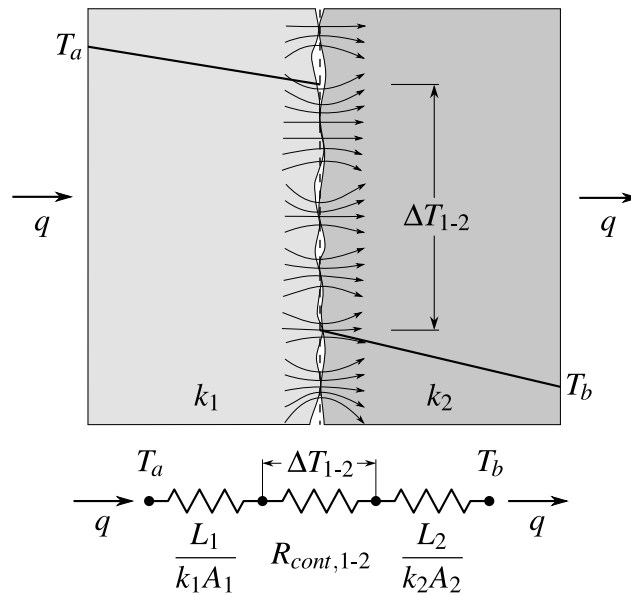
Figure 2.2: Qualitative illustration of the paths for heat transfer across the interface between two solids.

The example of the three layered plane wall can now be revisited and expanded to include the contributions of the contact resistances between the layers, as shown in Figure 2.3.

The overall value of the contact resistance can be minimized through two main approaches: maximizing the ratio of contact area to gap area and increasing the heat transfer across the gaps. The most obvious first step to decreasing the contact resistance is to make the two surfaces as smooth as possible. This causes there to be a larger number of smaller asperities, which leads to more contact points, thus increasing the contact area to gap area
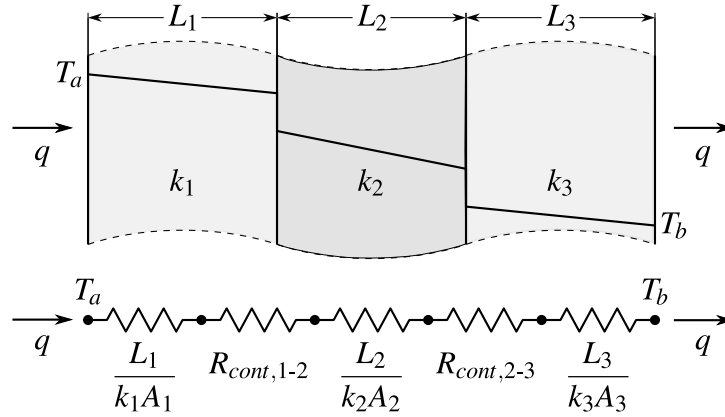
Figure 2.3: One dimensional conduction through a layered medium modeled with an equivalent thermal circuit including contact resistances.

ratio. Additionally, decreasing the height of the asperities on the two surfaces results in thinner gaps, which in turn decreases the resistance to conduction across the gaps.

Another step that can be taken is to increase the joint pressure of the surfaces, which has the same net effect as decreasing the roughness of the surfaces. Pressing the two materials together will cause the surfaces to deform, either plastically or elastically depending of the properties of the materials and the pressure being applied. As the amount of deformation increases, the contact area increases and the gap thickness decreases, thus leading to a lower thermal resistance.

A third way is to decrease the thermal resistance across the gaps is by increasing the thermal conductivity of the fluid within them. This is usually done through the use of an interfacial fluid, such as thermal grease.

Thermal Interface Materials

An alternative approach to minimizing thermal contact resistance is to introduce an additional layer of a third material between the two contacting surfaces. This third material is referred to as a thermal interface material (TIM). A TIM is usually made out of a soft, malleable material which will conform to the surfaces of the harder materials. This causes

the contact to gap ratio to be higher between the TIM and each of the surfaces than it would have been between the surfaces without the TIM.

The introduction of the TIM replaces one contact resistance ($R_{cont,\text{1-2}}$) with two contact resistances and a conductive resistance ($R_{cont,\text{1-TIM}} + R_{cond,\text{TIM}} + R_{cont,\text{TIM-2}}$), as illustrated in Figure 2.4. Therefore, in order for the TIM to be beneficial, it must be the case that

$$R_{cont,\text{1-TIM}} + R_{cond,\text{TIM}} + R_{cont,\text{TIM-2}} < R_{cont,\text{1-2}} \tag{2.8}$$
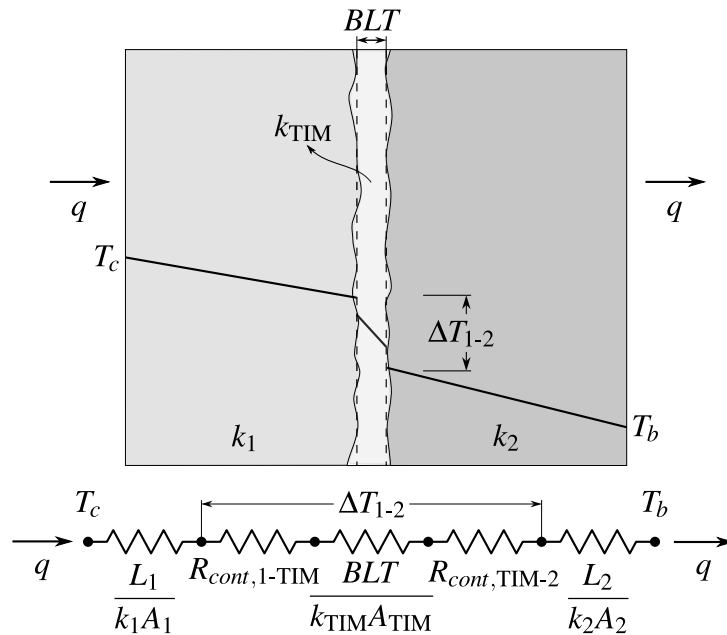
Figure 2.4: The introduction of a TIM between two surfaces can reduce the overall thermal interface resistance.

In order to minimize the contact resistances, $R_{cont,\text{1-TIM}}$ and $R_{cont,\text{TIM-2}}$, it is necessary to maximize the contact area at the interfaces between the TIM and the surfaces. For the case of a liquid TIM, it is only necessary to provide enough material to fill the gaps. For the case of a solid TIM, the interfacial layer must be sufficiently thick to allow deformation from both sides. This means that for a solid TIM, there is a minimum thickness which must be used to provide the optimum contact area.

11

The contribution of the conductive resistance of the TIM, $R_{cond,\mathrm{TIM}}$, is directly proportional to the thickness of the TIM, L_{TIM}. Therefore, in order to minimize the conductive resistance of the TIM it is necessary to minimize its thickness. Since the contribution of the conductive resistance and the contact resistances have a competing dependence on the thickness, it is desirable to have the least amount of TIM that will sufficiently conform to the surfaces.

2.1.3   Conduction in a Composite

When analyzing the flow of heat within a composite system it is often more convenient to use the effective thermal conductivity of the system as a whole rather than the thermal conductivities of the individual constituents. However, predicting the effective thermal conductivity is nontrivial, as it depends on more that just the properties of the individual components.

For the simple case of homogeneous spherical particles randomly distributed within a homogeneous material, as shown in Figure 2.5, Maxwell [10] used potential flow theory to predict the apparent thermal conductivity as

$$\lambda = k_m \frac{k_f + 2k_m + 2\Phi(k_f - k_m)}{k_f + 2k_m - \Phi(k_f - k_m)} \tag{2.9}$$

where k_f is the thermal conductivity of the filler particles, k_m is the thermal conductivity of the matrix material, and Φ is the volume fraction of the filler. However, this is only valid when the spheres are far enough apart that their effects are independent of one another. Therefore Eq. (2.9) is limited to low concentrations of filler particles.

Additional models have since been proposed which account for various shape and orientation parameters. An expression for platelets rather than spheres was developed by Bruggeman [11],

$$1 - \Phi = \frac{k_m - \lambda}{k_f - k_m} \left(\frac{k_m}{\lambda} \right)^{1/3}. \tag{2.10}$$

12
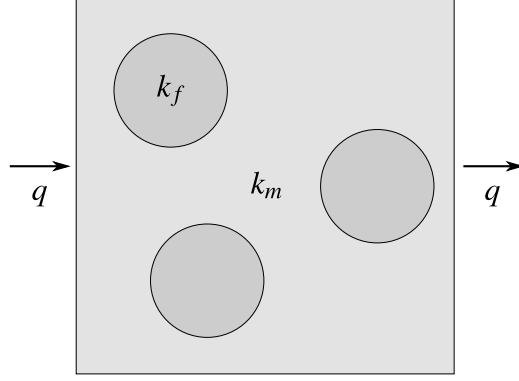
Figure 2.5: Homogeneous spherical filler particles randomly distributed within a homogeneous matrix material.

Cheng and Vachon [12] extended the probabilistic work of Tsao [13] to use a parabolic distribution,

$$
\frac{1}{\lambda} = \frac{1-B}{k_m} + \frac{1}{\{C(k_f - k_m)[k_m + B(k_f - k_m)]\}^{1/2}}
$$
$$
\cdot \ln \frac{[k_m + B(k_f - k_m)]^{1/2} + \frac{B}{2}[C(k_f - k_m)]^{1/2}}{(k_m + B(k_f - k_m))^{1/2} - \frac{B}{2}[C(k_f - k_m)]^{1/2}}, \tag{2.11}
$$

where

$$
B = \left(\frac{3\Phi}{2}\right)^{1/2}, \tag{2.12}
$$

$$
C = \left(\frac{2}{3\Phi}\right)^{1/2}. \tag{2.13}
$$

Lewis and Nielsen [14] modified the Halpin-Tsai equation [15] to account for the shape and orientation of the particles

$$
\frac{\lambda}{k_m} = \frac{1 + AB\Phi}{1 - B\psi\Phi} \tag{2.14}
$$

13

where

$$A = k_E - 1 \tag{2.15}$$

$$B = \frac{k_f/k_m - 1}{k_f/k_m + A}, \tag{2.16}$$

$$\psi = 1 + \frac{\Phi(1 - \Phi_{max})}{\Phi_{max}}, \tag{2.17}$$

k_E is the generalized Einstein coefficient [16], and Φ_{max} is the volume fraction of the filler corresponding to the maximum packing density. However, all of these models are still limited to low filler concentrations, since they assume the effects of the particles to be isolated from one another.

As the volume fraction of the filler particles increases, the particles begin to interact with one another and they can no longer be treated as isolated bodies. Additionally, at higher volume fractions, there is an increased chance of the particles touching one another, as illustrated in Figure 2.6. The contacting particles can form conductive chains in the direction of heat flow, which increases the effective thermal conductivity of the composite.
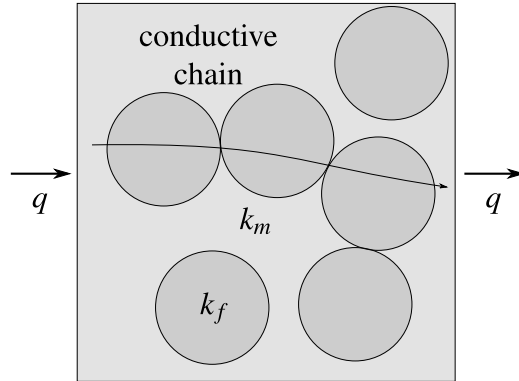
Figure 2.6: Contact between particles can create chained paths to promote conductive heat transfer.

A model which accounts for the forming of conductive chains was proposed by Agari and Uno [17],

$$\log \lambda = \Phi C_2 \log(k_f) + (1 - \Phi) \log(C_1 k_m) \tag{2.18}$$

where C_1 is a measure of the effect of the particles on the crystal structure of the polymer and C_2 is a measure of the ease in forming conductive chains of particles. The application of this model is primarily limited by the need to experimentally determine values for C_1 and C_2.

An additional parameter, not accounted for in the previous models, is the interfacial contact resistance between the particles and the matrix material. This resistance, sometimes called the Kapitza resistance [18, 19], can result from an imperfect mechanical or chemical adherence at the interface, which can be amplified by a CTE mismatch between the filler and matrix materials.

Hasselman and Johnson [20] and Benveniste [21] independently arrived at the same solution for including the effects of thermal contact resistance into the calculation of the effective thermal conductivity of a composite with spherical filler particles. Hasselman and Johnson used an identical approach to Maxwell [10] and Benveniste [21] used the Mori-Tanaka theory [22] for the mechanical properties of perfectly bonded composites. In both cases, the boundary condition at the interface between the filler particle and the matrix was modified, such that

$$\beta \, \Delta T_{mf} = -k_f \frac{\partial T_f}{\partial r}\bigg|_{r=a} \tag{2.19}$$

where ΔT_{mf} is the temperature drop across the interface, a is the radius of the filler particles, and β is the "skin constant" or thermal conductance across the interface. In both cases, the solution reduces to

$$\lambda = k_m \frac{k_f + 2k_m + 2\Phi(k_f - k_m) + 2\frac{k_f k_m}{a\beta}(1 - \Phi)}{k_f + 2k_m - \Phi(k_f - k_m) + 2\frac{k_f k_m}{a\beta}(2 + \Phi)}. \tag{2.20}$$

It should be noted that this is valid only for spherical, isolated particles. For the case of perfect contact between the matrix and the filler, i.e. $\beta \to \infty$, Eq. (2.20) reduces to the Maxwell-Eucken equation, Eq. (2.9).

The skin constant, β, is temperature dependant and was shown by Garrett and Rosenberg [23] to increase with temperature. Therefore, as the temperature increases, the improved thermal conductance across the matrix/filler interface will cause an increase in the effective thermal conductivity of the composite. However, since the thermal conductivity of most solids decreases with increasing temperature, the property change of the constituents will cause a decrease in the effective thermal conductivity of the composite. Due to these competing contributions, the net effect of an increase in temperature could be to increase or decrease the effective thermal conductivity of the composite depending on the materials being used and the configuration of the filler particles, i.e. size, surface roughness, orientation, and volume fraction.

It was reported by Batchelor [24] that the upper and lower bounds for the apparent thermal conductivity of a two phase composite were found by Hashin and Shtrikman [25] to be

$$\lambda_{lower} = k_m \left\{ 1 + \frac{\Phi(k_f - k_m)}{k_m + \frac{1}{3}(1 - \Phi)(k_f - k_m)} \right\} \tag{2.21}$$

$$\lambda_{upper} = k_f \left\{ 1 + \frac{(1 - \Phi)(k_m - k_f)}{k_f + \frac{1}{3}\Phi(k_m - k_f)} \right\} \tag{2.22}$$

where λ_{lower} is the lower bound and λ_{upper} is the upper bound for the apparent thermal conductivity of the composite.[1]

It should be noted that Eqs. (2.21) and (2.22) do not take into account the contribution of an interfacial resistance between the matrix and the filler particles. As a result of this, both the lower and upper bound will be overestimated. This can be illustrated by looking at the simplified case when $k_f = k_m$, which would result in $\lambda_{lower} = \lambda_{upper} = k_f = k_m$. However, it is possible for the effective conductivity of the two phase composite to be lower than the conductivities of either of the constituents if there is an interfacial resistance between the phases. For the case of the upper bound, the overestimation errs in the conservative

---

[1]this is the case for $k_m < k_f$, if the situation were reversed such that $k_f < k_m$ then Eq. (2.22) would give the lower bound and Eq. (2.21) would give the upper bound

direction, therefore the resulting bound should still apply. However, this is not the case for the lower bound. In general, it is not possible to predict a lower bound for the apparent thermal conductivity of a composite without taking into account the interfacial area (the surface area of the particles), the resistance to heat flow across the interface, and the effects of temperature on the interfacial resistance.

2.2 Measurement of Thermal Conductivity

Accurate values for the thermal conductivities of materials are crucial when designing thermal systems. However, there is currently no way to directly measure the thermal conductivity of a material; but rather, it must be derived from more fundamental measurements, namely temperature and heat flow. There are currently two main approaches to measuring thermal conductivity: steady state measurements and transient measurements.

2.2.1 Steady-State Measurement of Thermal Conductivity

The steady state, or static, method is so named because the system is allowed to reach a thermal equilibrium before the measured values are used to determine the thermal conductivity. A number of standards have been developed which describe how to measure the thermal conductivity of a material at steady state [26–32]. The various standards differ slightly in implementation/instrumentation, but they share a few key features.

In each steady state method, a sample of the material being measured is placed between two surfaces and heat is induced to flow across the sample from the hot surface to the cold surface. The sample and the two surfaces are insulated to avoid heat loss so that the heat flow can be approximated as one dimensional. The apparent thermal conductivity of the test material, λ, is then determined by combining the temperature difference between the two surfaces, ΔT, the heat flux through the sample, q'', and the thickness of the sample, L,

17

with the Fourier's Law and the assumption of one-dimensional steady state conduction,

$$q'' = -\lambda \frac{\Delta T}{L}. \tag{2.23}$$

Since measuring the thickness of the sample and the temperature at the two surfaces can be done using well established methods, the main challenge is the measurement of the heat flow. The heat flux term, q'' in Eq. (2.26), is commonly obtained by either generating a set amount of heat using a resistance heater or by mounting a heat flow meter in series with the sample.

Absolute Heat Generation

When using the absolute heat generation method, the amount of heat flowing through the sample is assumed to be equal to the amount of heat generated by the heater. This method is primarily limited by the difficulty in controlling the power dissipated by the heater to an acceptable degree. Since it is assumed that all heat generated by the heater is flowing through the sample, care must be taken to ensure that there are no losses in the radial directions or in the axial direction opposite the sample. Radial losses are usually minimized by wrapping the sample and heating surfaces with insulation or by conducting the experiment in an evacuated chamber. The axial losses are typically minimized by placing an additional guard heater on the opposite side of the primary heater from the sample. In this configuration, temperature sensors are either embedded in the two heaters or are placed adjacent to the heaters. The primary heater is powered at the desired level and the guard heater power is adjusted until the two heaters are at the same temperature. With the assumption of one dimensional heat flow, i.e. negligible losses in the non-axial directions, the guard heater forces there to be an adiabatic plane between the heaters thus acting as a shield to prevent heat losses from the primary heater. The main advantage of this method is that it is not necessary to know the thermal conductivities of any of the components of

the system prior to the test. A standard for using the absolute heat generation method with a guarded hot plate sandwiched between two specimens is described in ASTM C 177 [26].

Heat Flux Meter

An alternative to the absolute heat generation method is to insert a heat flux meter in series with the sample. The heat flux meter operates by measuring the temperature drop across a mass with known thermal conductivity and known thickness. Heat flux meters are usually made out of materials with low thermal conductivities, allowing the meter to be very thin while still generating a large enough temperature drop to be accurately measured. If the thermal conductivity, k_{FM}, thickness, L_{FM}, and temperature drop, ΔT_{FM}, are known for a flux meter and the flow is assumed to be one-dimensional, then the heat flow can be derived from the one-dimensional form of the Fourier's Law:

$$q'' = -k_{FM}\frac{\Delta T_{FM}}{L_{FM}}. \tag{2.24}$$

This method has the advantage of directly deriving the heat flux from the system, which precludes the need for an expensive, high-precision power supply. It also removes the effect of losses in the axial direction from the final measurement. Therefore, it is only necessary to provide radial insulation to ensure the heat flow is one dimensional in the region being monitored by the temperature sensors. Standards describing the use of a heat flux meter in a steady-state thermal conductivity test are described in ASTM C 518 [27] and ASTM E 1530 [31].

Comparative Cut Bar

Another approach, very similar to the heat flux meter method, is to obtain the heat flowing through the sample by using two metering bars with known thermal conductivities, typically greater than $50\,\mathrm{W/m \cdot K}$, to derive the heat flux from the temperature gradient in

the bars as described in ASTM E 1225 [30]. To do this, multiple temperature sensors are typically placed at equally spaced intervals above and below the sample. The temperature gradient in each metering bar, $\partial T / \partial x$, is obtained by fitting a linear line to the temperature readings, the slope of which can then be used to determine the heat flowing through the metering bar:

$$q'' = -k_{mb} \frac{\partial T}{\partial x} \tag{2.25}$$

The heat flux through the sample is typically taken to be the average of the heat fluxes through the two metering bars.

As with the heat flux meter method, since the heat flux is being measured in situ, it is only necessary to ensure the heat flow is one-dimensional in the region containing the temperature sensor by insulating against radial heat losses.

The primary hurdle to implementing the comparative cut bar method is the need for an accurate value for k_{mb}, which cannot be directly measured as stated previously. Additionally, since the final measurement has a strong dependence on k_{mb}, it may not be sufficient to simply use the vendor supplied thermal conductivity for the metering bar material.

ASTM D 5470

There are two standards, ASTM C 1045 [28] and ASTM D 5470 [29], which deal with some of the overarching issues affecting each of the previously described steady-state thermal conductivity measurement methods. Of particular interest here is ASTM D 5470 [29], since it focuses on the measurement of electronic insulation materials.

While the steady state method is relatively straight forward and the experimental apparatus is relatively inexpensive, it has a few disadvantages which limit its applicability. The first problem with this approach is that there will be an additional thermal contact resistance between each of the two surfaces and the sample being measured. This interface resistance is usually minimized by the incorporation of a TIM. However, it is still necessary to determine the value of the interface resistances so they can be subtracted from the apparent thermal

resistance of the sample. The preferred way of doing this is to test multiple samples of varying thicknesses.

The traditional method for determining the apparent thermal conductivity of the material and the interfacial resistance between the sample and the metering blocks is to plot the measured thermal impedance vs. the sample thickness. The thermal conductivity is then the reciprocal of the slope of the best fit line and the intercept at zero thickness is the interfacial resistance. However, in this study, a more general and slightly more straight forward method will be used. By forming a system of linear equations, the conductivity of the samples, λ, and the interfacial resistances between the samples and the metering block, R_{int}, can be found through a least squares solution to the following system of equations for an arbitrary number of samples:

$$
\begin{bmatrix}
2A_1 & L_1 \\
\vdots & \vdots \\
2A_i & L_i
\end{bmatrix}
\cdot
\begin{bmatrix}
R_{int} \\
\lambda^{-1}
\end{bmatrix}
=
\begin{bmatrix}
\Delta T_1/q_1'' \\
\vdots \\
\Delta T_i/q_i''
\end{bmatrix}
\tag{2.26}
$$

where A_i is the cross sectional area of, ΔT_i is the temperature drop across, and q_i'' is the heat flux through sample i.

An additional constraint placed by this approach is that each of the samples must be assumed to have the same thermal conductivity, which is a reasonable assumption if the material is homogeneous. However, if the material being tested is non-homogeneous and the conductivity is expected to vary between samples, then this approach will only allow for the determination of the average thermal conductivity of the samples tested. It must also be assumed that the interface resistances on either side of the samples are constant between tests, which is a reasonable assumption if a dry TIM is being used. However, if a wet TIM, such as thermal grease, is being used, care must be taken to ensure that it is applied in a consistent manner for each sample.

In the event that multiple samples of varying thickness cannot be obtained, a similar procedure can be used by stacking the samples. With this approach, each sample should

be measured individually and then in series. However, additional calculations must be per-formed to properly account for the additional thermal interface resistances between the stacked layers. Similar to the approach with multiple thicknesses, the stacking approach can only return the average thermal conductivity of the samples being tested.

A second disadvantage of the steady-state method is that it is has a strong dependence on the thickness of the sample. If the sample is rigid enough to not deform with the clamping pressure applied by the testing apparatus and the CTE is small enough that the change in thickness during the test is negligible, then it is sufficient to simply obtain an accurate measurement of the sample's thickness prior to testing. However, if the material is malleable enough to deform when clamped or the CTE is large enough to affect the results, then the change in thickness during the test will need to be accounted for. The two most common methods for dealing with this are to either use high precision shims, which fix the distance between the surfaces, or to perform in situ measurement of the sample thickness during the test.

2.2.2 Transient Measurement of Thermal Conductivity

An alternative to the steady state approach is to use a transient measurement method. When measuring the thermal conductivity using the transient method, it is not necessary to allow the system to come to steady state prior to taking measurements. The primary advantage of this approach is the decreased time required for a single test, that is a sample can be tested in minutes rather than hours. However, the decreased testing time comes at the cost of added complexity and more expensive equipment.

As with the steady state method, it is not possible to directly measure the thermal conductivity with the transient method. Instead, the thermal conductivity must be derived from more fundamental properties of the material. The density, ρ, and specific heat, c_p, of a material can be found in a relatively straight forward manner using well established methods. This being the case, if the thermal diffusivity, α, is known, then the definition of

thermal diffusivity,

$$\alpha = \frac{\lambda}{\rho \cdot c_p}, \tag{2.27}$$

can be rearranged to derive a value for the apparent thermal conductivity

$$\lambda = \alpha \rho c_p \tag{2.28}$$

However, there are a few drawbacks associated with deriving the thermal conductivity from other material properties. First, since each of the three properties used to derive the thermal conductivity must be measured individually, they will each have an uncertainty associated with them. Since the thermal conductivity is the product of the measured properties, errors in the component measurements are compounded in the final value for the thermal conductivity. This can be illustrated by looking at the propagation of uncertainty for Eq. (2.28).

If the constituent measurements are of the form $\alpha \pm \delta_\alpha$, $\rho \pm \delta_\rho$, and $c_p \pm \delta_{c_p}$, then, following the procedure presented by Moffat [33], the value of the thermal conductivity will be of the form $\lambda \pm \delta_\lambda$ where δ_λ is described as follows:

$$\delta_\lambda = \sqrt{\left(\frac{\partial \lambda}{\partial \alpha}\delta_\alpha\right)^2 + \left(\frac{\partial \lambda}{\partial \rho}\delta_\rho\right)^2 + \left(\frac{\partial \lambda}{\partial c_p}\delta_{c_p}\right)^2} \tag{2.29}$$

which reduces to

$$\delta_\lambda = \sqrt{(\rho c_p \delta_\alpha)^2 + (\alpha c_p \delta_\rho)^2 + \left(\alpha \rho \delta_{c_p}\right)^2} \tag{2.30}$$

This can be cast in terms of the percentage of the final value by dividing both sides by λ to get

$$\frac{\delta_\lambda}{\lambda} = \sqrt{\left(\frac{\delta_\alpha}{\alpha}\right)^2 + \left(\frac{\delta_\rho}{\rho}\right)^2 + \left(\frac{\delta_{c_p}}{c_p}\right)^2} \tag{2.31}$$

which leads to a final expression for λ of

$$\lambda = \alpha \rho c_p \left(1 \pm \sqrt{ \left(\frac{\delta_\alpha}{\alpha} \right)^2 + \left(\frac{\delta_\rho}{\rho} \right)^2 + \left(\frac{\delta_{c_p}}{c_p} \right)^2 } \right) \qquad (2.32)$$

Therefore, the percentage uncertainty of λ will be greater than the percentage uncertainty of each of the constituent properties. For example, if the uncertainty of α were 10% and the uncertainty of the other two properties were 1%, then the final uncertainty of λ would be 10.1%. However, if each of the properties had an uncertainty of 10%, then the final uncertainty of λ would be 17.3%.

An additional consequence of the sensitivity of λ to errors in each of the property measurements is that this method is limited to materials which are primarily homogeneous. If any of the properties of the material vary between samples, then each property will have to be measured for each sample independently or an unpredictable error will be introduced into the final value of λ. This could prove to be difficult as the equipment used to obtain the different values may require samples of varying size and shape.

Laser Flash

The most commonly used method for measuring thermal diffusivity is the flash method, which was first introduced in 1961 by Parker et al. [34]. In this method, a pulse of high-intensity light is absorbed on the front of a thin sample, and the temperature rise on the back side is recorded as a function of time. The temperature profile in the sample can be predicted by the equation for conduction within a solid of uniform thickness:

$$T(x,t) = \frac{1}{L} \int_0^L T(x,0)\, dx + \frac{2}{L} \sum_{n=1}^{\infty} \exp\left(\frac{-n^2 \pi^2 \alpha t}{L^2} \right) \cdot \cos \frac{n\pi x}{L} \int_0^L T(x,0) \cos \frac{n\pi x}{L}\, dx$$

where L is the thickness of the sample. By assuming that the energy in the pulse, Q, is absorbed in a very shallow region near the front surface and that the sample was isothermal

prior to the pulse, the temperature at the back surface can be expressed as

$$T(L,t) = \frac{Q}{\rho c_p L} \left[1 + 2 \sum_{n=1}^{\infty} (-1)^n \exp\left(\frac{-n^2 \pi^2}{L^2} \alpha t \right) \right] \tag{2.33}$$

By defining two dimensionless parameters,

$$V(L,t) = \frac{T(L,t)}{T_{max}} \tag{2.34}$$

$$\omega = \frac{\pi^2 \alpha t}{L^2} \tag{2.35}$$

where T_{max} is the maximum temperature reached by the back surface, Eq. (2.33) can be rewritten as

$$V = 1 + 2 \sum_{n=1}^{\infty} (-1)^n \exp(-n^2 \omega). \tag{2.36}$$

By defining $t_{1/2}$ as the time it takes the temperature of the back surface to reach half its maximum value, an expression for α can be derived from Eq. (2.36)

$$\alpha = \frac{1.38 L^2}{\pi^2 t_{1/2}} \tag{2.37}$$

where $t_{1/2}$ is empirically determined from the recorded temperature profile of the back surface. A noteworthy feature of Eq. (2.37) is that it does not depend on the amount of energy absorbed, the density, or the specific heat of the material.

A number of improvements have been made to this method over the years which correct for various errors, such as heat loss at high temperatures [35] and losses due to radiation [36]. These improvements are compiled in ASTM standards C 714 [37] and E 1461 [38]. Most modern systems use a laser to apply the energy pulse and an infrared sensor to record the temperature profile. The main challenges in using a modern day laser flash system stem from the difficulty in minimizing heat losses and involve sample preparation and calibration.

The surfaces of the sample should be flat and parallel. The optimum thickness of the samples depends on the diffusivity of the material, so an iterative process may need to be followed to determine the thickness needed. Both the absorption of the laser and the temperature measurement by the infrared sensor have a strong dependence on the emissivity of the surfaces of the sample. In order to control for this, the surfaces of the samples are usually coated with graphite or some other high emissivity coating. Lastly, since heat losses can not be completely eliminated, the accuracy, as determined by comparison to a reference material, can only be applied if the material being tested is very similar to the reference material in both size and properties.

The laser flash method can also be used to measure the specific heat of a material. If the amount of energy absorbed and the density of the sample are known, the specific heat of the sample can be determined from the expression,

$$c_p = \frac{Q}{\rho L T_{max}}. \tag{2.38}$$

This has the advantage of being able to determine the specific heat and thermal diffusivity of a single sample, which helps to alleviate some of the errors introduced when using a non-homogeneous material. However, there are a number of other, more accurate, methods for measuring specific heat which are usually preferred to this approach.

2.2.3 Measurement of Thermal Interface Materials

The selection of a TIM depends on many factors, which need to be analyzed differently for each specific application. Since the overall thermal resistance of a TIM includes the thermal resistance of the TIM itself as well as the interface resistances between the TIM and the surfaces it touches, the bulk thermal conductivity is insufficient to fully characterize a TIM. The inadequacies of ASTM standards for measuring the performance of TIMs, as detailed by Lasance [39], make design decisions based on vendor-supplied data difficult. The

data supplied by vendors are usually obtained with a standard pressure of 3 MPa being applied to the sample, which is much higher than what the TIM will experience in the field. It has been shown that contact resistance is greatly affected by changes in pressure [2]. Therefore, data collected with an unrealistically high pressure being applied cannot be reliably used to make design decisions for applications where the TIM will have a much lower pressure applied.

As suggested by Lasance [39], one possible solution to this problem is to implement application-specific tests. By applying various TIMs to a standardized package, meaningful comparisons can be made between various products with confidence that the resulting data is indicative of real world performance. While this approach is not as well suited for measuring the properties of the TIM alone as the methods previously discussed, it does give a better representation of how the TIM will interact with the other materials in the system. The main drawback to this approach is the required investment of time and money to set up a new test for each application.

2.3 Potting Compounds

A number of studies have looked at the effects of ceramic and metal powders in polymers. It has been shown that the mechanical properties [40, 41], electrical conductivity [42], dielectric constant [43], and thermal conductivity [41, 42] of metal and ceramic polymer composites show a beneficial increase with an increasing volume fraction of the embedded component. These attributes make it a good potting compound for harsh environment electronics.

This study will focus on a particular composite used to pot inductors and transformers. The composite consists of an epoxy, Stycast W-19, impregnated with tabular alumina, T64. The alumina granules were packed around the device to be potted and the structure was subjected to sonic vibrations as the epoxy resin was allowed to fill in the empty spaces around the alumina. The vibration and the incorporation of a range of particle sizes resulted in an alumina volume fraction of approximately 70-80%, as will be reported later. This is higher

than the expected maximum packing density for spherical particles of 64% [44]. As was discussed earlier, as the volume fraction of the filler particle increases, the particles begin to touch one another, thus creating conductive chains. The creation of these chains causes an exponential increase in the apparent thermal conductivity of the composite. Because of this effect, it is this high volume fraction of alumina that makes this composite useful as a potting compound.

In order to model and predict the performance of the system, it is necessary to have accurate values for the properties of the material. However, there are currently no models for predicting the thermal properties of such a composite which take into account the high packing density and wide range of particle shapes and sizes which are present in the composite of interest. Therefore, the density, volume fraction, heat capacity, and apparent thermal conductivity of the material will be determined experimentally. The density will be found by combining the mass of a sample with its volumetric displacement, the volume fraction will be found through the use of optical microscopy and image processing, the heat capacity will be measured by a differential scanning calorimeter (DSC), and the apparent thermal conductivity will be measured with a comparative cut bar apparatus based on ASTM D 5470 [29].

2.4 Thermal Adhesives

One TIM subclass is thermal adhesives, which are materials designed to mechanically bond two surfaces while also promoting the transfer of heat. Since thermal adhesives are often used to attach an electronic assembly to a heat sink with a very different CTE, it is desirable that the adhesive be malleable enough to absorb the CTE stresses produced by the operation of the components. This helps to prolong the life of both the electrical components and the adhesive.

As was discussed earlier, it is desirable, from a thermal perspective, for a TIM to be as thin as possible while still sufficiently conforming to the contacting surfaces. However,

since a thermal adhesive must also provide a mechanical bond and absorb CTE stresses, the thickness of the TIM (usually called bond line thickness, BLT) must often be increased from the thermal optimum for reliability reasons. The increased BLT distributes the CTE stresses over a larger distance, which leads to smaller stress concentrations at the interfaces.

This study will compare the thermal performance of two adhesives, PSA and a new proprietary alternative epoxy based adhesive. PSA tapes are used in a variety of applications from everyday consumer products to, more recently, electronics assembly [45]. In the area of electronics assembly, PSA tapes have been developed for electrical insulation, electrical conduction, and thermal conduction [46, 47]. Of interest, in this study, are the thermally conductive PSAs and their use as a TIM for connecting a printed circuit board (PCB) to an aluminum plate.

The modes of failure due to separation at a polymer-metal interface were reported by Yao and Qu [48], to be either adhesive failure or cohesive failure. Adhesive failure is when the separation occurs at the interface between the adhesive and the metal, while cohesive failure is when the separation occurs within the adhesive layer. It was reported that the mode of failure would depend primarily on the surface roughness of the metal.

The effects of creep on the mechanical strength of PSA for heat sink attachment under isothermal conditions were reported by Eveloy, et. al. [7]. This study will look at the effects of thermal cycling on the thermal resistance of PSA attached to an aluminum substrate. The thermal measurement method used to monitor the state of the adhesive is not able to distinguish between adhesive and cohesive failure, therefore a destructive analysis was performed at the conclusion of the study to determine the mode of adhesive delamination.

Similar work has been done by Eyman and Kromann [8] and Khuu, et. al. [9]. Eyman, et. al. [8] tested the effects of thermal cycling on the reliability of various methods for attaching heat sinks to plastic ball grid arrays (PBGA), with PSA and heat cured epoxy being among the methods tested. Electrical continuity was used as the criterion for failure; and it was reported that no failures occurred in the PSA attached heat sinks until 8,000

cycles, whereas a heat cured epoxy started failing at 300 cycles. Khuu, et. al. [9] used the laser flash method to measure the thermal performance of various thermal interface materials, with epoxy and gap pads attached with PSA among the tested materials; and reported small initial improvements but very little change in thermal resistance for each of the materials tested over the span of 760 cycles.

This study was conducted using a standardized package consisting of either a Flame Retardant 4 (FR4) or polyimide (denoted as Flex) PCB attached to an aluminum substrate with a thermal adhesive. The PCBs were attached to the aluminum substrate by the vendor to control for possible inconsistencies in manufacturing procedure. The two adhesives tested were PSA and an alternative adhesive (denoted as ALT). The boards were rapidly aged by thermally cycling from -40 to 125°C. The combined thermal resistance of the PCB, TIM, and aluminum substrate was measured every 250 cycles using a procedure similar to the one presented by Knight, et. al. [49].

This study will also look at the effects of overmolding, which plays a similar role to potting compounds discussed earlier, on the thermal performance of PSA. The overmoldings used are polyimide based and encapsulate the entire PCB and most of the aluminum substrate. Since it wraps around the PCB and substrate, the overmolding has the effect of mechanically holding the PCB in place. This will help to minimize the effects of delamination, however there is a trade off, as it inhibits the transfer of heat from the board. Two overmoldings were tested and they will be denoted as overmolding A and overmolding B.

While this study only measures the effects of thermal cycling on the thermal performance of the TIMs, related studies using the same standardized package have characterized the effects of thermal cycling on the reliability of the packages used to populate the board with PSA as the TIM [50, 51].

Chapter 3

Experimental Methodology

3.1 Volume Fraction Measurement through Image Processing

The volume fraction of alumina, Φ, present in the alumina/epoxy composite was determined through the use of optical microscopy and image processing. Micrographs were taken of locations near the top, bottom, and middle of the block.

The images were processed by using a threshold tool to convert the color image to a black and white image with the epoxy regions being black and the alumina regions being white, as shown in Figure 3.1. The images were imported with the Python Imaging Library (PIL) as a list of red, green, and blue (RGB) values. The white pixels, having an RGB value of (255,255,255), were counted and compared to the total number of pixels in the image to determine the percentage of the image occupied by the alumina.

$$\Phi = \frac{\text{Pixels}_{\text{alumina}}}{\text{Pixels}_{\text{total}}} \tag{3.1}$$

This was repeated for multiple samples and an average was taken to find the bulk volume fraction.

3.2 Specific Heat Measurement with a Differential Scanning Calorimeter

The specific heat of the alumina/epoxy composite was measured using a Differential Scanning Calorimeter (DSC). A DSC works by keeping the sample being measured at approximately the same temperature as a known reference material. The difference in the amount of heat needed to maintain the sample and the reference material at the same
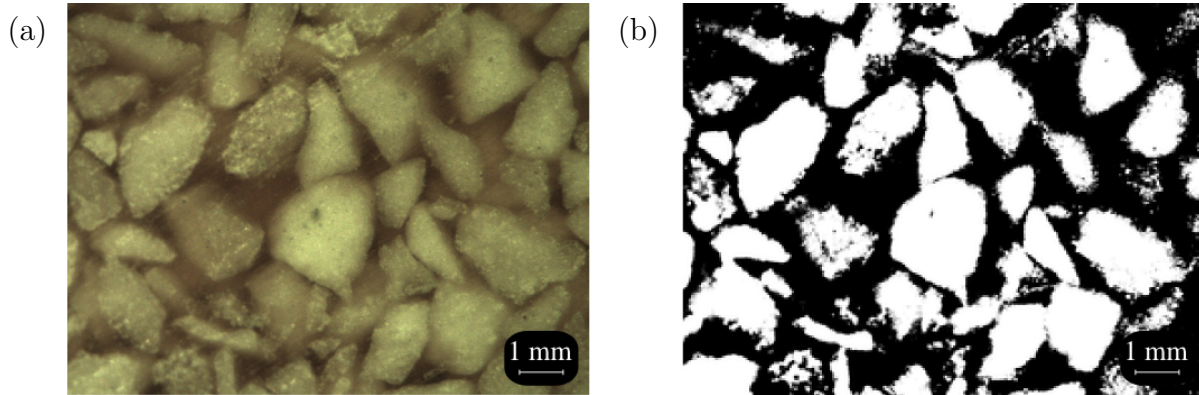
Figure 3.1: Image used to determine the volume fraction of epoxy, where (a) is the original image and (b) is the image after the threshold tool has been used to distinguish between the epoxy region and the alumina region.

temperature is used in conjunction with the known properties of the reference material to calculate the specific heat of the sample being measured.

The DSC can be used in two modes, ramp mode and scanning mode. In ramp mode, a constant amount of heat is applied to both the sample and the reference material so that the temperature rise of the reference material is approximately linear. The sample and the reference material are brought from room temperature to the target high end temperature and then cooled to the target low end temperature. During this process, the temperature of the sample is recorded and combined with the known amount of heat being applied to the sample to generate a curve of the specific heat over the given temperature range.

In scanning mode, the sample and the reference material are first brought to a target temperature. The sample and reference material are then repeatedly heated and cooled so that their temperatures oscillate around the target temperature. The difference in heat required to keep the sample and the reference material at the same temperature is recorded and used to calculate the specific heat of the sample at the target temperature. This process is repeated at multiple temperatures to find points that can be used to generate a curve. While scanning mode has the advantage of being more accurate at a given temperature, it has the disadvantage of not being a continuous measurement for all temperatures within a given temperature range.

3.3 Apparent Thermal Conductivity Measurement with a Comparative Cut Bar Apparatus

The thermal conductivity of the alumina/epoxy composite was measured using a comparative cut bar apparatus based on the ASTM D5470-06 [29]. The apparatus, shown in Figure 3, consists of two metering blocks, each with five thermocouples spaced 1 cm apart. The sample being measured is placed between the two metering blocks. A temperature gradient is imposed across the metering blocks and the sample. The temperature readings from the thermocouples are used to determine the heat flow through and the temperature drop across the sample. An apparent thermal conductivity can then be calculated for the sample material.
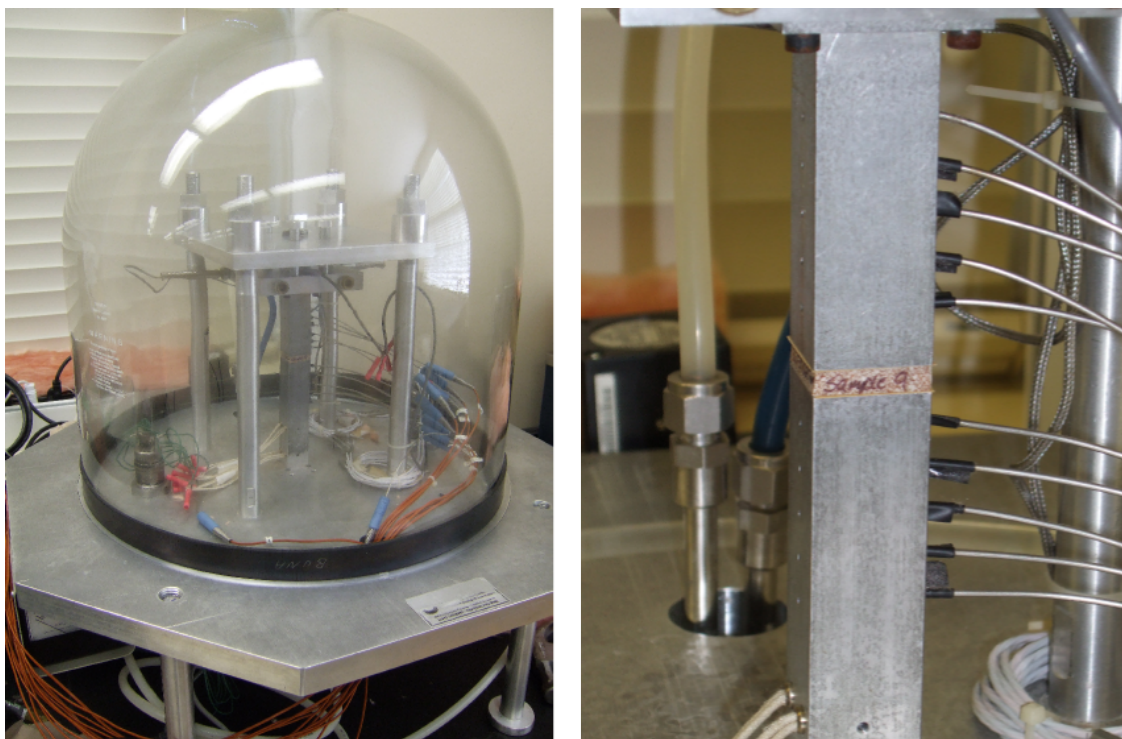
Figure 3.2: Guarded heater apparatus used to measure thermal conductivity.

The metering blocks were constructed from aluminum alloy 2024-T3. There are four resistance heaters, two rows of two, embedded below the thermocouples in the bottom metering block. A liquid cooled heat sink is mounted above the top metering block.

The thermal conductivity of the metering blocks, k_{mb}, was determined by using the guarded heater method. Two DC power supplies were used to power the two rows of heaters. The upper row of heaters heated the metering blocks while the lower row acted as guard heaters. The temperature of each row of heaters was monitored by a Resistance Temperature Detector (RTD) embedded between the heaters. The power levels were then adjusted so that the two rows of heaters were at the same temperature, forcing there to be an adiabatic plane between the rows which acted as a heat shield. The heat flowing through the metering blocks was calculated from the electrical power generated by the top row of heaters. A least squares fit of the temperatures in the metering block was used to determine the thermal conductivity of the metering block material to be $k_{mb} = 133 \pm 1 \, \mathrm{W/m \cdot K}$. Further details of the calibration process can be found in Elkady [52].

A constant force of 1925 N (435 lbs.) is applied to the sample during the test, which corresponds to a pressure of 3 MPa (435 psi). This is necessary because it will be assumed that the thermal interface resistance between the sample and the metering blocks will be constant between tests.

A TIM is placed between the sample and each of the clamping surfaces. This helps to minimize the interface resistance between the sample and the metering block, but more importantly it helps to keep the interface resistance constant between samples. The TIM chosen was Sil-Pad® 800 with a thickness of 0.127 mm (5 mil) and a manufacturer reported thermal conductivity of $1.6 \, \mathrm{W/m \cdot K}$. The contact resistances on either side of the TIM and the conductive resistance of the TIM will be combined into a single term, R_{int}, and are assumed to be constant between tests. The heat generated below the bottom metering block is removed by a serpentine liquid cooled heat sink mounted above the top metering block. The temperature of the inlet water to the heat sink is controlled by an external chiller.

The amount of heat flowing through the metering blocks is controlled by adjusting the power supplied to the heaters, which in turn controls the temperature drop across the sample. The temperature of the top metering block is controlled by adjusting the temperature of the

inlet water to the heat sink, which in turn controls the mean temperature of the sample. By adjusting the power supplied to the heaters and the temperature of the water supplied to the heat sink, the apparatus can be used to measure the apparent thermal conductivity of a material over a range of temperatures.

To test a sample, it is clamped between the metering blocks, with a layer of TIM on each side. The heaters are powered and the temperature of the inlet water is adjusted so the mean temperature of the sample is at the desired temperature. The system is assumed to be at steady state when the temperature readings have changed less than 0.1°C for at least 15 minutes.

A least squares fit of the thermocouple readings is extrapolated to find the temperature at each of the clamping surfaces, as illustrated in Figure 3.3. The slope of the least squares fit is also used, in conjunction with the known thermal conductivity of the metering blocks, to find the heat flux through each of the metering blocks.

$$q''_{bot} = -k_{mb} \left. \frac{\partial T}{\partial x} \right|_{bot} \tag{3.2}$$

$$q''_{top} = -k_{mb} \left. \frac{\partial T}{\partial x} \right|_{top} \tag{3.3}$$

The average of the heat fluxes through the metering blocks is taken to be the heat flux through the sample.

$$q'' = \frac{q''_{bot} + q''_{top}}{2} \tag{3.4}$$

Multiple samples of varying thicknesses are tested, and it is assumed that λ and R_{int} are constant between tests. The apparent thermal conductivity can then be obtained from
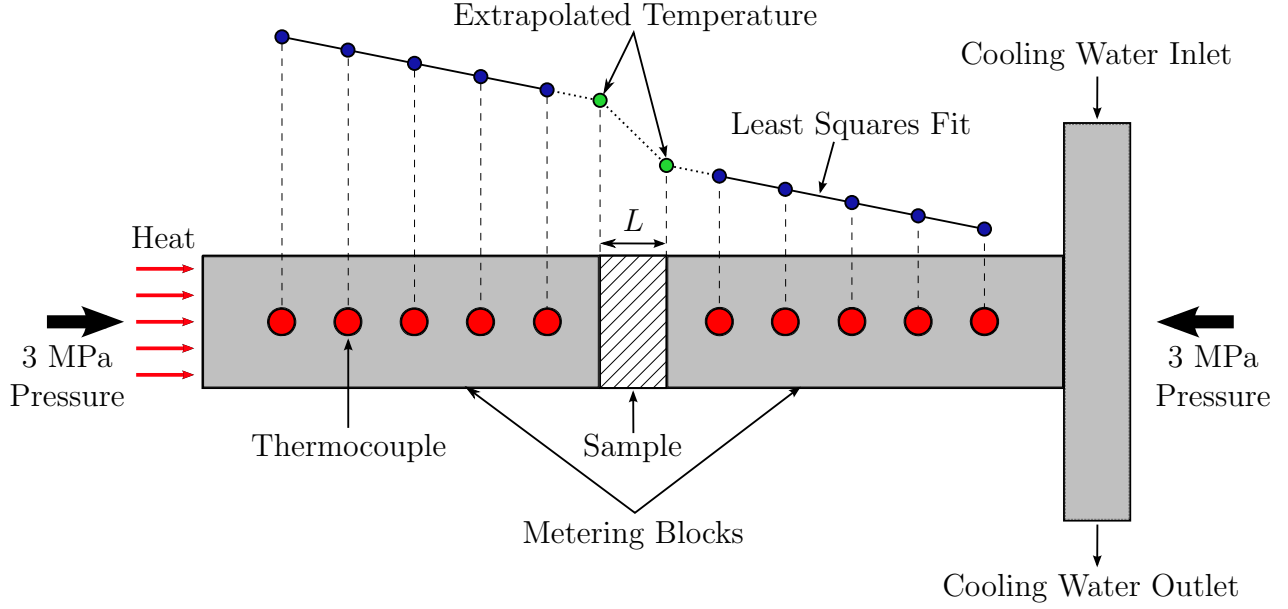
Figure 3.3: Thermocouple readings are extrapolated to determine the temperature at the clamping surface and the heat flowing through the sample.

the least squares solution to the following equation:

$$
\begin{bmatrix} 2A_1 & L_1 \\ \vdots & \vdots \\ 2A_i & L_i \end{bmatrix} \cdot \begin{bmatrix} R_{int} \\ \lambda^{-1} \end{bmatrix} = \begin{bmatrix} \Delta T_1/q_1'' \\ \vdots \\ \Delta T_i/q_i'' \end{bmatrix}
\tag{3.5}
$$

where A is the cross-sectional area of the sample, L is the length of the sample, R_{int} is the interfacial resistance between the sample and the metering block, λ is the apparent thermal conductivity of the sample, ΔT is the temperature drop across the sample, and q'' is the heat flux through the sample.

3.4   Thermal Resistance Measurement with a Comparative Cut Bar Apparatus

The same apparatus that was used to measure the apparent thermal conductivity of the alumina/epoxy composite was also used to compare the thermal performance of three sets of PCBs created with variations in the manufacturing process. Since the PCB samples could not be obtained with varying thickness, the absolute values of the thermal properties

36

were not obtained; but rather, the values were used to compare the boards relative to one another.

The heat flow through and the temperature drop across the samples were determined using the same procedure as was used for the alumina/epoxy samples. The only difference is that the interfacial resistance was not determined and thus each of the measurements of the PCB should be over estimated by the same amount.

3.5   In Situ Thermal Resistance Measurement

As discussed earlier, in order to properly characterize a TIM, it is necessary to include the effects of the bulk properties of the material as well as the interfacial resistances between the TIM and the rest of the system. Because of this, it is often necessary to use application specific tests which allow the performance of a TIM to be measured in situ. In this study, a test was constructed to compare the performance of two adhesives used to attach a PCB to an aluminum substrate.

A fixture was constructed to measure the temperature at the top and bottom of a package while a fixed amount of heat is generated on the top of the package. A composite thermal resistance can be calculated from the temperature drop across the PCB, TIM, and aluminum substrate.

$$R_{jx} = \frac{T_j - T_x}{P} = \frac{\Delta T_{jx}}{P} \tag{3.6}$$

where the junction temperature, T_j, comes from the thermistor on the top of the board and the reference temperature, T_x, comes from the thermocouple in the fluid below the board. The resulting junction resistance, R_{jx}, can be used to monitor the performance of the adhesive over the life of the board.

An operational schematic of the fixture used is shown in Figure 3.4. The aluminum substrate sits on top of a rubber gasket. The top of the fixture can be used to secure the sample in two ways. In the clamped configuration, the top of the fixture presses the PCB

against the aluminum substrate, which is pressed against the bottom rubber gasket; this configuration is shown in Figure 3.5 parts (a) and (b). In the unclamped configuration, the top of the fixture presses against only the aluminum substrate and the PCB is allowed to remain free, this configuration is shown in Figure 3.5 parts (c) and (d). In each method, the top of the fixture is secured to the bottom of the fixture by four screws, each tightened to 33.9 N · m (25 ft · lbs.) of torque, as shown in Figure 3.6.
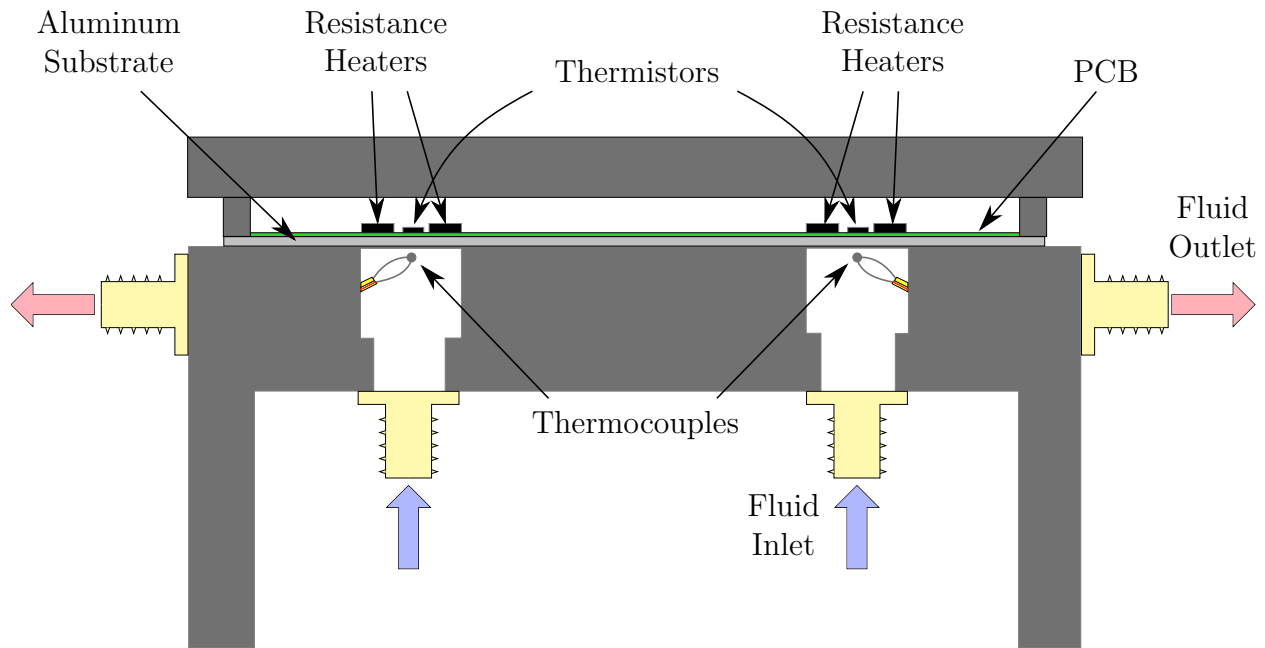
Figure 3.4: Fixture for measuring the junction resistance of a circuit board attached to an aluminum backing.

Once the package has been mounted in the fixture, ethylene glycol is impinged on the back of the aluminum substrate. The temperature of the ethylene glycol is maintained at approximately 22°C by an automated chiller. A thermocouple is used to monitor the temperature of the fluid, T_x, and a thermistor, mounted on the PCB, is used to measure the temperature at the top of the board, T_j. Four resistance heaters are used to generate a fixed amount of heat on the top surface of the board. The fixture is then sufficiently insulated
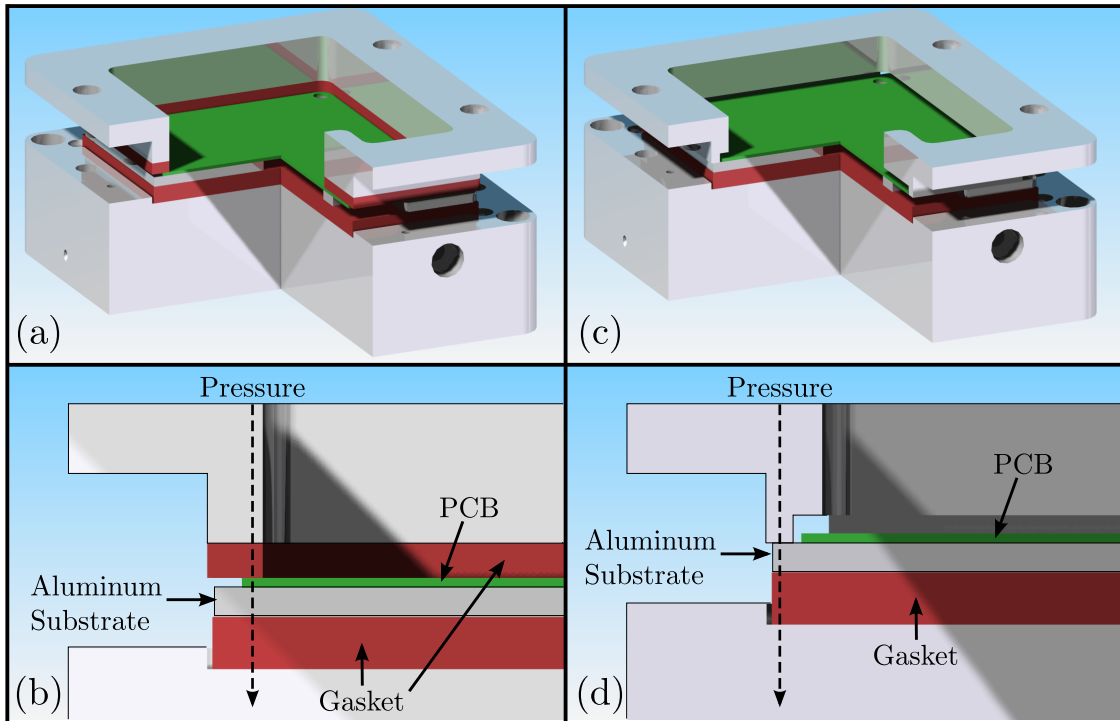
Figure 3.5: Mounting configurations for measuring junction resistance: (a) Clamped configuration (b) Detail view of clamped configuration (c) Unclamped configuration (d) Detail view of unclamped configuration
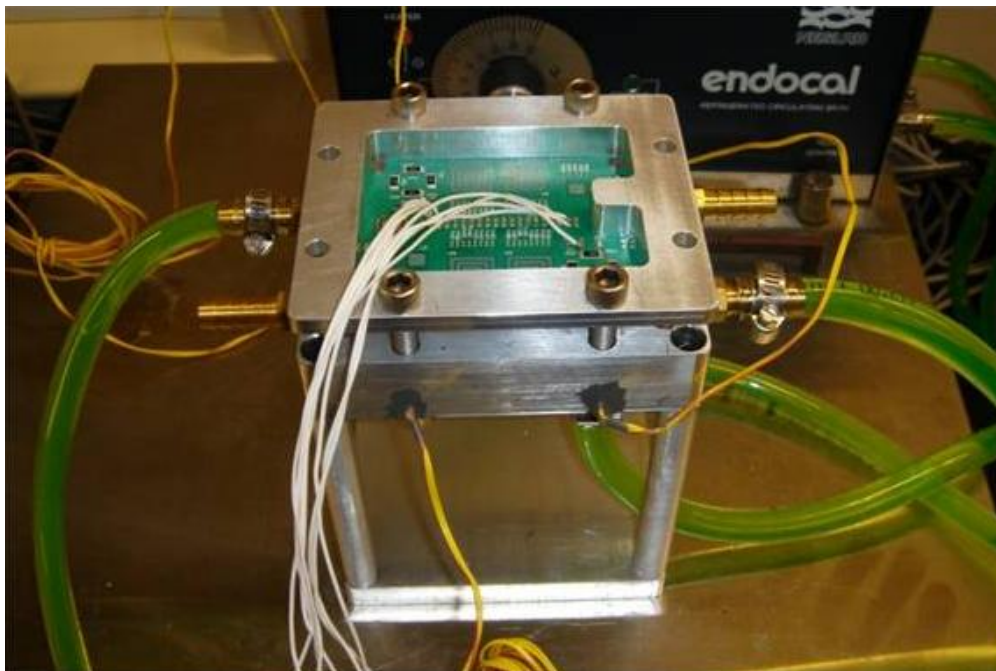
Figure 3.6: PCB mounted in junction resistance measurement fixture.

so as to force heat from the resistors to move through the board and into the fluid on the backside of the metal plate, as shown in Figure 3.7.

Figure 3.7: Insulation used to minimize heat losses to the environment junction resistance measurement fixture.

Temperature readings were taken once the system reached steady state with each set of heaters generating 0, 0.5, 1.0, 1.5, and 2.0 W. Steady state was determined to have occurred when the temperature changed less than 0.01°C for 25 readings, which occurred in approximately five minutes. The temperature difference between the thermistor on the circuit board and the thermocouple in the fluid was then used to determine the junction resistance using a linear regression fit to the power data with an uncertainty of 0.2K/W. A sample set of measurements is shown in Figure 3.8.

The junction resistance is primarily a function of the thermal conductivities of the PCB, adhesive, and substrate; the contact areas of the PCB/adhesive and adhesive/substrate interfaces; and the convective resistance between the bottom surface of the aluminum substrate and the fluid. CTE stresses induced by thermal cycling can degrade the adhesive bond between the TIM and the PCB or aluminum substrate. This leads to a decrease in the contact

40
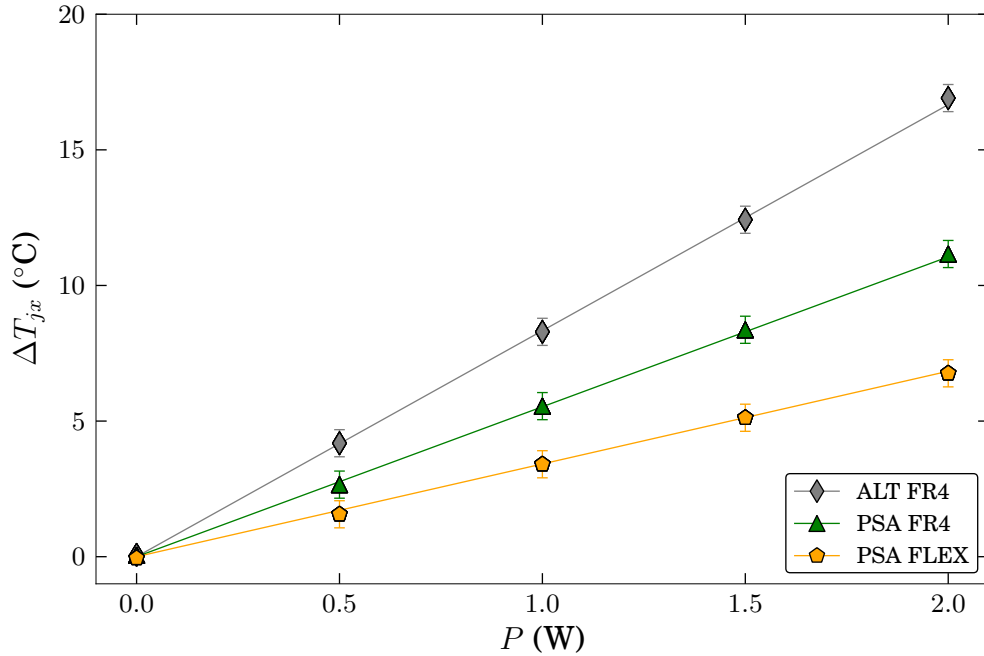
Figure 3.8: Typical thermal resistance data

area, due to delamination, which increases the junction resistance. Exposure to high temperatures during thermal cycling can also cause an increase in thermal conductivity, due to curing, which decreases the junction resistance. In order to isolate the influence of these competing effects, the boards were tested in both the clamped and unclamped configurations.

When the boards are clamped, the fixture presses the PCB against the aluminum substrate, which causes an increase in contact area at the interfaces on either side of the TIM. This increase in contact area minimizes the contribution of the interfacial resistances on either side of the TIM while preserving the contributions of the conductive resistance across the TIM and the convective resistance into the fluid.

When the boards are unclamped, the PCB is not pressed against the aluminum substrate, so the PCB is only held in place by the adhesive. In this configuration, the contributions of the interfacial resistances on either side of the TIM, the conductive resistance across the TIM, and the convective resistance into the fluid are left unaltered.

Since the conductive resistance across the TIM and the convective resistance into the fluid should be approximately the same in both configurations, any difference between the clamped and unclamped readings can be attributed to the interfacial resistances on either side of the TIM. Therefore, the degree of delamination can be monitored by measuring the difference between the junction resistances of a board in the clamped and unclamped configurations.

3.6 Test Matrix

3.6.1 Alumina Granule/Epoxy Potting Compound

A large roughly cylindrical block, nominally 200 mm in diameter and 100 mm in height, of the alumina granule/epoxy potting compound was cast by the vendor to be representative of the final product as it would appear in a packaged device. The block was fabricated by packing tabular alumina granules, T64, into a container and then pouring an epoxy, Stycast W-19, from the top while sonically vibrating the container. The epoxy was allowed to fill in the gaps between the granules. Upon completion of the procedure there was a layer of extra epoxy at the top of the block. A cross section of the cylindrical block is shown in Figure 3.9; where the dark red/black layer at the top of the image is the epoxy only region, the pink/white region in the middle is where the material was broken apart, and the dark regions on either side of the pink/white region were cut using a rotary mill. The regions that were cut with the rotary mill are darker than the broken region because the tool caused the epoxy to be smeared across the alumina granules during the cutting process.

In order to check for variations in thermal properties by location, samples for the density, volume fraction and specific heat measurements were taken from various locations throughout: near the top, bottom, sides and middle, as illustrated in Figure 3.10. The sectioning was done using a high-speed rotary diamond saw.

The apparent thermal conductivity measurements of the alumina/epoxy composite were performed on three samples of varying thickness and a nominal cross sectional area of 6.45
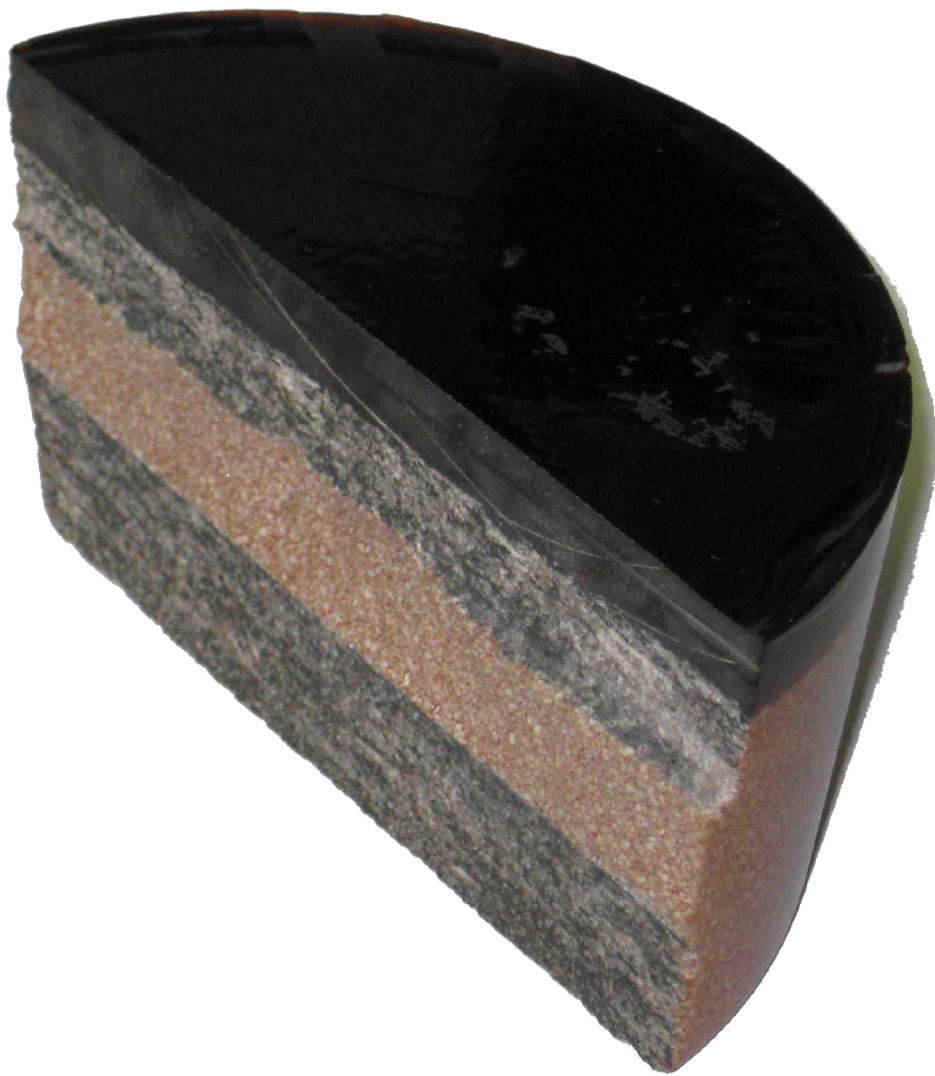
Figure 3.9: Cross section of alumina granule/epoxy sample block.
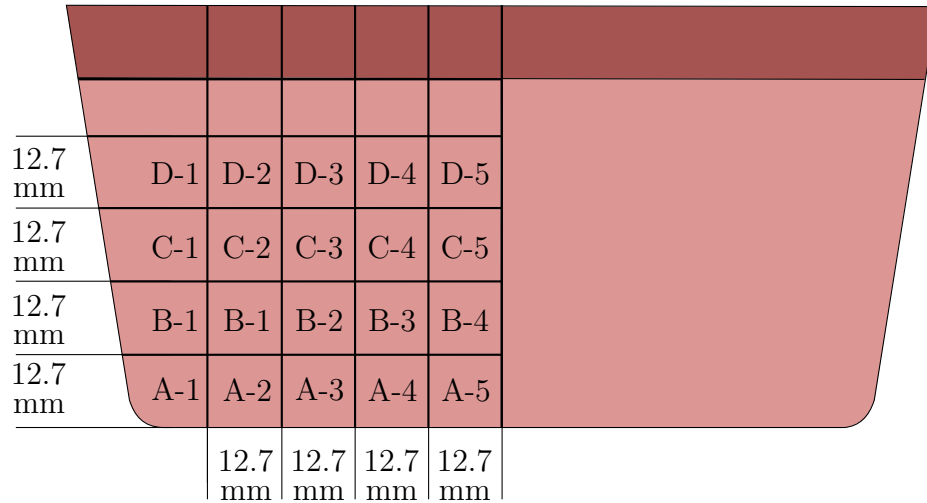
Figure 3.10: Schematic representation of an alumina/epoxy cast block and the location from which samples were taken to determine the properties of the material.

cm^2 ($1'' \times 1''$). The nominal thicknesses of the three samples were 7.30 mm, 15.59 mm, and 19.64 mm. Due to the larger sample size needed for the apparent thermal conductivity test, these samples did not follow the map in Figure 3.10, rather they were taken from the middle of the block. The three samples used for the apparent thermal conductivity measurements are shown in Figure 3.11.
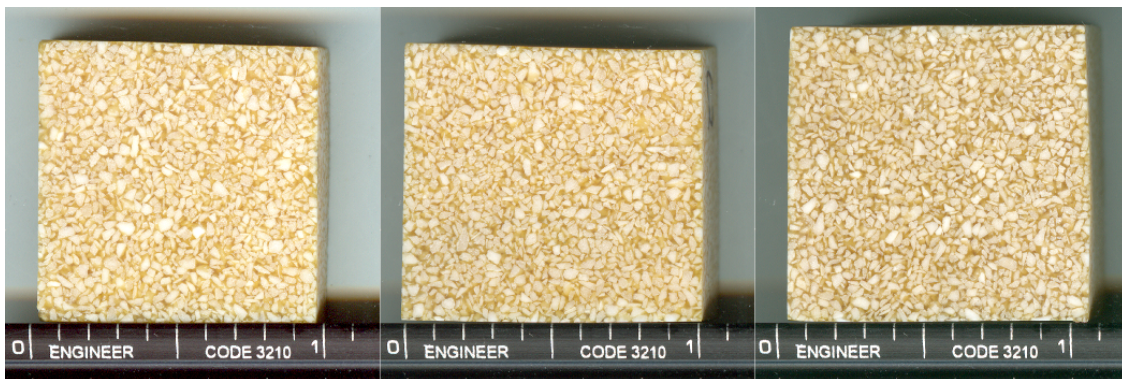
Figure 3.11: Alumina/epoxy samples used for the apparent thermal conductivity measurements. (Note: the scale is in inches)

3.6.2 PCB Comparison

The PCB comparison was done on three sets of boards. The first set was a comparison of two PCBs, Q and V, manufactured by different vendors. The vendors were given the same PCB design, however manufacturing decisions were made which resulted in slightly different stack-ups. The stack-up of each PCB consisted of 6 layers of copper with three layers of pre-preg and two layers of core, however there was some variation in the thicknesses of the layers between the PCBs from the two vendors. The front and back sides of these samples can be seen in Figures 3.12 and 3.13. Each sample was nominally 1.6 mm thick with a nominal surface area of 6.45 cm^2 ($1'' \times 1''$).
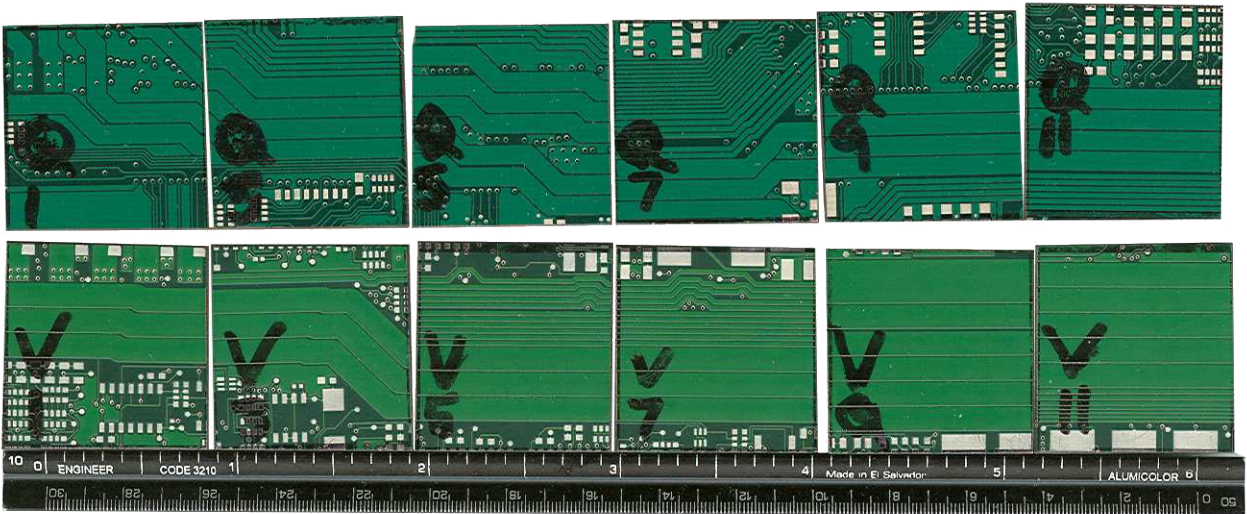
Figure 3.12: Front side of PCB configurations Q and V samples.

The second set of PCB samples, QB, was a follow up to the first set where a third vendor was asked to manufacture a PCB with an identical stack-up to the one used for the Q boards in the first set. The front and back sides of these samples can be seen in Figures 3.14 and 3.15. As with the previous set, each sample was nominally 1.6 mm thick with a nominal surface area of 6.45 cm^2 ($1'' \times 1''$).

The third set of PCB samples compared the difference between vias filled with an epoxy and unfilled vias. There were four samples with filled vias (denoted as set F), and there were four samples with unfilled vias (denoted as U). The four samples for each configuration
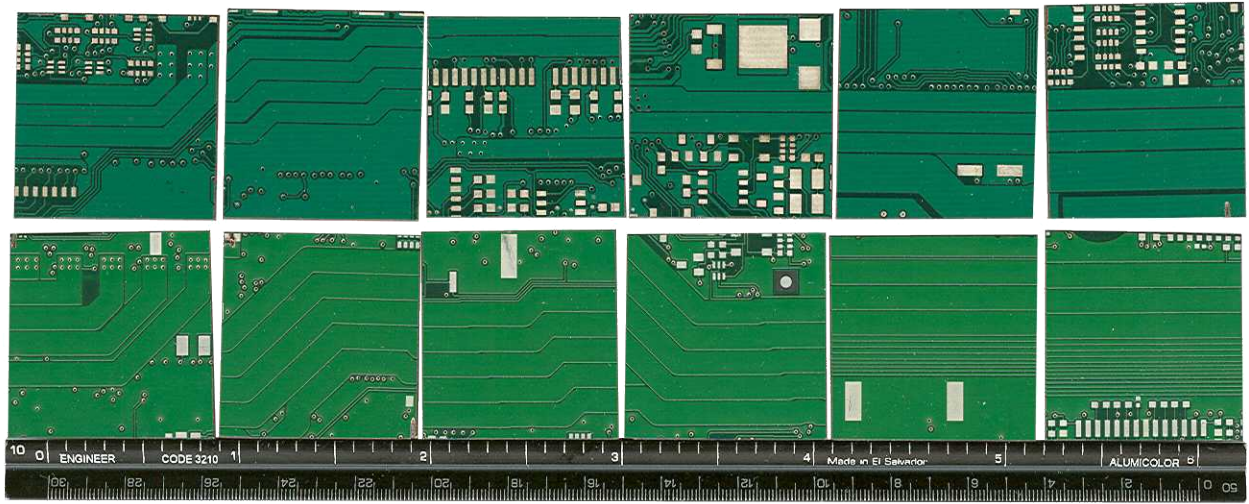
Figure 3.13: Back side of PCB configurations Q and V samples.
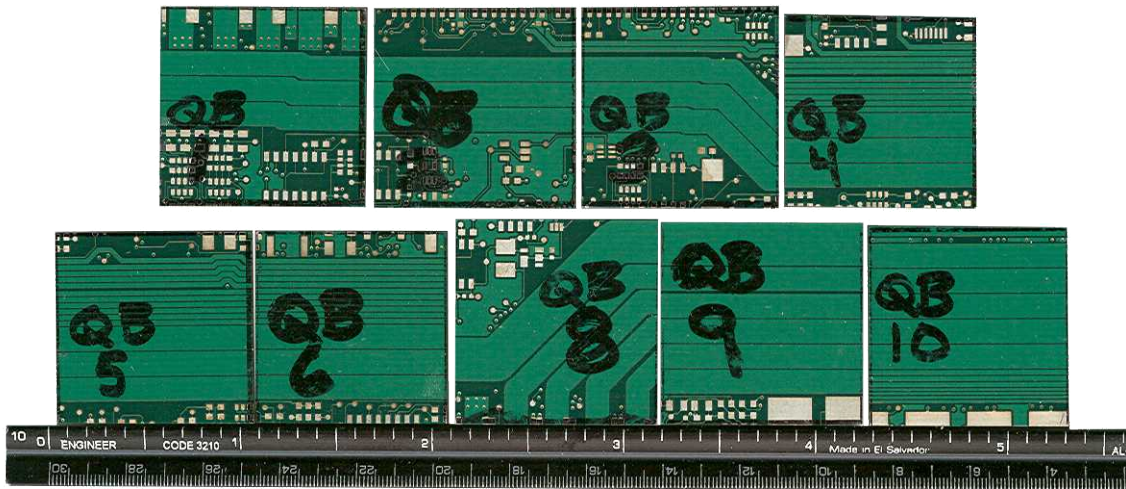
Figure 3.14: Front side of PCB configuration QB samples.
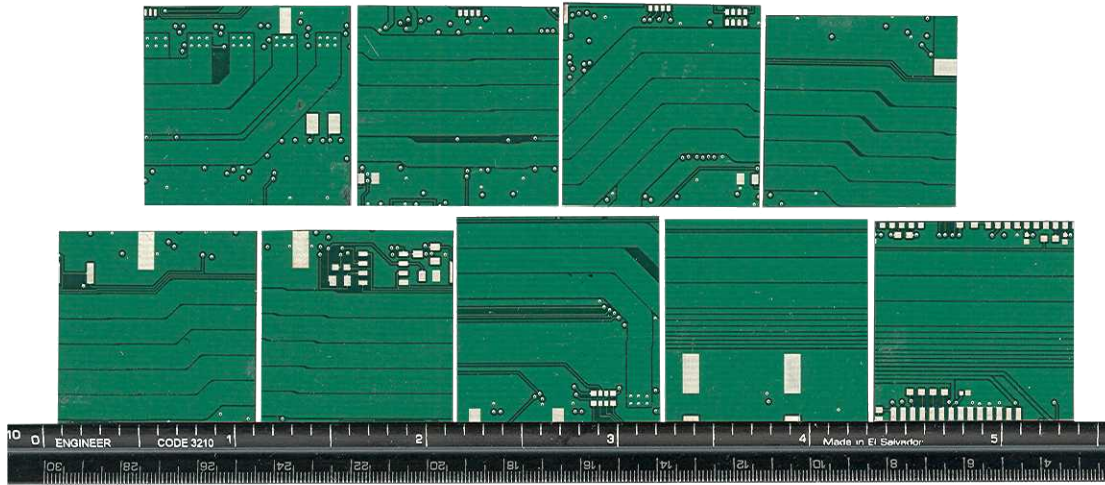
Figure 3.15: Back side of PCB configuration QB samples.

were taken from comparable locations on a larger board such that the only difference was the filling in the vias. The front and back sides of these samples can be seen in Figures 3.16 and 3.17, where the filled vias are in the top row in each image. The samples with the filled vias were all nominally 0.99 mm thick with a nominal surface area of 6.45 cm^2 ($1'' \times 1''$), and the samples with the unfilled vias were nominally 0.96 mm thick with a nominal surface area of 6.45 cm^2 ($1'' \times 1''$).
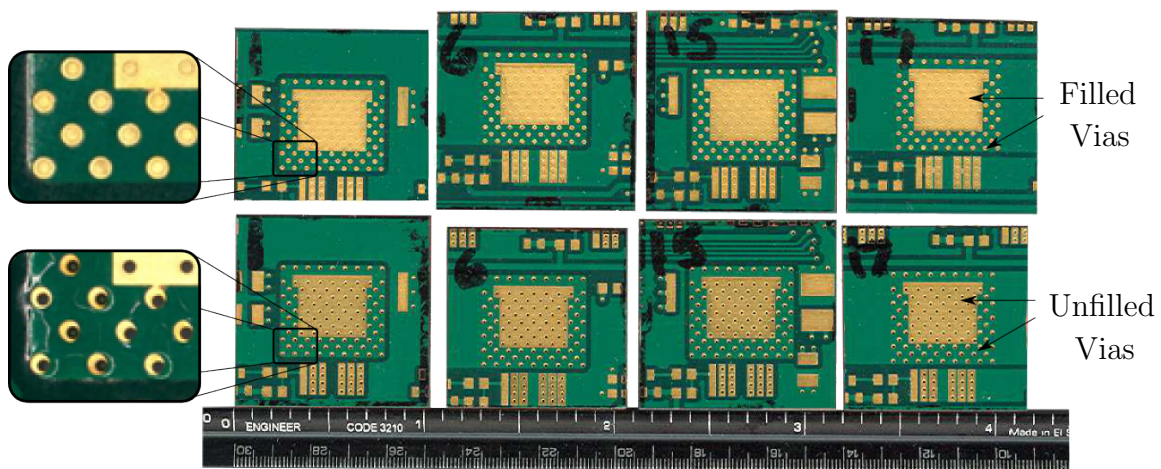
Figure 3.16: Front side of PCB configurations U and F samples.

47
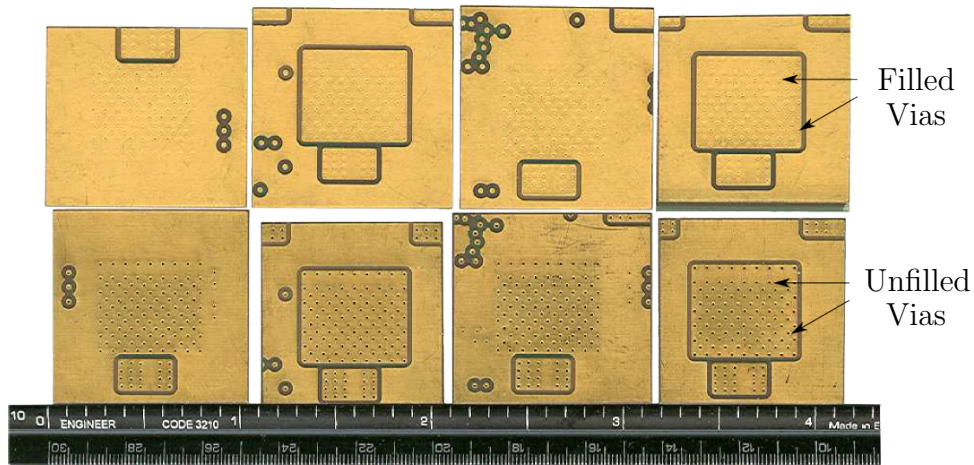
Figure 3.17: Back side of PCB configurations U and F samples.

The properties were measured at an average sample temperature of 25 and 50°C. Similar boards were tested in an external lab which reported a directional dependence where there was approximately a $0.1 \text{ W/m} \cdot \text{K}$ difference in the thermal conductivity depending on which side of the sample was in contact with the cold surface. Because of this, the samples were tested in two orientations, label-hot and label-cold, to check for directional dependence.

3.6.3 Thermal Adhesives

The thermal adhesive comparison study was conducted on five different configurations of board, adhesive, and overmolding. Each board had the standardized layout shown in Figure 3.18, with two test locations per board. Each test location consisted of a thermistor with four resistance heaters. The resistance heaters were arranged in a square to simulate the presence of a heat producing electronic component. The configurations tested are listed in Table 3.1 and sample boards are shown in Figure 3.19. The PCBs were attached to the aluminum substrate by the vendors. There were two adhesives tested, PSA and ALT; and two overmoldings, OM-A and OM-B, which varied in chemical composition but were identical in thickness and appearance.

48

Resistance
Heaters

Thermistor
(Junction)
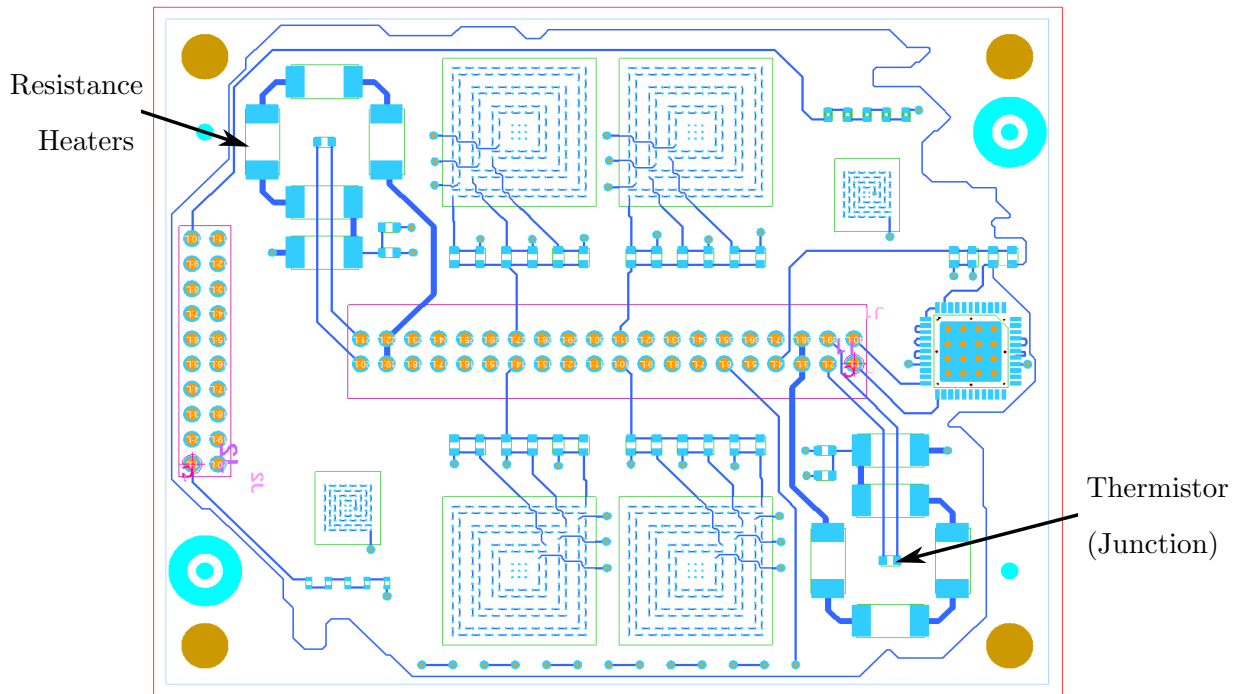
Figure 3.18: Circuit layout for test vehicle

Table 3.1: PCB and thermal adhesive configurations tested

# of Boards	PCB	Adhesive	Overmolding
10	Flex	PSA	
9	FR4	PSA	
17	FR4	ALT	
4	FR4	PSA	A
5	FR4	PSA	B
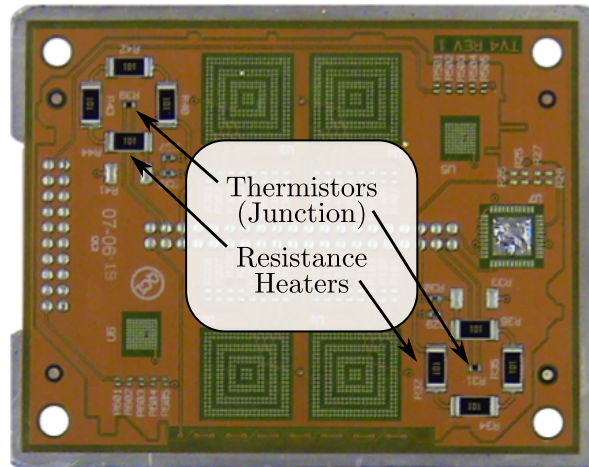
(a)
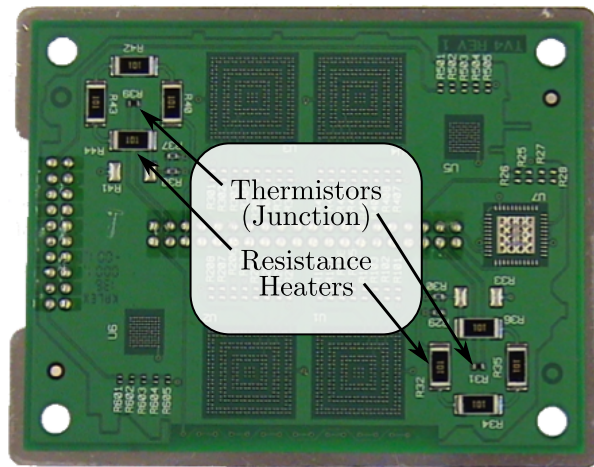
(b)
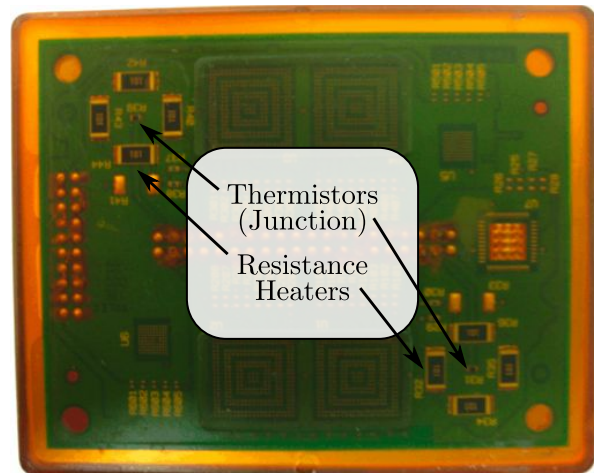
(c)

Figure 3.19: Aluminum substrate attached to (a) Flex PCB, (b) FR4 PCB, and (c) FR4 PCB with overmolding.

Chapter 4

Experimental Results

4.1 Volume Fraction of Alumina

The volume fraction of alumina in an alumina/epoxy composite was determined by taking the average of 20 samples. The samples were taken from four stratified layers, with five samples per layer, as shown in Figure 3.10.

Since the particles of alumina were heterogeneous in both size and shape, there was significant variation in the volume fraction by location. This variation occurred in both the axial and radial directions. Small alumina particles settled amongst the larger particles near the bottom of the cast block. Near the top of the cast block, there were relatively fewer smaller particles present, so the compound was proportionally more epoxy. Due to this, the volume fraction tended to decrease with increasing axial height. However, there was also some radial variation, i.e. two locations at the same stratum had different volume fractions of alumina, as illustrated in Figure 4.1. Therefore, in general, the volume fraction varied unpredictably by location. The results of combining the measurements from the 20 locations are summarized in Table 4.1.

Table 4.1: Volume fraction of alumina calculated using images taken from 20 locations.

	Volume Fraction, Φ (%)
Mean	74
Maximum	83
Minimum	69
σ	4
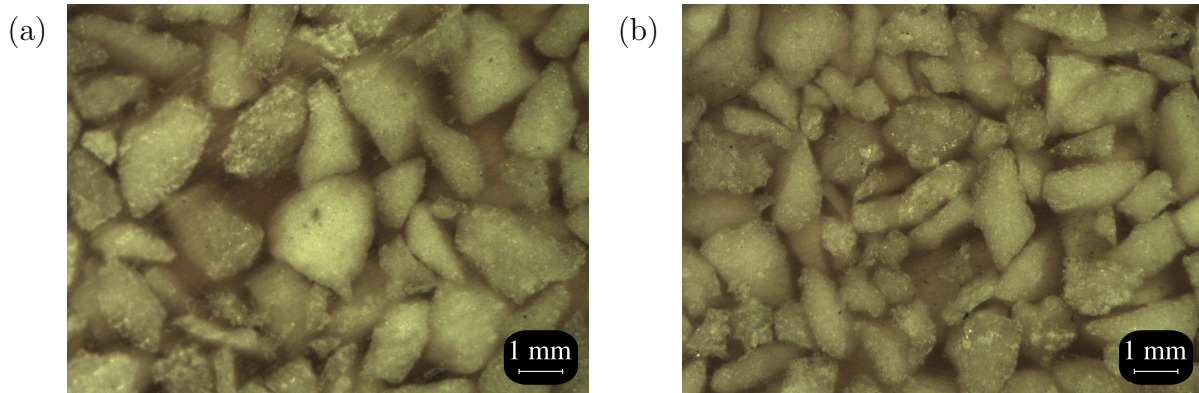
Figure 4.1: Micrographs illustrating the variation in volume fraction of alumina by location, where (a) came from location C-3 and (b) came from location C-5.

4.2   Specific Heat of an Alumina/Epoxy Composite

The specific heat of an alumina/epoxy composite was found by measuring 20 samples, five radially spaced samples from four axial locations. Each sample was cut into the shape of a disc with a thickness of 1 mm and a diameter of 5 mm.

The samples were first tested in ramp mode and then in scanning mode. The results of the scanning mode test showed a significant departure from the results of the ramp mode test. In the first ramp mode test, as shown by the red line in Figure 4.2, the specific heat increases between 20 and 60°C, decreases drastically between 60 and 80°C, and then increases again between 80 and 135°C. However, as shown by the red circles in Figure 4.2, the first scanning mode test shows a steady increase in thermal conductivity with temperature over the entire temperature range. The trend seen in the scanning mode test is more representative of what was expected for this material. Because of this discrepancy, the samples were tested in both modes a second time, shown in blue in Figure 4.2. The second set of tests showed consistent readings for both modes. This suggests there was a residual chemical reaction which occurred when the sample was heated during the first tests and that the reaction had completed by the time the second tests were run.

The specific heat was found to vary unpredictably with both axial and radial location. For example, as seen in Figure 4.3, at a given axial height, the sample taken from
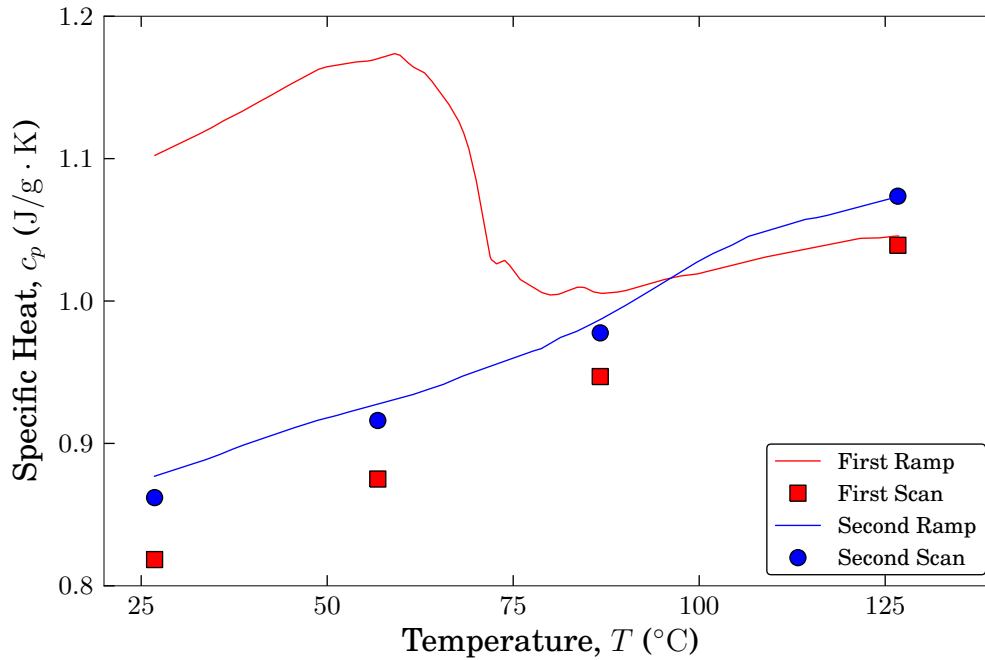
Figure 4.2: Specific heat of a single sample measured four times with a DSC, twice in ramp mode and twice in scan mode.

an outer radial location, C-2, and an inner radial location, C-5, yielded values that were lower than that of an intermediate sample, C-4. The values for the specific heat ranged from 0.86-1.14 $J/g \cdot K$ at 25°C and 1.07-1.37 $J/g \cdot K$ at 125°C. This is consistent with the conclusion of other authors [40–43] that the thermal properties are strongly dependent on volume fraction.

4.3 Apparent Thermal Conductivity of Alumina/Epoxy Composite

The thermal conductivity of an alumina/epoxy composite was measured using three samples of varying thicknesses. However, after completing the measurements, it was observed that the samples being tested had changed color, which suggests that they continued to cure during the test. As seen in Figure 4.4, the bottom surface, which was in contact with the hot metering block, was much darker than the top surface, which was in contact with the cold metering block. This color change is better illustrated by Figure 4.4(b) where it can be
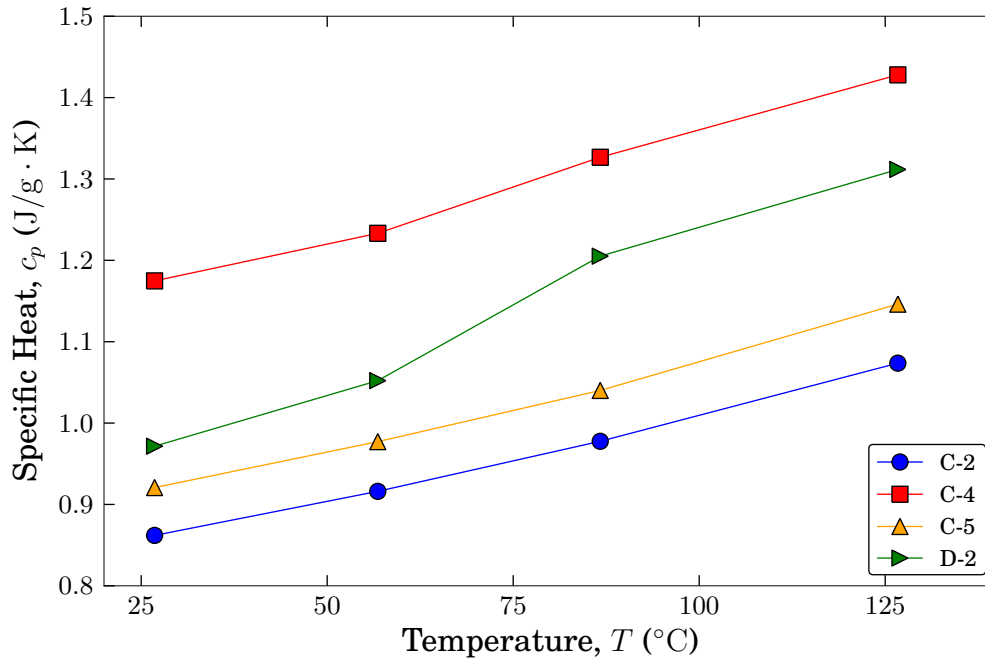
Figure 4.3: Typical specific heat values for different locations.

seen that the color gradient follows the imposed temperature gradient of dark to light and hot to cold respectively. Although not shown in these images, the color of the material prior to the conductivity test was closer to that of Figure 4.4(c) than Figure 4.4(a).
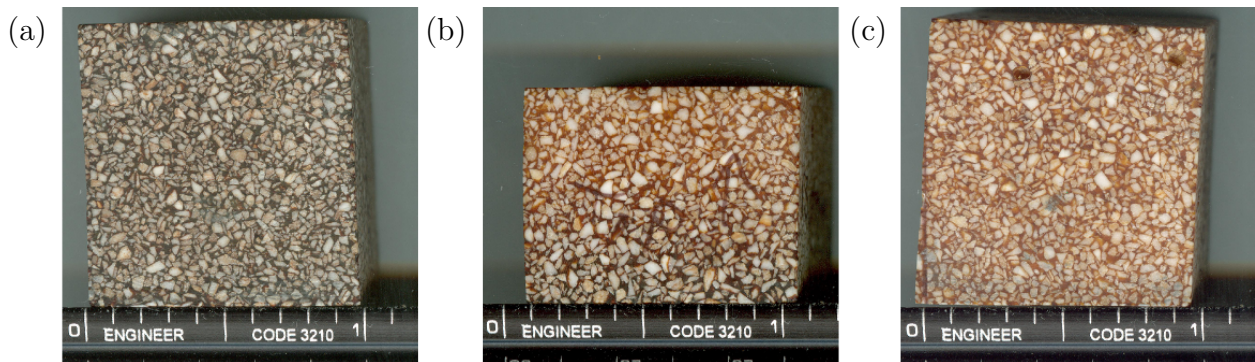
Figure 4.4: Images of sample after performing a conductivity test, where (a) is the bottom, (b) is the side, and (c) is the top. (Note: the scale is in inches).

The method used to determine the apparent thermal conductivity of the sample is dependent upon the system being at steady state. Therefore, it is not possible to reliably determine the apparent conductivity of the material if the properties of the material are

changing during the test, which in this case they appeared to be. Not only did the material appear to change during the test, but it also appeared to change non-uniformly, i.e. the top and bottom of the sample may not have the same properties since they appeared to have cured different amounts.

Since the discrepancies in the specific heat measurements appeared to be resolved by keeping the samples heated for an extended period of time, a similar process was taken to ensure that any residual chemical reactions were completed prior to re-measuring the thermal conductivity. Portions of the material were placed in a chamber at 125°C and checked periodically for changes. The changes that were observed are illustrated in Figure 4.5. The exterior surfaces that were exposed to the air in the chamber became increasingly darker over time. However, the interior, shown by the cross-sections in Figure 4.5, continued to get lighter over time. The difference in the interior and exterior color is illustrated in Figure 4.6, where it can be seen that the darkening of the exterior surface only extends approximately 2 mm deep. The slit, shown in Figure 4.6, was cut prior to placing the material in the chamber, and inspection of the discoloration along its surface shows that the darkening of the exterior occurred wherever the material was exposed to air.

A section of the material was placed in a chamber at 125°C and monitored for changes in color and changes in mass until it reached a steady state. Three samples, with nominal thicknesses of 7.30 mm, 15.59 mm, and 19.64 mm were then cut from this section to perform the thermal conductivity tests, as shown in Figure 3.11. They were tested with mean sample temperatures of 25, 75, and 100°C. The apparent thermal conductivities at these temperatures are shown in Table 4.2 along with the theoretical upper and lower bounds for an ideal composite with no interfacial resistance between the matrix material and the filler particles.

The upper and lower bounds for the apparent thermal conductivity were calculated using the Hashin and Shtrikman correlations, Eqs. (2.21) and (2.22), using estimated values for the thermal conductivities of the constituents and measured values for the volume fraction.

Figure 4.5: Changes in the material after being exposed exposed to 125°C for the given time, where at 3 days and 2 weeks the darker surfaces are the exterior color and the lighter surfaces are cross sections to show the interior color.
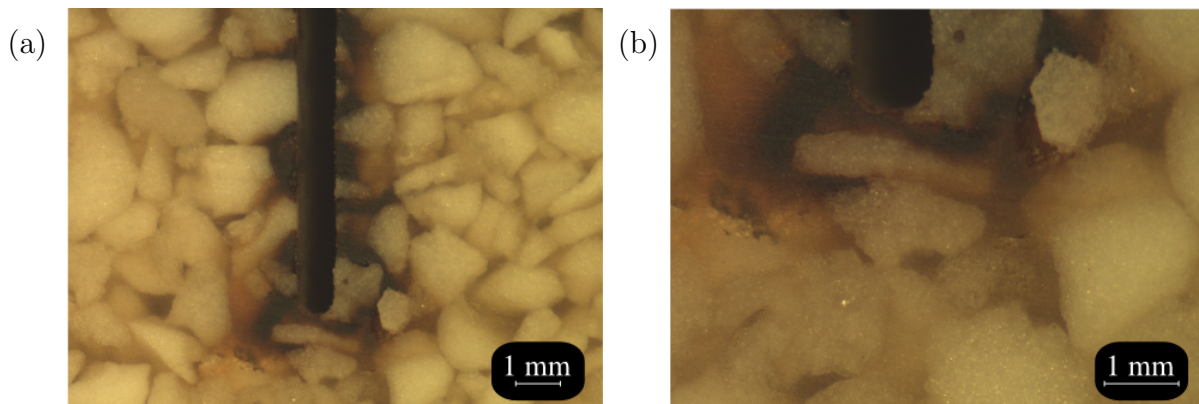
Figure 4.6: Micrographs showing the surface effects which occurred after being held at 125°C for 2 weeks.

The epoxy matrix material is expected to have a thermal conductivity of $0.5 \leq k_m \leq 1.5$, the tabular T64 alumina (99.5% aluminum oxide) filler particles are expected to have a thermal conductivity of $k_f = 35 \text{ W/m} \cdot \text{K}$, and the volume fraction was measured to be $0.69 \leq \Phi \leq 0.83$. Using the low values in these ranges for λ_{lower} and the high values for λ_{upper} gives the results shown in Table 4.2,[1] where it can be seen that the measured thermal conductivities are not bound by the theoretical predictions of Eqs. (2.21) and (2.22). As discussed earlier, since these correlations do not account for interfacial resistance between the matrix and the filler particles, both the upper and lower bounds are overestimated.

Table 4.2: Apparent thermal conductivity values of alumina/epoxy composite.

Temperature (°C)	λ (W/m · K)		
	λ_{meas}	λ_{lower}	λ_{upper}
25	2.0		
75	2.9	3.42	27.25
100	3.2		

It should be noted that this method assumes the thermal conductivity to be the same for each sample. However, it is expected that the thermal conductivity will vary with the volume fraction, particle size, and number of particles of alumina. Since the volume fraction was found to vary by location, and therefore by sample, it is not possible to determine the local thermal conductivity of a specific sample. Rather, the values reported represent the average apparent thermal conductivity of the three samples tested. Also, thermal conductivity decreases with increasing temperature for most homogeneous solids, however this material did the opposite. This behaviour could be caused by CTE effects on the interfacial resistances between the matrix and the filler particles causing the apparent thermal conductivity to increase even while the conductivities of the constituent materials decrease.

---

[1]the correlations for the upper and lower bounds do not account for temperature

4.4 Comparison of PCB Thermal Performance

A comparative cut bar apparatus was used to compare the thermal performance of various PCB configurations. Since multiple thickness were not available, the measurements were used to compare the relative performance of the boards rather than to determine their absolute thermal properties since the contributions of the interfacial resistances were not removed.

The first set consisted of two groups of boards, Q and V, manufactured from the same PCB design by different vendors. The apparent thermal conductivity and thermal impedance of the Q and V boards are listed in Tables 4.4 and 4.3. The properties were measured at an average sample temperature of 25 and 50°C, and the samples were tested in both orientations to check for directional dependence. It was found that the Q boards performed better than the V boards at both temperatures and that variations in thermal resistance due to orientation fell within the measured uncertainty.

Table 4.3: Thermal impedance measurements for PCB configurations Q and V.

			Thermal Impedance, $A \cdot R$ (10^{-3}m^{2}K/W)							
			1	3	5	7	9	11	**mean**	**σ**
Q	25°C	Label-Cold	2.6	3.4	2.8	3.1	3.3	3.4	**3.1**	**0.3**
	50°C	Label-Cold	2.7	3.2	2.7	2.9	3.2	3.2	**3.0**	**0.2**
		Label-Hot	2.5	3.3	2.6	3.0	3.2	3.2	**3.0**	**0.3**
V	25°C	Label-Cold	3.4	4.6	4.7	4.6	4.5	4.6	**4.4**	**0.5**
	50°C	Label-Cold	3.1	4.0	4.3	4.4	4.2	4.1	**4.0**	**0.5**
		Label-Hot	3.4	3.8	4.1	4.4	4.3	4.2	**4.0**	**0.4**

The second set of boards, QB, was a follow up to the first set where a vendor was asked to manufacture a PCB with a stack-up identical to the Q boards from the first set. The apparent thermal conductivity and thermal impedance measurements for the QB group are listed in Tables 4.6 and 4.5. As was expected, it was found that the QB boards performed better than the V boards, however they did not perform as well as the Q. As with the first

Table 4.4: Apparent thermal conductivity measurements for PCB configurations Q and V.

| | | | Thermal Conductivity, λ (W/m·K) | | | | | | | |
			1	3	5	7	9	11	**mean**	**σ**
Q	25°C	Label-Cold	0.62	0.47	0.58	0.51	0.48	0.47	**0.52**	**0.06**
	50°C	Label-Cold	0.60	0.51	0.59	0.56	0.50	0.50	**0.54**	**0.05**
		Label-Hot	0.63	0.48	0.61	0.53	0.51	0.51	**0.54**	**0.06**
V	25°C	Label-Cold	0.47	0.35	0.34	0.34	0.35	0.35	**0.37**	**0.05**
	50°C	Label-Cold	0.51	0.40	0.37	0.37	0.38	0.39	**0.40**	**0.05**
		Label-Hot	0.48	0.42	0.39	0.37	0.38	0.38	**0.40**	**0.04**

set, the orientation did not appear to have any statistically significant effect on the thermal properties.

Table 4.5: Thermal impedance measurements for PCB configuration QB.

| | | | Thermal Impedance, $A \cdot R$ (10^{-3}m^{2}K/W) | | | | | | | | | |
			1	2	3	4	5	6	8	9	10	**mean**	**σ**
QB	25°C	Label-Cold	2.9	3.4	3.7	4.2	4.1	4.1	3.5	4.1	3.8	**3.8**	**0.4**
		Label-Hot			3.8		4.2			4.1		**4.1**	**0.3**
	50°C	Label-Cold	2.5	3.0	3.5	3.6	3.8	3.6	3.2	3.7	3.3	**3.4**	**0.4**
		Label-Hot	2.6	3.1		3.8		3.8	3.1		3.3	**3.3**	**0.5**

Table 4.6: Apparent thermal conductivity measurements for PCB configuration QB.

| | | | Thermal Conductivity, λ (10^{-1}W/m·K) | | | | | | | | | |
			1	2	3	4	5	6	8	9	10	**mean**	**σ**
QB	25°C	Label-Cold	5.5	4.7	4.3	3.8	3.8	3.9	4.4	3.9	4.2	**4.3**	**0.6**
		Label-Hot			4.2		3.7			3.9		**3.9**	**0.3**
	50°C	Label-Cold	6.4	5.2	4.6	4.4	4.2	4.5	4.8	4.3	4.8	**4.8**	**0.7**
		Label-Hot	6.1	5.1		4.1		4.2	5.0		4.8	**4.9**	**0.7**

The third set of boards was thinner than the previous sets and compared filled vias (F) to unfilled vias (U). The apparent thermal conductivity and thermal impedance measurements for the F and U boards are listed in Tables 4.8 and 4.7. It was found that the boards with

the unfilled vias performed slightly better than the filled vias at both 25 and 50°C and that the orientation did not have a statistically significant effect on the thermal properties.

Table 4.7: Thermal impedance measurement for PCB configurations U and F.

			Thermal Impedance, $A \cdot R$ $(10^{-3}\mathrm{m^2K/W})$					
			1	6	15	17	**mean**	**σ**
F	25°C	Label-Cold	1.6	1.6	1.6	1.5	**1.6**	**0.1**
		Label-Hot	1.6		1.6		**1.6**	**0.1**
	50°C	Label-Cold	1.5	1.4	1.5	1.4	**1.4**	**0.1**
		Label-Hot		1.5		1.4	**1.4**	**0.0**
U	25°C	Label-Cold	1.4	1.3	1.4	1.3	**1.3**	**0.1**
		Label-Hot		1.3		1.3	**1.3**	**0.0**
	50°C	Label-Cold	1.4	1.2	1.3	1.2	**1.3**	**0.1**
		Label-Hot	1.4		1.3		**1.3**	**0.1**

Table 4.8: Apparent thermal conductivity measurements for PCB configurations U and F.

			Thermal Conductivity, λ $(\mathrm{W/m \cdot K})$					
			1	6	15	17	**mean**	**σ**
F	25°C	Label-Cold	0.62	0.63	0.63	0.67	**0.64**	**0.02**
		Label-Hot	0.61		0.63		**0.62**	**0.02**
	50°C	Label-Cold	0.67	0.69	0.66	0.73	**0.69**	**0.03**
		Label-Hot		0.67		0.70	**0.69**	**0.02**
U	25°C	Label-Cold	0.67	0.75	0.68	0.76	**0.71**	**0.05**
		Label-Hot		0.75		0.76	**0.76**	**0.00**
	50°C	Label-Cold	0.69	0.77	0.73	0.79	**0.74**	**0.05**
		Label-Hot	0.69		0.76		**0.72**	**0.05**

While at first glance this seems to suggest that the material used to fill the vias did a poorer job of transferring heat than the air it was replacing, it is more likely that filling the vias caused a degradation in one of the other links in the thermal path. One possible explanation for this is that the filled vias had approximately 50% less copper around the edge of the vias, as illustrated in Figure 4.7, due to the point in the manufacturing process at which the vias were filled. It is also possible that the measurements could have been skewed

by differences in contact resistance between the PCB and the Sil-Pad. As was mentioned earlier, the boards with the filled vias were approximately 0.3 mm thicker than the boards with the unfilled vias. As seen in Figure 3.16, the filled vias were located in a square region at the center of the board. The filling of the vias caused the square region to be raised more on the boards with the filled vias than on the boards with the unfilled vias. Because of this the top surfaces of the filled via boards were less planar than those of the unfilled via boards. This could have led a larger thermal interface resistance between the filled via boards and the Sil-Pad than was present with the unfilled via boards, which could explain the poorer performance of the filled via boards.
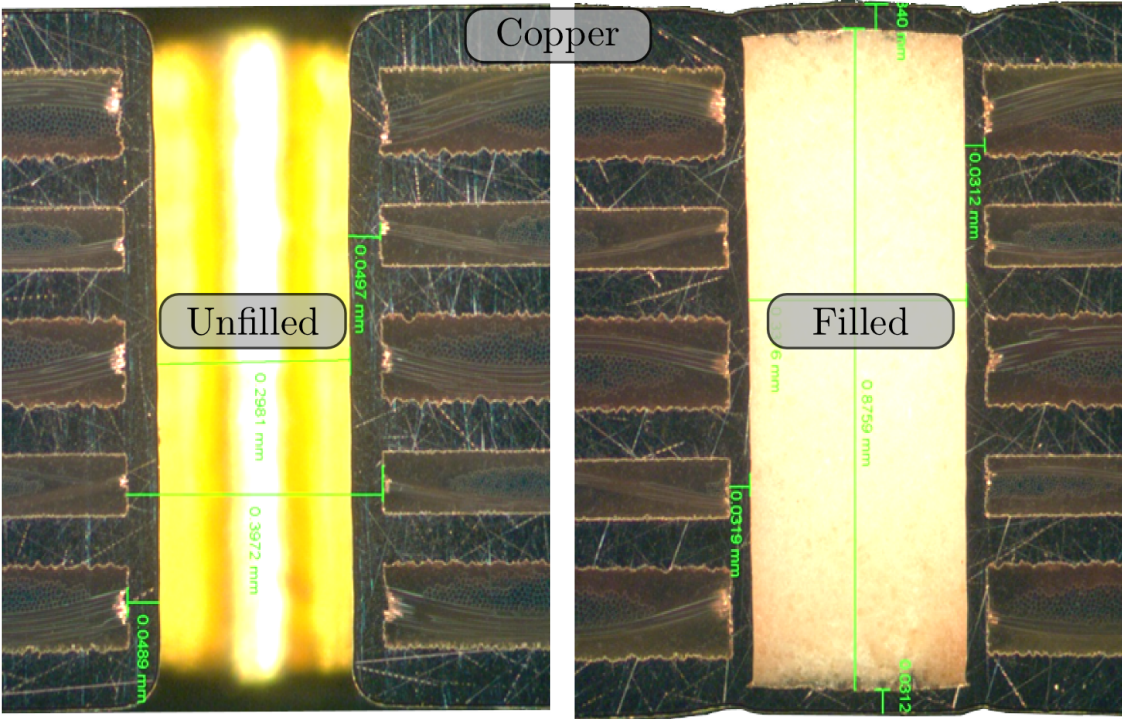
Figure 4.7: Cross sections of filled and unfilled vias showing a thicker layer of copper lining the inside wall of via in the unfilled boards than in the filled boards.

4.5　Effects of Thermal Cycling on Thermal Adhesives

Two thermal adhesives, a standard PSA and an alternative epoxy based adhesive, were compared using a standardized package to measure the effects of thermal cycling on the thermal junction resistance of a PCB attached to an aluminum substrate.

Prior to cycling, measurements were taken for each board as a baseline. The baseline measurements for PSA and the alternative adhesive on FR4 boards are shown in Figure 4.8, where it can be seen that the alternative adhesive exhibited a larger range of thermal resistances than did the PSA. The alternative adhesive boards ranged from 4.65 to 8.33 K/W with a standard deviation of 0.95 K/W, while the PSA boards ranged from 5.23 to 6.35 K/W with a standard deviation of 0.26 K/W. Since both sets used the same type of PCB and substrate, the difference between the two can be attributed to the contribution of the TIM component to the overall junction resistance. The wider range of values for the epoxy boards suggest a non-uniform application of the alternative adhesive during assembly, which may be a result of the wet process used to apply the epoxy as opposed to the dry process used to apply the PSA tape.

After the baseline measurements were taken, the boards were thermally cycled in a Thermotron S-4C chamber from -40°C to 125°C on a 90 minute cycle with 15 minute dwells at the target temperatures following the JEDEC standard JESD 22-A104C [53]. A sample temperature profile is shown in Figure 4.9. The method used to measure the junction resistance requires that the system be at steady state, or a thermal equilibrium. Therefore, the junction resistance was not monitored continuously while the boards were in the chamber, but rather they were removed from the chamber for junction resistance measurements every 250 cycles. This means that the boards were thermally cycled for 250 cycles and then allowed to sit at room temperature for 2 weeks, while the junction resistance measurements were taken, before being placed back in the chamber for the next 250 cycles.
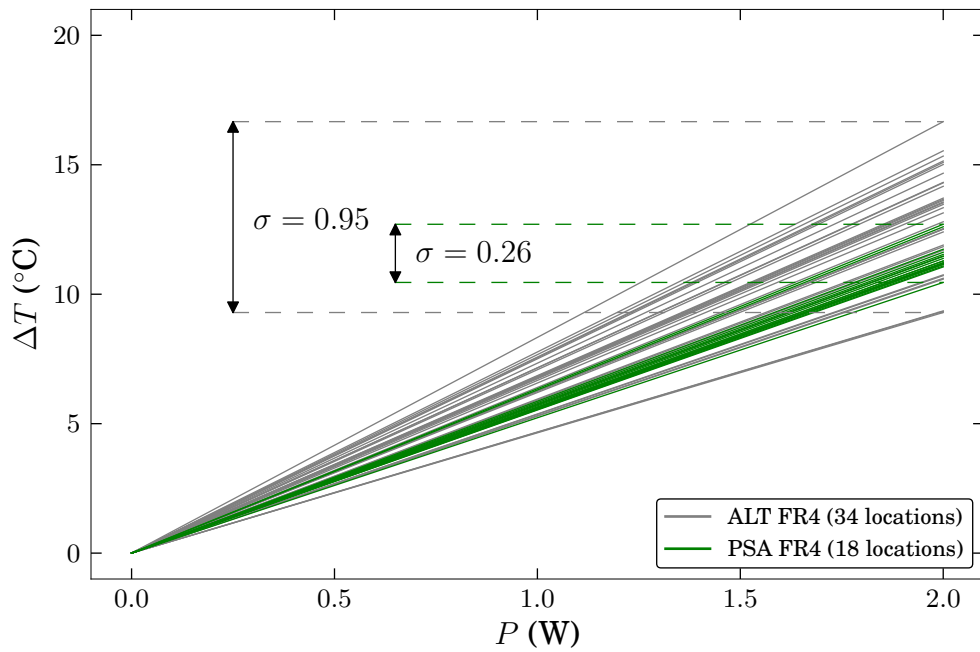
Figure 4.8: Thermal resistances of FR4 boards with PSA and an alternative adhesive prior to cycling. Measurements are shown for 2 locations per board on 17 ALT FR4 boards and 9 PSA FR4 boards.
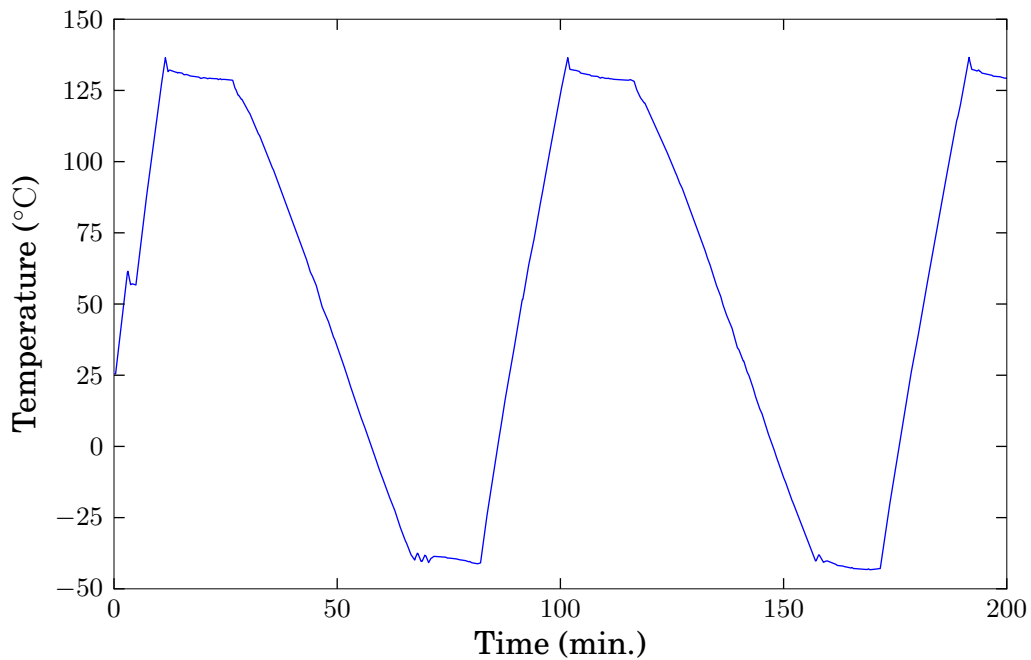
Figure 4.9: Thermal cycling profile

4.5.1 Clamped Junction Resistance

The thermal resistances of the boards while clamped are shown in Figure 4.10, where it can be seen that the Flex boards had a lower junction resistance than the FR4 boards. This difference is primarily due to the smaller contribution of the Flex PCB to the junction resistance since the Flex is thinner than the FR4. The configurations with the FR4 boards all had comparable thermal resistances, with the PSA boards having a slightly lower average thermal resistance than the alternative adhesive boards.
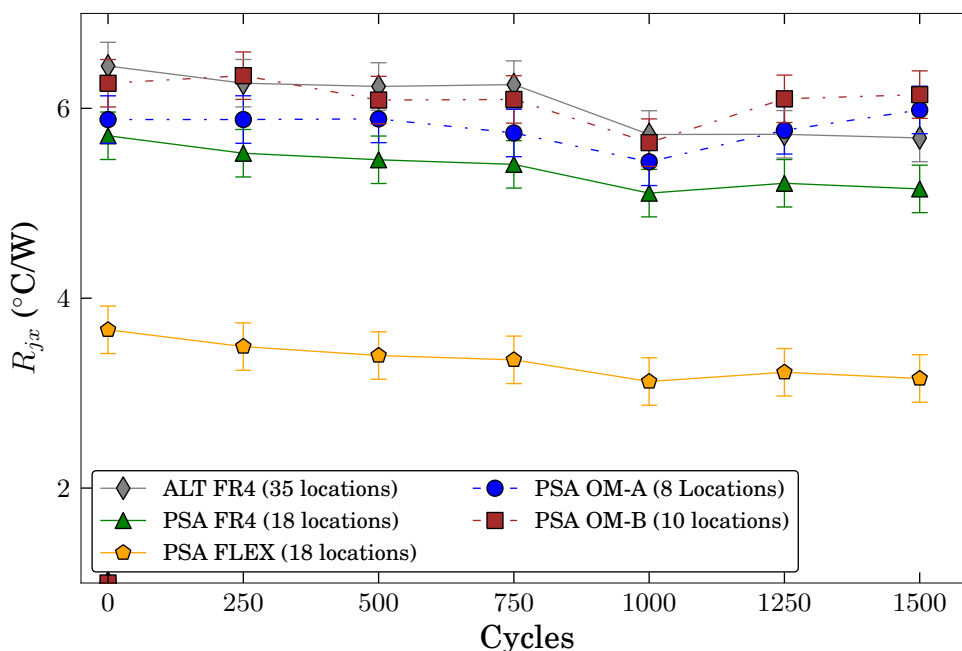
Figure 4.10: Average junction resistance with cycling

Figure 4.11 shows the change in the junction resistance of the boards while clamped as a function of the number of thermal cycles. In each of the non-overmolded configurations, the thermal performance improved with thermal cycling, with the exceptions to this trend falling within the measured uncertainty. This improvement is possibly due to curing of the adhesive, which increases its thermal conductivity. Since the PCBs were being pressed against the aluminum substrate, the changes observed are primarily due to changes in material properties, namely thermal conductivity. Similar initial improvements in thermal performance

were reported by Khuu, et. al. [9] for both PSA, which showed a 25% reduction in thermal resistance between 0 and 255 cycles and then no change between 255 and 760 cycle; and an epoxy based adhesive, which showed an 11% reduction in thermal resistance between 0 and 255 cycles and then a 10% increase between 255 and 760 cycles.
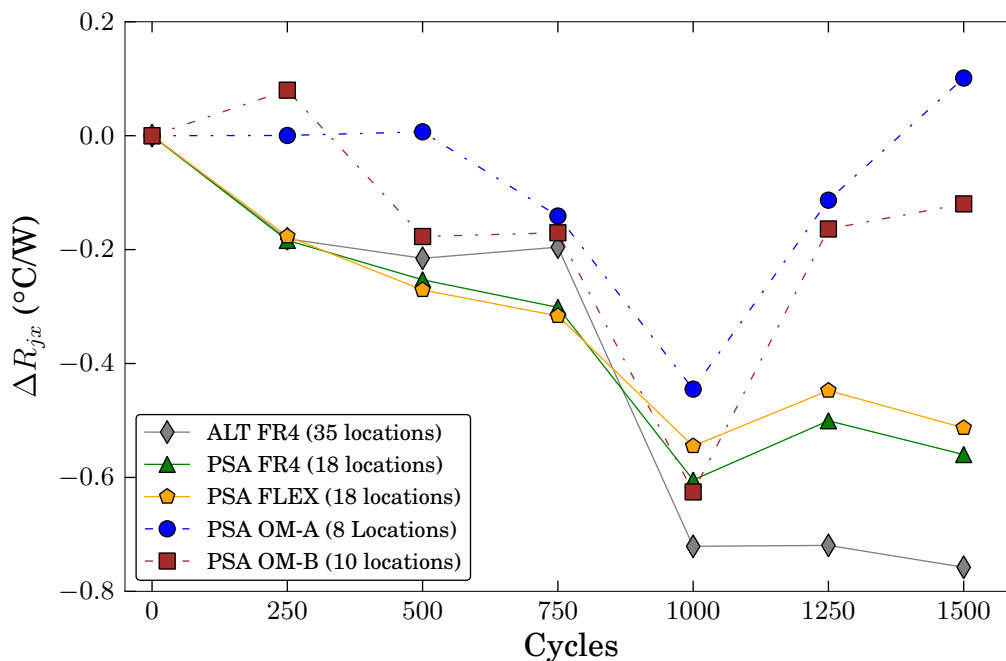
Figure 4.11: Average change in junction resistance with cycling

4.5.2 Unclamped Junction Resistance

The delamination of the PCB from the aluminum substrate causes a significant increase in the contact resistance between the board and the substrate due to decreased contact area. Comparing the difference between the junction resistances while pressing and not pressing on the board allows for the detection of delamination.

The boards were separated into three categories: no delamination, partial delamination, and full delamination. A board was considered to have partial delamination if the unclamped junction resistance was 25% greater than the clamped junction resistance or full

delamination if it was 50% greater. Typical results for the alternative adhesive boards showing no delamination, partial delamination, and full delamination are shown in Figure 4.12, and the percent difference between the clamped and unclamped configurations for each of the alternative adhesive boards is shown in Figure 4.13.
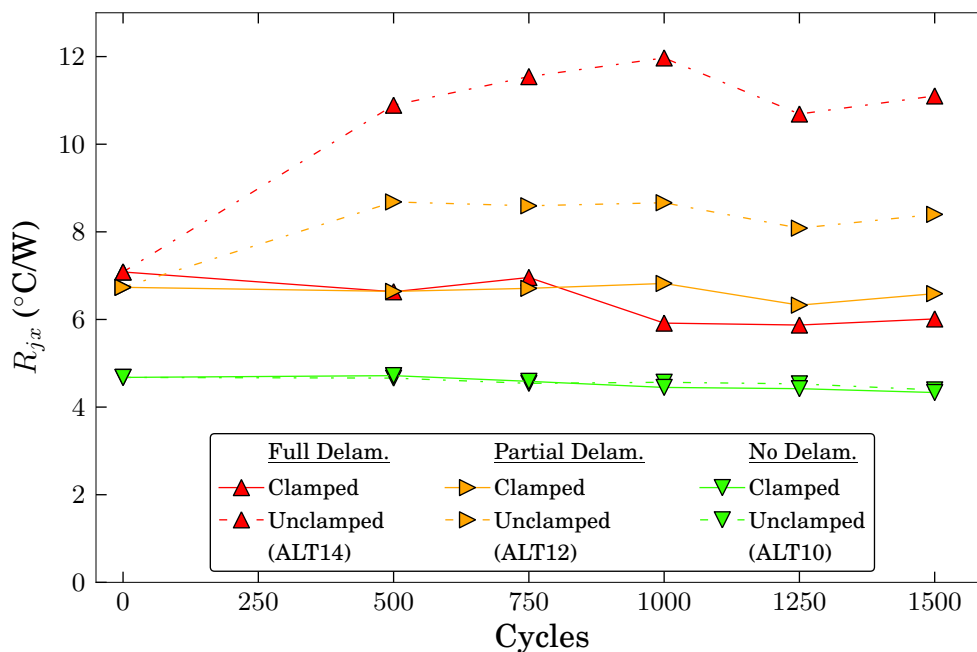
Figure 4.12: Comparison of junction resistance for clamped and unclamped boards

It was found that there was no significant difference between the clamped and unclamped readings for the PSA boards after 1500 cycles, therefore it was determined that no delamination had occurred. However, there were significant differences between the clamped and unclamped readings for the alternative adhesive boards resulting in partial delamination being present at four locations and full delamination at 12 locations after 1500 cycles, as shown in Figures 4.13-4.14[2]. This supports the findings of Eyman, et. al. [8], who reported no failures in PSA attached heat sinks until around 8,000 cycles, where as a heat cured epoxy started failing at around 300 cycles.

---

[2]What appears to be a reversal in trend between 1250 and 1500 cycles in Figure 4.14 was caused by small changes in the measurements of boards that were near the threshold used to distinguish between the different types of delamination
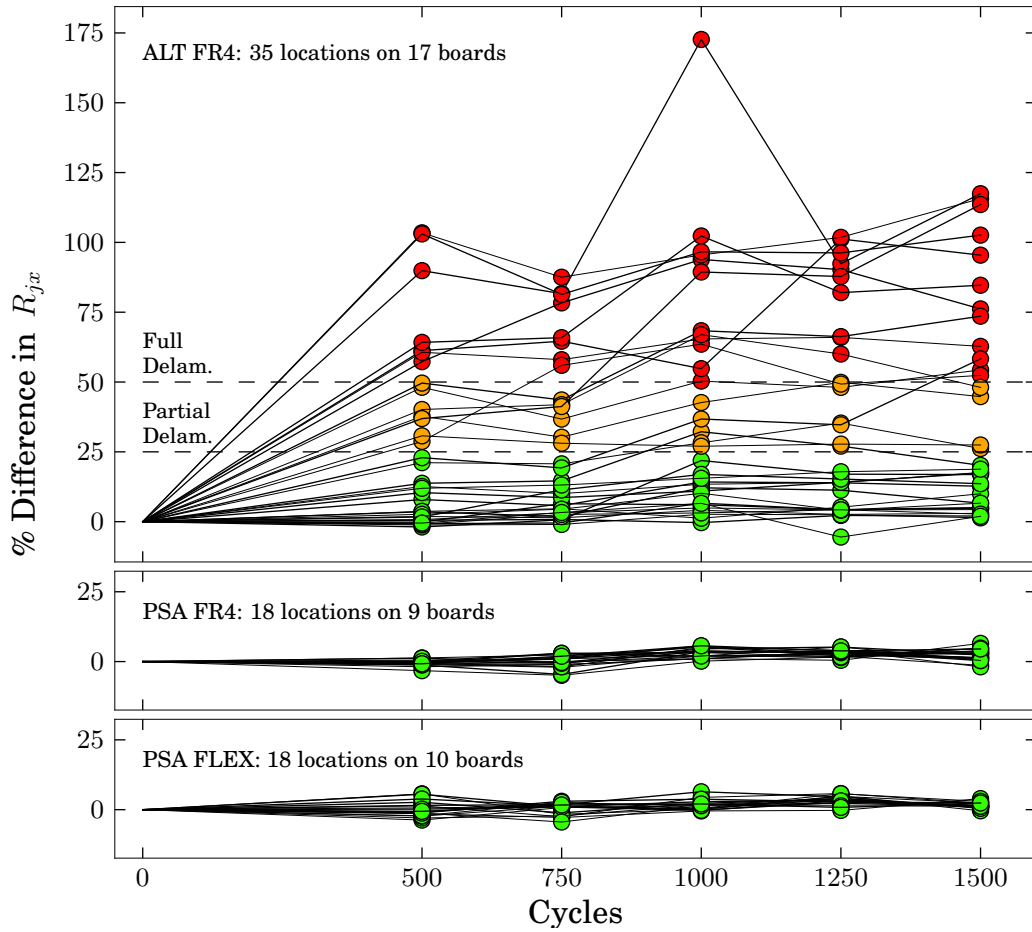
Figure 4.13: Percent change in junction resistance of boards without clamping
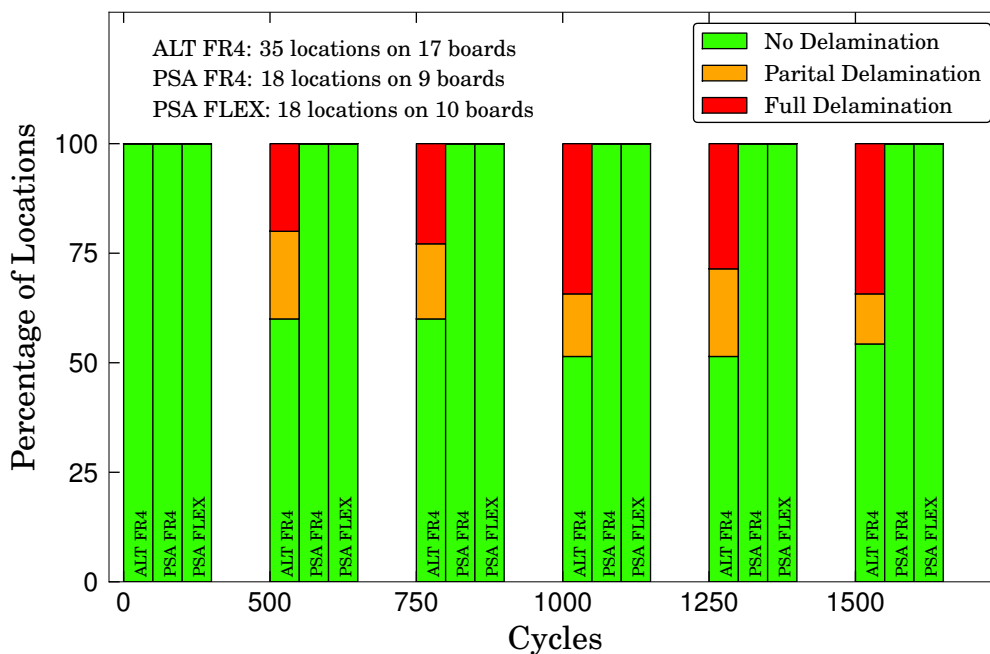
Figure 4.14: Percentage of locations where delamination has occurred.

It is not possible to distinguish between an adhesive failure, separation at the interface between the adhesive and the PCB or substrate, and a cohesive failure, separation within the adhesive layer, by simply measuring the junction resistance. Therefore, it was necessary to perform a destructive analysis to determine the mode of delamination. This was done by pulling a partially delaminated PCB from the substrate to cause the remaining adhesive to separate, an example of which is shown in Figure 4.15.

The region above the black line, in Figure 4.15, delaminated during the course of thermal cycling. The PCB was then peeled/pulled from the substrate which caused the delamination below the black line. The green areas in the left image are the bare PCB, which means there was an adhesive failure at the interface between the epoxy and the PCB; while the grey areas in the left image are the epoxy, which means there was an adhesive failure at the interface between the epoxy and the aluminum substrate. The light-grey areas below the black line are regions where cohesive failure occurred within the epoxy.
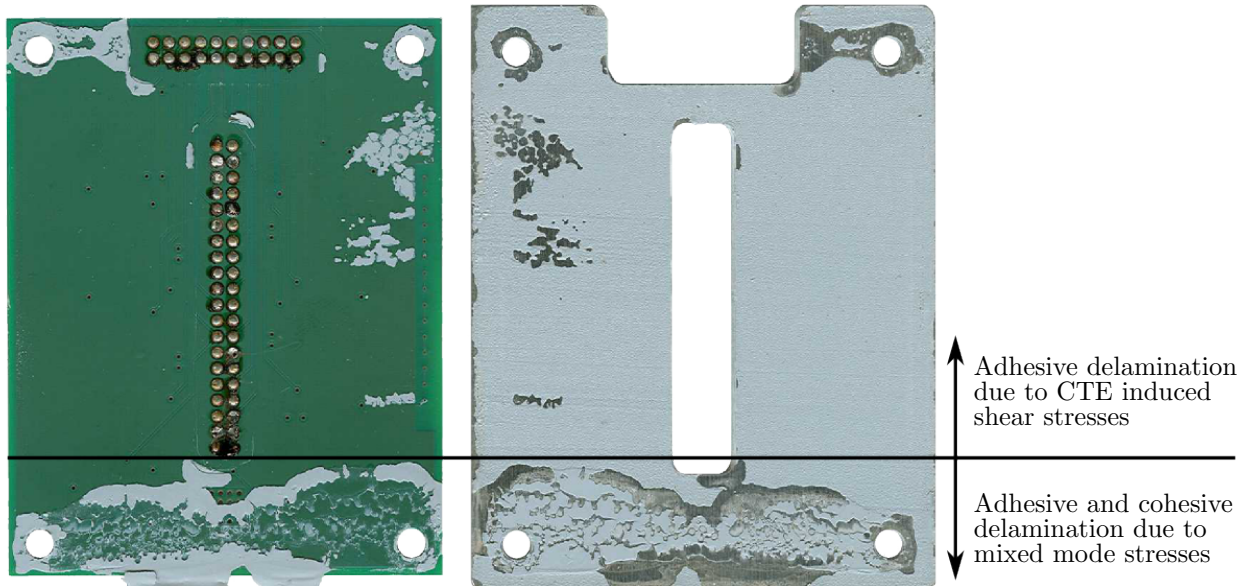
Figure 4.15: The primary mode of delamination caused by CTE stress in the ALT adhesive was adhesive failure at the interface between the epoxy and the PCB, however mixed mode stresses induced by pulling/peeling the PCB from the substrate resulted in adhesive failure at both interfaces and cohesive failure within the epoxy.

The primary stresses exerted on the adhesive bond during thermal cycling will be CTE induced shear stresses. From Figure 4.15 it can be seen that the majority of the delamination due to thermal cycling was adhesive failure at the interface between the epoxy and the PCB. When peeling/pulling the PCB from the substrate, there were mixed mode normal and shear stresses exerted on the adhesive bond. From Figure 4.15 it can be seen that the majority of the delamination due to pulling was still adhesive failure at the interface between the epoxy and the PCB, but a significant portion of the delamination also occurred as cohesive failure within the epoxy and adhesive failure at the interface between the epoxy and the aluminum substrate.

As seen in Figure 4.12, the contact resistance at the PCB adhesive interface contributes a significant portion of the overall junction resistance of the assembled package. In order to improve the reliability of the adhesive, the bond at the interface between the PCB and epoxy needs to be enhanced, since that is where the majority of the failure due to thermal cycling occurred. Two possible methods for achieving this are to either roughen or clean the PCB

surface prior to applying the adhesive. Roughening the PCB surface increases the number of mechanical interlocking sites which leads to a stronger bond. Treating the surface of a PCB with plasma can improve an adhesive bond by removing contaminants and activating the surface.

4.5.3 Overmolding

There was an initial increase in the junction resistance for both types of overmolding, however this increase was within the measured uncertainty. Between 250 cycles and 1000 cycles, the overmolded boards showed an initial improvement in performance, while clamped, similar to the non-overmolded boards. However, between 1000 and 1500 cycles, there was a degradation in thermal performance. This degradation could be caused by a relaxation of the overmolding.

Due to the way the overmolded boards are constructed, it is not possible to hold them in the fixture without applying downward pressure on the circuit board. Because of this, the presence of delamination cannot be conclusively determined using from the measurement of the junction resistance. It was seen that overmolding A exhibited cracks as early as 250 cycles, while overmolding B showed no cracks after 1500 cycles. It should be noted that portions of the overmolding had to be carved away from the backs of the overmolded boards in order to mount them in the fixtures, and that the cracks in overmolding A initially started where the material had been removed and then propagated into the unaltered regions, as shown by Cracks 2, 3, and 5 in Figure 4.16. However, additional cracks appeared at later cycles which were isolated from the damaged regions, as shown by Cracks 1 and 4 in Figure 4.16. Additionally, the overmolding B boards received the same modifications and still did not exhibit any cracking, as shown in Figure 4.17.
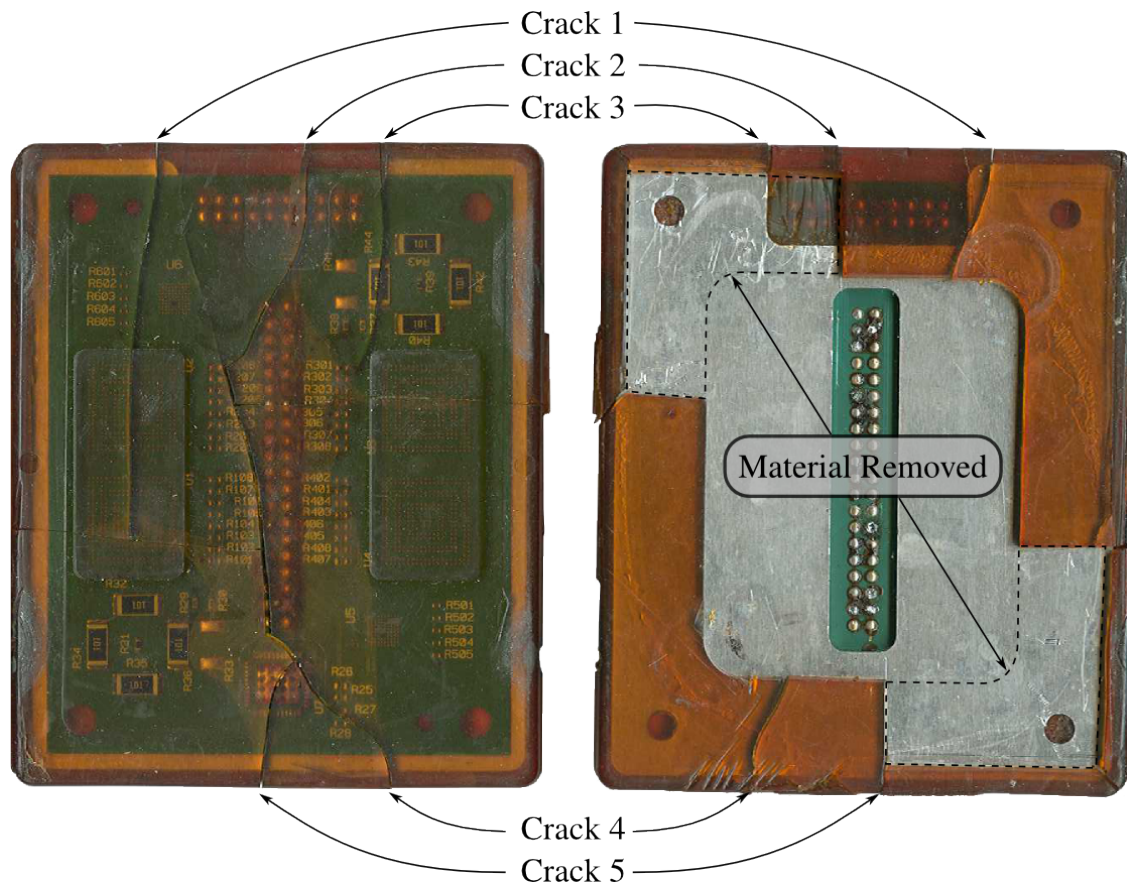
Figure 4.16: Front and back images of overmolding A showing material removed and crack propagation from back to front
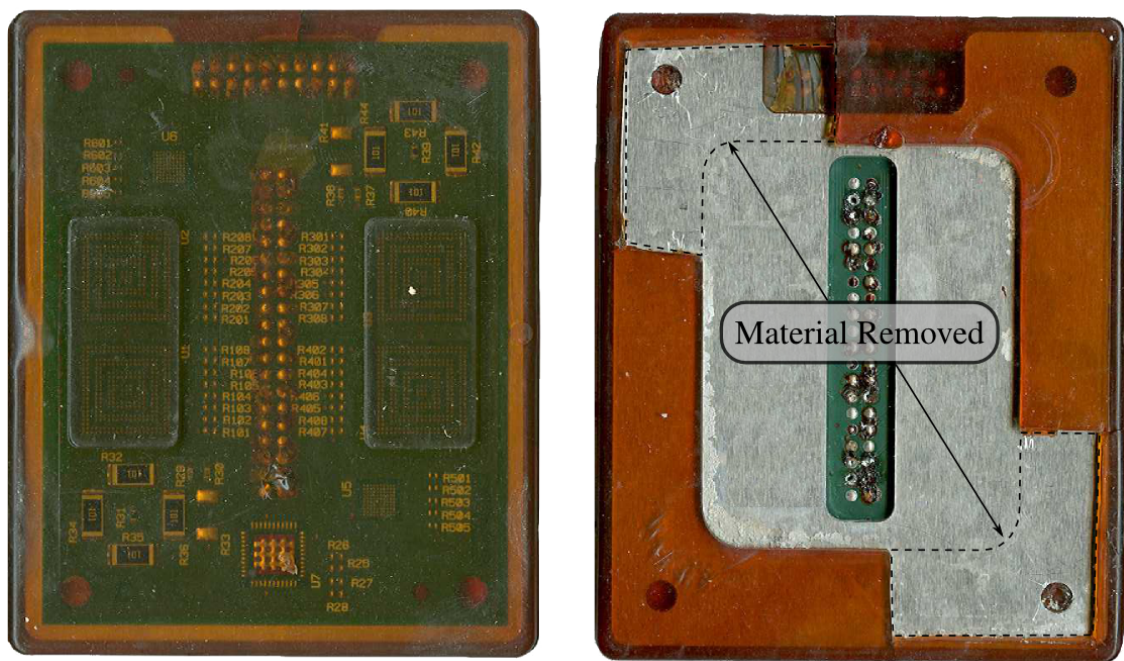
Figure 4.17: Front and back images of overmolding B showing material removed.

Chapter 5

Conclusion

Steady state thermal conductivity measurements were used to characterize and compare three types of electronic packaging materials: an alumina granule/epoxy potting compound, various PCB configurations, and two thermal adhesives.

5.1   Alumina Granule/Epoxy Composite Characterization

The volume fraction, specific heat, and thermal conductivity of an epoxy impregnated with alumina granules used to pot magnetic devices, such as large inductors and power transformers, were measured. The properties were found to be non-uniform both spatially and temporally.

The volume fraction of alumina was measured using optical microscopy and image processing. It was found to vary by location, both axially and radially. However, even the lowest volume fractions measured were still higher than the statistically predicted volume fraction for spherical particles [44]. This is attributed to the process used to combine the epoxy and alumina granules as well as the range of particle shapes and sizes present in the mixture.

The specific heat was measured with a DSC and was found to vary by location, ranging from 0.86–1.14 J/g · K at 25°C and 1.07–1.37 J/g · K at 125°C. The apparent thermal conductivity was measured using a comparative cut bar apparatus based on ASTM D5470 [29] and was found to range from 1.96 W/m · K at 25°C to 3.17 W/m · K at 100°C.

There were changes in thermal properties and coloration with exposure to temperatures above 60°C. This is attributed to the epoxy not being fully cured as delivered by the vendor. Since these temperatures are within the operating range of many electronics, care needs to be taken to ensure that the potting compound is fully cured prior to deployment. Otherwise,

73

the properties of the potting compound could change drastically and non-uniformly over the life of the product, leading to unpredictable behavior.

Epoxy with embedded alumina granules can be used to improve the thermal performance and reliability of electronics in harsh environments. However, users of such compounds should be aware that the thermal properties are not necessarily constant in time or uniform, and assuming that they are could lead to significant errors when modeling their performance.

5.2   PCB Comparison

The apparent thermal conductivity and thermal impedance of three sets of PCBs were measured using a comparative cut bar apparatus based on ASTM D 5470 [29]. In the first comparison, two PCBs were manufactured from the same design by different vendors. The manufacturing decisions made by the vendors resulted in slightly different stack-ups for the two boards. The Q boards had a lower average thermal resistance, $0.0031\,\mathrm{m^2K/W}$ at $25°C$ and $0.0030\,\mathrm{m^2K/W}$ at $100°C$, than did the V boards, $0.0044\,\mathrm{m^2K/W}$ at $25°C$ and $0.0040\,\mathrm{m^2K/W}$ at $100°C$.

The second set of boards was a follow up to the first set where a vendor was asked to manufacture boards with a stack-up identical to the Q boards from the first set. The average thermal resistance of the QB boards was found to be $0.0038\,\mathrm{m^2K/W}$ at $25°C$ and $0.0034\,\mathrm{m^2K/W}$ at $100°C$.

The third set of boards consisted of two groups: one with filled vias and one with unfilled vias. It was found that the average thermal resistance of the boards with the filled vias was $0.0016\,\mathrm{m^2K/W}$ at $25°C$ and $0.0014\,\mathrm{m^2K/W}$ at $100°C$, while the boards with the unfilled vias had a lower average thermal resistance of $0.0013\,\mathrm{m^2K/W}$ at both 25 and $100°C$. Although the apparent thermal conductivity of the boards with the unfilled vias was higher than that of the filled boards, it is unlikely that the filled vias transmitted heat less effectively than the filled vias. Rather, it is more likely that filling the vias either caused a degradation in one of the other thermal paths through the PCB or it caused an increase in the interfacial

resistance between the top of the PCB and the Sil-Pad used as a TIM between the metering block and the sample. In general, the third set of boards performed better than the first two sets on both a thermal resistance and an apparent thermal conductivity basis.

5.3   In Situ Thermal Adhesive Measurement

A non-destructive method was used to monitor the effect of thermal cycling on the thermal conductivity and delamination of two thermal adhesives. By testing on a standardized, application-specific package the data obtained can be used to make design decisions with confidence that the results are indicative of real world performance.

It was found that the clamped PSA, unclamped PSA, and the clamped alternative adhesive showed an increase in thermal performance with cycling, possibly due to curing, which supports earlier findings in the literature. There were no signs of delamination in the PSA after 1000 cycles. However, delamination was detected at 17 out of the 35 locations tested in the boards attached with the alternative adhesive.

While the method used is not capable of detecting the presence of delamination in overmolded boards, it was seen that the thermal conductivity of the PSA adhesive showed similar improvements initially due to curing with the overmolding as it did without the overmolding. It was also found that severe cracking occurred in overmolding A as early as 250 cycles while no cracking occurred in overmolding B after 1500 cycles.

Bibliography

[1] J. P. Gwinn and R. L. Webb, "Performance and testing of thermal interface materials," *Microelectronics Journal*, vol. 34, pp. 215–222, 2003.

[2] W. Nakayama and A. Bergles, "Thermal interfacing techniques for electronic equipment—a perspective," *Journal of Electronic Packaging*, vol. 125, pp. 192–199, June 2003.

[3] C. T. Murray, R. L. Rudman, M. B. Sabade, and A. V. Pocius, "Conductive adhesives for electronic assemblies," *MRS Bulletin*, pp. 449–454, June 2003.

[4] S. Murray, C. Hillman, and M. Pecht, "Environmental aging and deadhesion of siloxane-polyimide-epoxy adhesive," *IEEE Transactions on Components and Packaging Technologies*, vol. 26, pp. 524–531, September 2003.

[5] T. Tuhus and A. Bjorneklett, "Thermal cycling reliability of die bonding adhesives," in *Proceeding of 31st Annual International Reliability Physics Symposium*, pp. 204–208, March 1993.

[6] W.-S. Kwon, M.-J. Yim, K.-W. Paik, S.-J. Ham, and S.-B. Lee, "Thermal cycling reliability and delamination of anisotropic conductive adhesives flip chip on organic substrates with emphasis on the thermal deformation," *Journal of Electronic Packaging*, vol. 127, pp. 86–90, June 2005.

[7] V. Eveloy, P. Rodgers, and M. Pecht, "Reliability of pressure-sensitive adhesive tapes for heat sink attachment in air-cooled electronic assemblies," *IEEE Transactions on Device and Materials Reliability*, vol. 4, pp. 650–657, December 2004.

[8] L. M. Eyman and G. B. Kromann, "Investigation of heat sink attach methodologies and the effects on package structural integrity and interconnect reliability of the 119-lead plastic ball grid array," in *Proceedings of 47th Electronic Components and Technology Conference*, pp. 1068–1075, May 1997.

[9] V. Khuu, M. Osterman, A. Bar-Cohen, and M. Pecht, "Thermal performance measurements of thermal interface materials using the laser flash method," in *Proceedings of IPACK2007*, no. 33554, July 2007.

[10] J. C. Maxwell, *A Treatise on Electricity and Magnetism.* London: Oxford, 1st ed., 1873.

[11] D. A. G. Bruggeman, "Dielectric constant and conductivity of mixtures of isotropic materials," *Annalen der Physik*, vol. 24, pp. 636–679, 1935.

[12] S. C. Cheng and R. I. Vachon, "The prediction of the thermal conductivity of two and three phase solid heterogeneous mixtures," *International Journal of Heat and Mass Transfer*, vol. 12, pp. 249–263, 1969.

[13] G. T.-N. Tsao, "Thermal conductivity of two-phase materials," *Industrial and Engineering Chemistry*, vol. 53, pp. 395–397, May 1961.

[14] L. E. Nielsen, "Thermal conductivity of particulate-filled polymers," *Journal of Applied Polymer Science*, vol. 17, pp. 3819–3820, December 1973.

[15] J. C. Halpin, "Stiffness and expansion estimates for oriented short fiber composites," *Journal of Composite Materials*, vol. 3, no. 4, p. 732, 1969.

[16] A. Einstein, "A new determination of molecular dimensions," *Annalen der Physik*, vol. 19, no. 4, p. 289, 1906.

[17] Y. Agari and T. Uno, "Estimation on thermal conductivities of filled polymers," *Journal of Applied Polymer Science*, vol. 32, pp. 5705–5712, 1986.

[18] P. L. Kapitza, "Heat transer and superfluidity of helium ii," *Physical Review*, vol. 60, pp. 354–355, August 1941.

[19] E. T. Swartz and R. O. Pohl, "Thermal boundary resistance," *Reviews of Modern Physics*, vol. 61, pp. 605–668, July 1989.

[20] D. P. H. Hasselman and L. F. Johnson, "Effective thermal conductivity of composites with interfacial thermal contact resistance," *Ceramic Engineering and Science Proceedings*, vol. 7, pp. 1011–1013, August 1986.

[21] T. Benveniste, "Effective thermal conductivity of composites with a thermal contact resistance between the constituents: Nondilute case," *Journal of Applied Physics*, vol. 61, pp. 2840–2843, April 1987.

[22] T. Mori and K. Tanaka, "Average stress in matrix and average elastic energy of materials with misfitting inclusions," *Acta Metallurgica*, vol. 21, pp. 571–574, May 1973.

[23] K. W. Garrett and H. M. Rosenberg, "The thermal conductivity of epoxy-resin/powder composite materials," *Journal of Physics D: Applied Physics*, vol. 7, no. 9, pp. 1247–1258, 1974.

[24] G. K. Batchelor, "Transport properties of two-phase materials with random structure," *Annual Review of Fluid Mechanics*, vol. 6, pp. 227–255, 1974.

[25] Z. Hashin and S. Shtrikman, "A variational approach to the theory of the effective magnetic permeability of multiphase materials," *Journal of Applied Physics*, vol. 33, pp. 3125–3131, October 1962.

[26] ASTM C 177-04, *Standard Test Method for Steady-State Heat Flux Measurements and Thermal Transmission Properties by Means of the Guarded-Hot-Plate Apparatus*. ASTM International, PA, United States, 2004.

[27] ASTM C 518-04, *Standard Test Method for Steady-State Thermal Transmission Properties by Means of the Heat Flow Meter Apparatus.* ASTM International, PA, United States, 2004.

[28] ASTM C 1045-07, *Standard Practice for Calculating Thermal Transmission Properties Under Steady-State Conditions.* ASTM International, PA, United States, 2007.

[29] ASTM D 5470-06, *Standard Test Method for Thermal Transmission Properties of Thermally Conductive Electrical Insulation Materials.* ASTM International, PA, United States, 2006.

[30] ASTM E 1335-04, *Standard Test Method for Thermal Conductivity of Solids by Means of the Guarded-Comparative-Longitudinal Heat Flow Technique.* ASTM International, PA, United States, 2004.

[31] ASTM E 1530-06, *Standard Test Method for Evaluating the Resistance to Thermal Transmission of Materials by the Guarded Heat Flow Meter Technique.* ASTM International, PA, United States, 2006.

[32] ASTM F 433-02, *Standard Practice for Evaluating Thermal Conductivity of Gasket Materials.* ASTM International, PA, United States, 2002.

[33] R. J. Moffat, "Describint the uncertainties in experimental results," *Experimental Thermal and Fluid Sciences*, vol. 1, pp. 3–17, 1998.

[34] W. J. Parker, R. J. Jenkins, C. P. Butler, and G. L. Abbott, "Flash method of determining thermal diffusivity, heat capacity, and thermal conductivity," *Journal of Applied Physics*, vol. 32, pp. 1679–1684, September 1961.

[35] R. D. Cowan, "Pulse method of measuring thermal diffusivity at high temperatures," *Journal of Applied Physics*, vol. 34, pp. 926–927, April 1963.

[36] L. M. Clark III and R. E. Taylor, "Radiation loss in the flash method for thermal diffusivity," *Journal of Applied Physics*, vol. 46, pp. 714–719, February 1975.

[37] ASTM C 714-05, *Standard Test Method for Thermal Diffusivity of Carbon and Graphite by Thermal Pulse Method.* ASTM International, PA, United States, 2005.

[38] ASTM E 1461-07, *Standard Test Method for Thermal Diffusivity by the Flash Method.* ASTM International, PA, United States, 2007.

[39] C. J. M. Lasance, "The urgent need for widely-accepted test methods for thermal interface materials," *19th IEEE SEMI-THERM Symposium*, pp. 123–128, 2003.

[40] L. M. McGrath, R. S. Parnas, S. H. King, J. L. Schroeder, D. A. Fischer, and J. L. Lenhart, "Investigation of the thermal, mechanical, and fracture properties of alumina-epoxy composites," *Polymer*, vol. 49, no. 4, pp. 999–1014, 2008.

[41] C. P. Wong and R. S. Bollamplaly, "Thermal conductivity, elastic modulus, and co-efficient of thermal expansion of polymer composites filled with ceramic particles for electronic packaging," *Journal of Applied Polymer Science*, vol. 74, no. 14, pp. 3396–3403, 1999.

[42] Y. P. Mamunya, V. V. Davydenko, P. Pissis, and E. V. Lebdev, "Electrical and thermal conductivity of polymers filled with metal powders," *European Polymer Journal*, vol. 38, no. 9, pp. 1887–1897, 2002.

[43] V. Singh, A. R. Kulkarni, and T. R. R. Mohan, "Dielectric properties of aluminum-epoxy composites," *Journal of Applied Polymer Science*, vol. 90, pp. 3602–3608, 2003 2003.

[44] R. K. McGeary, "Mechanical pacing of spherical particles," *Journal of the American Ceramic Society*, vol. 44, no. 10, pp. 513–522, 1961.

[45] C. Creton, "Pressure-sensitive adhesives: An introductory course," *MRS Bulletin*, pp. 434–439, June 2003.

[46] R. Conner and J. Peterson, "Electrical grade pressure sensitive adhesive tapes," *Electrical Electronics Insulation Conference*, pp. 697–700, September 1995.

[47] D. Klosterman, L. Li, and J. E. Morris, "Materials characterization, conduction development, and curing effects on reliability of isotropically conductive adhesives," *IEEE Transactions on Components, Packaging, and Manufacturing Technology–Part A*, vol. 21, pp. 23–31, March 1998.

[48] Q. Yao and J. Qu, "Interfacial versus cohesive failure on polymer-metal interfaces in electronic packaging – effects of interface roughness," *Journal of Electronic Packaging*, vol. 124, pp. 127–134, June 2002.

[49] R. W. Knight, Y. Elkady, J. C. Suhling, and P. Lall, "Causes of degradation of thermal performance of ball grid arrays after thermal cycling," in *Proceedings of IPACK2007*, no. 33626, 2007.

[50] P. Lall, M. Islam, J. Evans, J. Suhling, and T. Shete, "Damage mechanics of electronics on metal-backed substrates in harsh environments," *IEEE Transactions on Components and Packaging Technologies*, vol. 29, pp. 204–212, March 2006.

[51] J. L. Evans, P. Lall, R. Knight, E. Crain, T. Shete, and J. R. Thompson, "System design issues for harsh environment electronics employing metal-backed laminate substrates," *IEEE Transactions on Components and Packaging Technologies*, vol. 31, pp. 74–85, March 2008.

[52] Y. A. Elkady, *Thermal Performance of Ball Grid Arrays and Thin Interface Materials*. Ph.D. dissertation, Auburn University, Auburn, AL, United States, 2005.

[53] JESD22-A104C, *Temperature Cycling*. JEDEC Solid State Technology Association, Arlington, VA, May 2005.

[54] T. G. Beckwith, R. D. Marangoni, and J. H. Lienhard V, *Mechnical Measurements*. Prentice Hall, sixth ed., 2007.

Appendices

Appendix A

Junction Resistance Measurements

Table A.1: Thermal resistance values for clamped PSA FLEX boards.

		R_{jx} (°C/W)						
Board		0 Cycles	250 Cycles	500 Cycles	750 Cycles	1000 Cycles	1250 Cycles	1500 Cycles
PSA-1 FLEX	R_{jx_1}	3.55	3.36	3.27	3.18	3.00	3.14	2.89
	R_{jx_2}	3.66	3.55	3.50	3.47	3.18	3.33	3.27
PSA-2 FLEX	R_{jx_1}	3.47	3.30	3.23	3.13	3.03	3.08	3.12
	R_{jx_2}	3.67						
PSA-3 FLEX	R_{jx_1}	3.84	3.43	3.29	3.36	3.21	3.18	3.11
	R_{jx_2}	3.98	3.49	3.45	3.47	3.28	3.37	3.28
PSA-4 FLEX	R_{jx_1}	3.42	3.24	3.19	3.17	2.99	3.05	3.05
	R_{jx_2}	3.84	3.64	3.54	3.50	3.12	3.30	3.32
PSA-5 FLEX	R_{jx_1}	3.68	3.42	3.32				
	R_{jx_2}	3.65	3.53	3.55	3.38	3.08	3.15	
PSA-6 FLEX	R_{jx_1}	3.69	3.48	3.45	3.47	3.04	3.15	3.13
	R_{jx_2}	3.76	3.51	3.45	3.46	3.04	3.22	3.26
PSA-7 FLEX	R_{jx_1}	3.51	3.43	3.39	3.30	3.15	3.17	3.21
	R_{jx_2}	3.74	3.57	3.57	3.49	3.36	3.44	3.41
PSA-8 FLEX	R_{jx_1}	3.48	3.37	3.28	3.23	2.92	3.02	3.01
	R_{jx_2}	3.67	3.64	3.50	3.35	2.97	3.14	3.16
PSA-9 FLEX	R_{jx_1}	3.60	3.48	3.45	3.31	3.19	3.29	3.07
	R_{jx_2}	3.73	3.71	3.55	3.47	3.41	3.61	3.27
PSA-10 FLEX	R_{jx_1}	3.65	3.55	3.23	3.19	2.97	3.03	2.96
	R_{jx_2}	3.76	3.59	3.41	3.39	3.21	3.22	3.11
Average		3.67	3.49	3.40	3.35	3.12	3.22	3.15
σ		0.15	0.12	0.12	0.13	0.14	0.15	0.13

Table A.2: Thermal resistance values for unclamped PSA FLEX boards.

Board		500 Cycles	750 Cycles	1000 Cycles	1250 Cycles	1500 Cycles
		R_{jx} (°C/W)				
PSA-1 FLEX	R_{jx_1}	3.22	3.10	2.99	3.13	3.01
	R_{jx_2}	3.47	3.55	3.24	3.41	3.32
PSA-2 FLEX	R_{jx_1}	3.11	3.16	3.07	3.18	3.16
	R_{jx_2}					
PSA-3 FLEX	R_{jx_1}	3.34	3.28	3.36	3.36	3.18
	R_{jx_2}	3.54	3.43	3.35	3.51	3.31
PSA-4 FLEX	R_{jx_1}	3.37	3.12	2.99	3.20	3.03
	R_{jx_2}	3.73	3.54	3.21	3.41	3.36
PSA-5 FLEX	R_{jx_1}	3.24	3.26			
	R_{jx_2}	3.46	3.39	3.04	3.25	
PSA-6 FLEX	R_{jx_1}	3.34	3.40	3.09	3.28	3.15
	R_{jx_2}	3.51	3.53	3.23	3.37	3.27
PSA-7 FLEX	R_{jx_1}	3.41	3.34	3.16	3.32	3.28
	R_{jx_2}	3.71	3.53	3.36	3.53	3.49
PSA-8 FLEX	R_{jx_1}	3.21	3.27	2.93	3.13	3.05
	R_{jx_2}	3.46	3.45	3.09	3.23	3.20
PSA-9 FLEX	R_{jx_1}	3.37	3.40	3.20	3.48	3.16
	R_{jx_2}	3.56	3.51	3.40	3.73	3.32
PSA-10 FLEX	R_{jx_1}	3.19	3.05	3.01	3.08	3.00
	R_{jx_2}	3.39	3.45	3.28	3.24	3.18
Average		3.41	3.36	3.17	3.33	3.20
σ		0.17	0.16	0.14	0.17	0.13

Table A.3: Thermal resistance values for clamped PSA FR4 boards.

Board		R_{jx} (°C/W)						
		0 Cycles	250 Cycles	500 Cycles	750 Cycles	1000 Cycles	1250 Cycles	1500 Cycles
PSA-1 FR4	R_{jx_1}	5.23	5.14	5.03	5.00	4.70	4.87	4.77
	R_{jx_2}	5.60	5.30	5.26	5.16	4.95	4.95	5.00
PSA-2 FR4	R_{jx_1}	5.59	5.36	5.34	5.27	5.10	5.11	4.96
	R_{jx_2}	6.35	5.84	5.66	5.63	5.26	5.28	5.21
PSA-3 FR4	R_{jx_1}	5.58	5.33	5.43	5.38	5.15	5.11	5.12
	R_{jx_2}	5.64	5.46	5.41	5.33	4.99	5.24	5.12
PSA-4 FR4	R_{jx_1}	5.53	5.39	5.33	5.32	5.10	5.20	4.96
	R_{jx_2}	5.73	5.56	5.52	5.45	5.12	5.32	5.25
PSA-5 FR4	R_{jx_1}	5.55	5.44	5.37	5.30	4.98	5.09	5.02
	R_{jx_2}	5.61	5.38	5.29	5.22	4.83	5.14	5.09
PSA-6 FR4	R_{jx_1}	5.74	5.58	5.46	5.45	5.17	5.22	5.03
	R_{jx_2}	5.77	5.58	5.56	5.47	5.21	5.32	5.30
PSA-7 FR4	R_{jx_1}	5.81	5.69	5.62	5.64	5.29	5.34	5.30
	R_{jx_2}	6.30	5.90	5.77	5.85	5.30	5.40	5.26
PSA-8 FR4	R_{jx_1}	5.64	5.53	5.44	5.42	5.07	5.16	5.36
	R_{jx_2}	5.87	5.72	5.65	5.63	5.33	5.44	5.44
PSA-9 FR4	R_{jx_1}	5.57	5.62	5.50	5.39	5.22	5.23	5.31
	R_{jx_2}	5.69	5.67	5.62	5.46	5.15	5.38	5.23
Average		5.71	5.53	5.46	5.41	5.11	5.21	5.15
σ		0.26	0.19	0.17	0.19	0.16	0.15	0.17

Table A.4: Thermal resistance values for unclamped PSA FR4 boards.

Board		R_{jx} (°C/W)				
		500 Cycles	750 Cycles	1000 Cycles	1250 Cycles	1500 Cycles
PSA-1 FR4	R_{jx_1}	5.10	5.11	4.85	4.96	4.96
	R_{jx_2}	5.27	5.32	5.04	5.09	5.07
PSA-2 FR4	R_{jx_1}	5.36	5.27	5.15	5.30	5.03
	R_{jx_2}	5.73	5.61	5.50	5.56	5.35
PSA-3 FR4	R_{jx_1}	5.33	5.33	5.20	5.27	5.19
	R_{jx_2}	5.40	5.41	5.25	5.35	5.36
PSA-4 FR4	R_{jx_1}	5.27	5.26	5.16	5.23	5.28
	R_{jx_2}	5.51	5.51	5.31	5.48	5.41
PSA-5 FR4	R_{jx_1}	5.31	5.19	5.08	5.19	4.95
	R_{jx_2}	5.26	5.28	5.10	5.26	5.14
PSA-6 FR4	R_{jx_1}	5.44	5.50	5.29	5.29	5.27
	R_{jx_2}	5.53	5.64	5.39	5.53	5.43
PSA-7 FR4	R_{jx_1}	5.44	5.36	5.30	5.42	5.47
	R_{jx_2}	5.70	5.58	5.49	5.57	5.45
PSA-8 FR4	R_{jx_1}	5.41	5.32	5.32	5.36	5.26
	R_{jx_2}	5.65	5.60	5.52	5.63	5.45
PSA-9 FR4	R_{jx_1}	5.45	5.37	5.32	5.51	5.33
	R_{jx_2}	5.58	5.56	5.44	5.58	5.47
Average		5.43	5.40	5.26	5.36	5.27
σ		0.16	0.15	0.17	0.18	0.17

Table A.5: Thermal resistance values for clamped ALT FR4 boards.

Board		R_{jx} (°C/W)						
		0 Cycles	250 Cycles	500 Cycles	750 Cycles	1000 Cycles	1250 Cycles	1500 Cycles
ALT-2	R_{jx_1}	6.83	7.08	6.98	7.17	6.24	6.19	6.19
	R_{jx_2}	8.33	7.72	8.16	7.96	6.67	6.34	6.61
ALT-3	R_{jx_1}	5.37	5.25	5.19	5.13	4.94	4.99	5.02
	R_{jx_2}	5.60	5.48	5.58	5.42	5.05	5.15	5.02
ALT-4	R_{jx_1}	6.78	6.81	6.57	6.66	6.19	6.03	6.17
	R_{jx_2}	7.77	7.14	7.28	7.30	6.16	6.37	6.36
ALT-5	R_{jx_1}	6.86	6.53	6.60	6.90	6.65	6.44	6.35
	R_{jx_2}	6.20	6.31	6.26	6.00	5.26	5.37	5.23
ALT-6	R_{jx_1}	6.57	6.46	6.45	6.50	6.28	6.18	5.87
	R_{jx_2}	6.76	6.67	6.71	6.67	6.15	6.09	6.08
ALT-7	R_{jx_1}	7.16	6.86	6.59	6.91	7.08	6.41	6.14
	R_{jx_2}	7.50	6.92	7.32	7.01	5.97	6.07	6.17
ALT-8	R_{jx_1}	6.26	6.29	6.20	6.31	5.67	5.72	5.85
	R_{jx_2}	4.65	4.45	4.41	4.36	4.20	4.12	4.13
ALT-9	R_{jx_1}	6.67	6.71	6.59	6.75	6.41	6.39	6.16
	R_{jx_2}	5.29	5.17	5.05	4.99	4.82	4.86	4.77
ALT-10	R_{jx_1}	4.68	4.76	4.72	4.59	4.45	4.42	4.33
	R_{jx_2}	6.26	6.16	6.00	6.02	5.40	5.39	5.59
ALT-11	R_{jx_1}	5.31	5.15	5.08	4.97	4.91	4.82	4.76
	R_{jx_2}	7.55	6.99	6.94	6.83	5.06	6.28	6.38
ALT-12	R_{jx_1}	6.73	6.79	6.64	6.71	6.82	6.33	6.59
	R_{jx_2}	7.57	7.18	7.11	7.20	6.29	6.67	6.64
ALT-13	R_{jx_1}	6.81	6.81	6.67	6.75	6.32	6.26	6.15
	R_{jx_2}	6.40	6.30	6.28	6.20	5.83	5.76	5.59
ALT-14	R_{jx_1}	4.67	4.38	4.39	4.28	4.18	4.15	4.25
	R_{jx_2}	7.08	6.67	6.63	6.96	5.92	5.87	6.01
ALT-15	R_{jx_1}	5.92	5.66	5.54	5.34	5.04	5.15	5.17
	R_{jx_2}	7.34	7.07	6.97	7.20	6.07	6.29	6.11
ALT-16	R_{jx_1}	5.36	5.34	5.33	5.19	5.02	4.86	4.90
	R_{jx_2}	6.26	6.29	6.22	6.50	6.04	6.13	6.16
ALT-17	R_{jx_1}	5.85	5.63	5.74	5.47	5.22	5.79	5.75
	R_{jx_2}	7.67	7.28	7.05	7.56	6.62	6.30	6.60
ALT-18	R_{jx_1}	5.95	5.93	5.83	5.77	5.61	5.45	5.26
	R_{jx_2}	7.15	6.77	6.75	6.94	6.11	6.04	5.04
ALT-19	R_{jx_1}		4.81	4.73	4.75	4.60	4.48	4.23
Average		6.45	6.26	6.23	6.25	5.72	5.73	5.69
	σ	0.93	0.84	0.87	0.95	0.75	0.69	0.72

Table A.6: Thermal resistance values for unclamped ALT FR4 boards.

Board		R_{jx} (°C/W) 500 Cycles	750 Cycles	1000 Cycles	1250 Cycles	1500 Cycles
ALT-2	R_{jx_1}	10.34	9.80	9.38	9.16	9.56
	R_{jx_2}	13.15	13.10	10.32	12.75	12.91
ALT-3	R_{jx_1}	5.28	5.20	5.14	5.12	5.17
	R_{jx_2}	5.54	5.40	5.38	5.37	5.26
ALT-4	R_{jx_1}	9.06	8.68	8.84	9.04	8.93
	R_{jx_2}	11.45	13.02	11.95	12.11	11.21
ALT-5	R_{jx_1}	10.61	10.91	11.00	10.69	10.33
	R_{jx_2}	7.13	6.88	6.96	6.83	6.29
ALT-6	R_{jx_1}	7.26	7.15	7.12	7.05	6.90
	R_{jx_2}	7.24	7.05	7.02	6.94	6.85
ALT-7	R_{jx_1}	13.41	12.95	13.84	12.94	13.23
	R_{jx_2}	7.18	7.05	7.28	7.10	7.21
ALT-8	R_{jx_1}	7.51	7.62	7.27	7.74	7.38
	R_{jx_2}	4.43	4.39	4.19	4.21	4.21
ALT-9	R_{jx_1}	8.49	10.52	10.49	9.54	9.39
	R_{jx_2}	5.05	5.31	5.11	5.07	5.01
ALT-10	R_{jx_1}	4.66	4.54	4.57	4.53	4.39
	R_{jx_2}	6.21	6.13	6.06	6.00	5.96
ALT-11	R_{jx_1}	5.27	5.20	4.97	5.07	5.23
	R_{jx_2}	13.17	12.40	13.80	12.08	13.87
ALT-12	R_{jx_1}	8.68	8.59	8.66	8.08	8.40
	R_{jx_2}	10.63	10.34	10.59	11.10	11.52
ALT-13	R_{jx_1}	9.35	9.58	10.55	10.02	9.10
	R_{jx_2}	6.93	6.74	6.46	6.58	6.56
ALT-14	R_{jx_1}	4.42	4.41	4.38	4.32	4.43
	R_{jx_2}	10.89	11.54	11.97	10.69	11.10
ALT-15	R_{jx_1}	5.69	5.57	5.55	5.36	5.51
	R_{jx_2}	9.54	10.18	11.50	11.82	13.05
ALT-16	R_{jx_1}	5.28	5.32	5.18	5.06	5.03
	R_{jx_2}	6.33	7.24	7.06	7.07	7.00
ALT-17	R_{jx_1}	5.71	5.65	5.56	5.47	5.86
	R_{jx_2}	14.31	13.72	13.01	12.37	13.38
ALT-18	R_{jx_1}	6.52	6.52	6.48	6.42	6.25
	R_{jx_2}	8.29	8.27	8.36	8.13	7.98
ALT-19	R_{jx_1}	4.65	4.67	4.65	4.49	4.40
Average		7.99	8.05	8.02	7.90	7.97
σ		2.81	2.83	2.88	2.76	2.96

Table A.7: Thermal resistance values for PSA OM-A boards.

Board		R_{jx} (°C/W)						
		0 Cycles	250 Cycles	500 Cycles	750 Cycles	1000 Cycles	1250 Cycles	1500 Cycles
OM-A-1	R_{jx_1}	5.81	5.74	5.77	5.62	5.33	5.58	6.06
	R_{jx_2}	5.81	6.02	5.63	5.68	5.41	5.94	6.24
OM-A-2	R_{jx_1}	5.93	5.76	6.04	5.81	5.47	5.70	6.04
	R_{jx_2}	6.39	6.48	5.81	5.80	5.44	5.96	
OM-A-3	R_{jx_1}	6.00	5.94	6.12	5.80	5.46	5.68	5.80
	R_{jx_2}	6.15	6.33	6.12	6.02			
OM-A-5	R_{jx_1}	5.86	5.95	5.89	5.80	5.51	5.95	5.78
	R_{jx_2}	6.12	6.04	5.73	6.19	5.40	5.87	
Average		5.88	5.88	5.89	5.74	5.44	5.77	5.98
σ		0.07	0.11	0.18	0.08	0.06	0.15	0.17

Table A.8: Thermal resistance values for PSA OM-B boards.

Board		R_{jx} (°C/W)						
		0 Cycles	250 Cycles	500 Cycles	750 Cycles	1000 Cycles	1250 Cycles	1500 Cycles
OM-B-1	R_{jx_1}	5.71	6.14	5.99	6.12	5.48	6.13	6.28
	R_{jx_2}	6.48	6.80	6.50	6.69	5.76	6.05	6.24
OM-B-2	R_{jx_1}	6.17	6.10	5.89	5.98	5.47	5.88	6.03
	R_{jx_2}	6.37	6.89	6.42	6.77	5.84	6.31	6.25
OM-B-3	R_{jx_1}	6.19	6.14	5.96	5.91	5.68	6.24	6.11
	R_{jx_2}	6.77	6.28	6.44	6.17	5.79	6.14	6.10
OM-B-4	R_{jx_1}	5.91	5.99	5.93	5.75	5.42	5.83	5.95
	R_{jx_2}	6.28	6.24	5.92	5.95	5.85	6.43	6.36
OM-B-5	R_{jx_1}	6.38	5.89	5.83	5.71	5.42	5.82	5.93
	R_{jx_2}	6.37	6.98	6.00	5.90	5.69	6.17	6.20
Average		6.26	6.34	6.09	6.09	5.64	6.10	6.14
σ		0.28	0.38	0.24	0.35	0.17	0.19	0.14

Appendix B

Thermocouple Calibration

Prior to their use in the experiments, the thermocouples were calibrated against a thermistor with an uncertainty of 0.01°C. This was done by submerging the thermocouples and the thermistor into a temperature controlled bath. Measurements were taken over the range of interest and a linear fit was applied to calibrate the thermocouple readings to the thermistor readings. The uncertainty of the resulting calibration curve was calculated using the procedure presented in Beckwith, et. al. [54]. The calibration curves were of the form

$$y_{cal} = a + bx \tag{B.1}$$

with an offset uncertainty of

$$\delta_a = \pm t_{\alpha,\nu} S_{y/x} \sqrt{\frac{1}{n} + \frac{\overline{x}^2}{S_{xx}^2}} \tag{B.2}$$

and a scale uncertainty of

$$\delta_b = \pm \frac{t_{\alpha,\nu} S_{y/x}}{S_{xx}} \tag{B.3}$$

where n is the number of measurements, $t_{\alpha,\nu}$ is calculated from the Student's t probability density function (PDF), $\overline{x}$ is the mean of the measured values,

$$S_{xx}^2 = \sum (x_i - \overline{x})^2, \tag{B.4}$$

and

$$S_{y/x} = \sqrt{\frac{\sum (y_i - y_{cal}(x_i))^2}{n - 2}} \tag{B.5}$$

where $y_{cal}(x_i)$ is the calibrated measured value. A 95% confidence interval was used when calculating $t_{\alpha,\nu}$.

The resulting calibration curves with their uncertainties for the thermocouples used in the comparative cut bar apparatus are:

$$T_{cal,1} = 0.993198\,x + 0.491284\,\text{K} \pm (0.001057\,x + 0.029911\,\text{K}) \tag{B.6}$$

$$T_{cal,2} = 0.993409\,x + 0.460432\,\text{K} \pm (0.001040\,x + 0.029476\,\text{K}) \tag{B.7}$$

$$T_{cal,3} = 0.994218\,x + 0.519466\,\text{K} \pm (0.001012\,x + 0.028594\,\text{K}) \tag{B.8}$$

$$T_{cal,4} = 0.995766\,x + 0.517962\,\text{K} \pm (0.001062\,x + 0.029956\,\text{K}) \tag{B.9}$$

$$T_{cal,5} = 0.995253\,x + 0.592676\,\text{K} \pm (0.001070\,x + 0.030109\,\text{K}) \tag{B.10}$$

$$T_{cal,6} = 0.994244\,x + 0.653899\,\text{K} \pm (0.001138\,x + 0.031983\,\text{K}) \tag{B.11}$$

$$T_{cal,7} = 0.992889\,x + 0.670189\,\text{K} \pm (0.001263\,x + 0.035534\,\text{K}) \tag{B.12}$$

$$T_{cal,8} = 0.992723\,x + 0.467853\,\text{K} \pm (0.001131\,x + 0.032059\,\text{K}) \tag{B.13}$$

$$T_{cal,9} = 0.993347\,x + 0.481838\,\text{K} \pm (0.001002\,x + 0.028370\,\text{K}) \tag{B.14}$$

$$T_{cal,10} = 0.993602\,x + 0.532932\,\text{K} \pm (0.001082\,x + 0.030558\,\text{K}) \tag{B.15}$$

Appendix C

Uncertainty Analysis

C.1 Volume Fraction Measurement through Image Processing

The volume fraction of the alumina granules in the epoxy was determined through the use of image processing. Micrographs were taken from various location throughout the sample. A threshold tool was used to convert the pixels in the epoxy regions to black and the pixels in the alumina regions to white. The number of white and black pixels were counted to determine the percentage of the image occupied by each material,

$$\Phi = \frac{\text{Pixels}_{\text{alumina}}}{\text{Pixel}_{\text{total}}} \tag{C.1}$$

There are three main contributions to the uncertainty in the final reading: the assumptions that the material is nominally isotropic and that the two-dimensional representation is not dependent on orientation, the resolution of the image used, and the accuracy of the value chosen for the threshold parameter.

The uncertainty contributed by the isotropic assumption was minimized by using images from 20 different locations. The images were also taken from different orientations, i.e. some were perpendicular to the axial direction and some were parallel to the axial direction. Since, there was significant variation between locations, the final value should be interpreted as a bulk property with the knowledge that the local properties will vary.

The resolution of the image introduces an uncertainty through pixelation at the boundaries between the materials. This was minimized by using a resolution where the pixels were many order of magnitude smaller than the smallest feature size of interest. Therefore, the

uncertainty introduced through pixelation will be negligible in comparison to the uncertainty introduced by the threshold parameter.

The largest source of uncertainty in the process comes from the selection of the threshold criterion. The selection of the epoxy region was done on a color basis. However, the epoxy is translucent which makes it difficult to accurately determine the grain boundary of the alumina granules. The uncertainty introduced by the selection of the threshold criterion was determined by using the best values for the parameters along with values which intentionally over- and under-estimated the location of the grain boundary. This was repeated for each image and the Student's t probability density function for small sample sizes was used to determine the 95% confidence interval to be approximately

$$\delta_\Phi = \pm 10\%. \tag{C.2}$$

C.2   Specific Heat Measurement with a Differential Scanning Calorimeter

The specific heat of the alumina granule/epoxy composite was measured with a TA Q2000 DSC. There are three sources of uncertainty which propagate into the final measurement: uncertainty in the system calibration due to uncertainties in the properties of the reference material, uncertainty in the baseline calibration for the test, and uncertainty in the measurements during the test. The resulting combination of the uncertainties is estimated to be

$$\delta_{C_p} = \pm 5\% \text{ of the measured value.} \tag{C.3}$$

C.3   Thermal Conductivity Measurement with a Comparative Cut Bar Apparatus

The thermal impedance of the sample being measured in the comparative cut bar apparatus was calculated from the heat flowing through the sample and the temperature drop across the sample. The heat flowing through the sample was calculated from the thermal

conductivity of the metering bars and the temperature gradient in the metering bars, which was calculated from the thermocouple measurements and the locations of the thermocouples. Since it is perhaps more illustrative to view the thermal impedance on a flux basis when comparing samples, the thermal impedance values were presented in Chapter 4 as the area of the sample times the measured thermal impedance, $A_s \cdot R$, Therefore, propagation of error causes the uncertainty of the calculated value of the thermal impedance on a flux basis to depend on the uncertainties of:

- the thermocouple temperature measurements, given by Eqs. (B.6)-(B.15),

- the locations of the thermocouples, $\delta_x = \pm 10^{-7}$ m,

- the thermal conductivity of the metering bar, $\delta_{k_{mb}} = \pm 1$ W/m $\cdot$ K,

- the cross-sectional area of the metering bar, $\delta_{A_{mb}} = \pm 3.6 \times 10^{-7}$ m^2, and

- the cross-sectional area of the sample[1], $\delta_{A_s} \approx \pm 3.6 \times^{-7}$ m^2.

The effect of the uncertainties listed above on the final value was found by propagating them into the thermal impedance calculations through the method of sequential perturbations as presented by Moffat [33]. In this approach the best guess values for each of the measurements are used to calculate the parameter of interest which is stored. Each of the constituent measurements are then individually perturbed by their uncertainty and the difference between the new value and the original value is stored. Once all the variables have been perturbed, the differences are added in quadrature. The resulting uncertainty can be expressed as

$$\delta_{AR} = \pm \sqrt{\sum_i (AR_o - AR_{i+\delta_i})^2} \tag{C.4}$$

$$= \pm \sqrt{\left(AR_o - AR_{T_1+\delta_{T_1}}\right)^2 + \left(AR_o - AR_{T_2+\delta_{T_2}}\right)^2 + \ldots} \tag{C.5}$$

[1]this assumes the sample being measured has approximately the same area as the metering bar

where AR_o is the original value that would have been calculated if the uncertainties were ignored and $AR_{i+\delta_i}$ is the value that would have been calculated if the ith measurement had been perturbed by its uncertainty. The final value for the uncertainty of $A \cdot R$ using this method was

$$\delta_{AR} = \pm 10^{-4} \text{m}^2 \cdot \text{K/W} \tag{C.6}$$

The apparent thermal conductivity was calculated with Eq. (3.5), which has the same uncertainty propagation as the thermal impedance plus an additional uncertainty introduced by the sample thickness, $\delta_L = \pm 10^{-7}$ m. Applying the sequential perturbations method yielded an uncertainty of

$$\delta_\lambda = \pm 0.1 \, \text{W/m} \cdot \text{K} \tag{C.7}$$

C.4 In Situ Thermal Resistance Measurement of a PCB Attached to an Aluminum Substrate

The junction resistance, R_{jx}, was found by extracting the slope from a linear least squares fit to the measurement of power, P, and the temperature drop across the package, ΔT_{jx}, such that

$$R_{jx} = \frac{\Delta T_{jx}}{P} = \frac{T_j - T_x}{P} \tag{C.8}$$

where the junction temperature, T_j, was measured by a thermistor mounted to the PCB, the reference temperature, T_x, was measured by a type k thermocouple below the aluminum substrate, and the power, P, was generated by four resistance heaters mounted to the PCB. In order to determine the uncertainty in the junction resistance measurement it is necessary to first determine the uncertainty in the constituent measurements.

The reference temperature was measured with an AMETHERM SM06 502350 negative thermal coefficient (NTC) thermistor. The resistance of the thermistor, R_T, was measured by an HP 34401A multimeter, which has an uncertainty of $\delta_{R_T} = \pm 0.001 \, \text{k}\Omega$. The measured resistance was used to interpolate the temperature from a calibration curve supplied by the

vendor. The resulting uncertainty for the junction temperature measurement is

$$\delta_{T_j} = \pm 0.01°\text{C}. \tag{C.9}$$

The reference temperature was measured with a type k thermocouple. The thermocouple voltage was measured with a National Instruments TBX-68T breakout box with built-in cold junction compensation. The resulting uncertainty of the reference temperature measurement is

$$\delta_{T_x} = \pm 0.5°\text{C}. \tag{C.10}$$

The power was produced by four resistance heaters, which were powered by an Agilent E3695A power supply. A voltage potential across the resistance heaters was generated by the power supply. The current through the resistors was then measured by the power supply. The power through the heaters was calculated by multiplying the voltage by the current. The power was then compared to the desired power, the voltage was adjusted, and the process was repeated throughout the test. The uncertainty in the voltage potential is $\delta_V = \pm 0.001\,\text{V}$, and the uncertainty in the current measurement is $\delta_I = 0.001$ A. The uncertainty in the power generated can then be determine by analyzing the propagation of uncertainty in the power equation,

$$P = VI \tag{C.11}$$

which has an uncertainty of

$$\delta_P = \pm\sqrt{\left(\frac{\partial P}{\partial V}\delta_V\right)^2 + \left(\frac{\partial P}{\partial I}\delta_I\right)^2} \tag{C.12}$$

$$= \pm\sqrt{(I\delta_V)^2 + (V\delta_I)^2}. \tag{C.13}$$

V and I are inversely proportional to one another in Eq. (C.11), and they are related to one another by the resistance through the equation

$$V = IR. \tag{C.14}$$

Therefore, since the resistance of the heaters drives the selection of the voltage and current for a desired power, it is convenient to write Eq. (C.13) in terms of the resistance of the heaters, R_e, and the desired power.

$$\delta_P = \pm P^{1/2} \sqrt{\frac{(0.001 \text{ V})^2}{R_e} + R_e(0.001 \text{ A})^2}. \tag{C.15}$$

Since the resistance heater arrays have a nominal resistance of $4 \text{ k}\Omega$, Eq. (C.15) can be further reduced to

$$\delta_P = \pm 0.063 \text{ W}^{1/2} \cdot P^{1/2} \tag{C.16}$$

The uncertainties of the powers used in this study are then

$$\delta_{P=0.5 \text{ W}} = \pm 0.045 \text{ W} \tag{C.17}$$

$$\delta_{P=1.0 \text{ W}} = \pm 0.062 \text{ W} \tag{C.18}$$

$$\delta_{P=1.5 \text{ W}} = \pm 0.077 \text{ W} \tag{C.19}$$

$$\delta_{P=2.0 \text{ W}} = \pm 0.089 \text{ W} \tag{C.20}$$

The uncertainty of the junction resistance was found by propagating the uncertainties of the temperatures and powers into the linear fit through the method of sequential

perturbations as presented by Moffat [33]. The resulting uncertainty can be expressed as

$$\delta_{R_{jx}} = \pm \sqrt{\sum_i (R_{jx,o} - R_{jx,i+\delta_i})^2} \tag{C.21}$$

$$= \pm \sqrt{\left(R_{jx,o} - R_{jx,P_1+\delta_{P_1}}\right)^2 + \left(R_{jx,o} - R_{jx,P_2+\delta_{P_2}}\right)^2 + \dots} \tag{C.22}$$

where $R_{jx,o}$ is the original value that would have been calculated if the uncertainties were ignored and $R_{jx,i+\delta_i}$ is the value that would have been calculated if the ith measurement had been perturbed by its uncertainty. The final value for the uncertainty of R_{jx} using this method was

$$\delta_{R_{jx}} = \pm 0.2 \, \text{K/W} \tag{C.23}$$

C.5   Summary

The uncertainties of the primary measured quantities used in this study are summarized in Table C.1.

Table C.1: Tabulated uncertainties of measured quantities.

Measured Quantity	Symbol	Uncertainty
Volume Fraction	Φ	$\pm 10\%$
Specific Heat	C_p	$\pm 5\%$
Thermal Resistance	$A \cdot R$	$\pm 10^{-4} \, \text{m}^2 \cdot \text{K/W}$
Apparent Thermal Conductivity	λ	$\pm 0.1 \, \text{W/m} \cdot \text{K}$
Junction Resistance	R_{jx}	$\pm 0.2 \, \text{K/W}$

Appendix D

Source Code

D.1 Volume Fraction Measurement through Image Processing

CountPixels.py

```python
#!/usr/bin/env python
from PIL import Image
import os


def CountPixels(file,color=(255,255,255)):
    """ Count the number of pixels in an image that match the given rgb
    color (default is pure white) """


    # Import the image using the 'Image.open()' command and create a list
    # of tuples using the '.getdata()' attribute.  The resulting list will
    # be a list of tuples with the rgb values for each pixel,
    # i.e. (255,255,255) for a white pixel
    pixels = Image.open(file).getdata()


    # iterate over each pixel and count the number of pixels that
    # match 'color'
    matching_pixels = 0
    for pixel in pixels:
        if pixel == color:
```

```python
            matching_pixels += 1

    # the total number of pixels in the image is the length of the
    # 'pixels' list
    total = len(pixels)

    # calculate the percentage of the pixels that are white
    percent_matching = float(matching_pixels)/float(total)

    # output data
    print "Total number of pixels: %s" % total
    print "Number of matching pixels: %s" % matching_pixels
    print "Percentage of matching pixels %s" % percent_matching

    return total, matching_pixels, percent_matching

startdir = os.getcwd()

imagedir = "Path/To/Images"

# open a file to write the results to
os.chdir(startdir)
output = open('results.csv','w')
output.write('Filename, Total Pixels, Alumina Pixels, Percentage of \
Alumina\n')

# get a list of the images in the directory
```

```python
os.chdir(imagedir)
images = os.listdir(os.getcwd())


for image in images:
    if '.tif' not in image: continue
    total, matching_pixels, percent_matching = CountPixels(image)
    output.write("%s,%f,%f,%f\n" % (image, total, matching_pixels, \
    percent_matching))


output.close()
```

D.2 Apparent Thermal Conductivity Measurement with a Comparative Cut Bar Apparatus

D.2.1 Data Acquisition
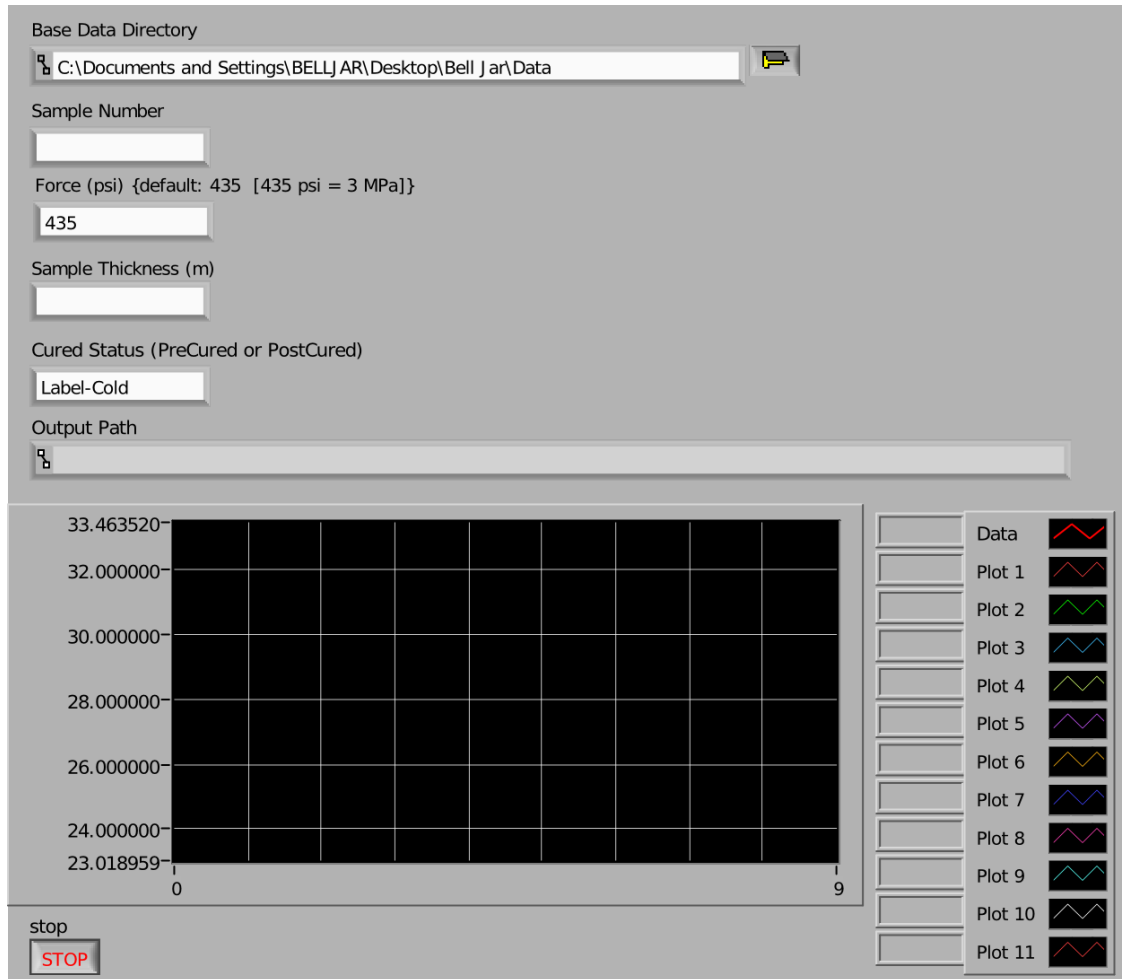
Figure D.1: LabView front panel for comparative cut bar temperature measurement.
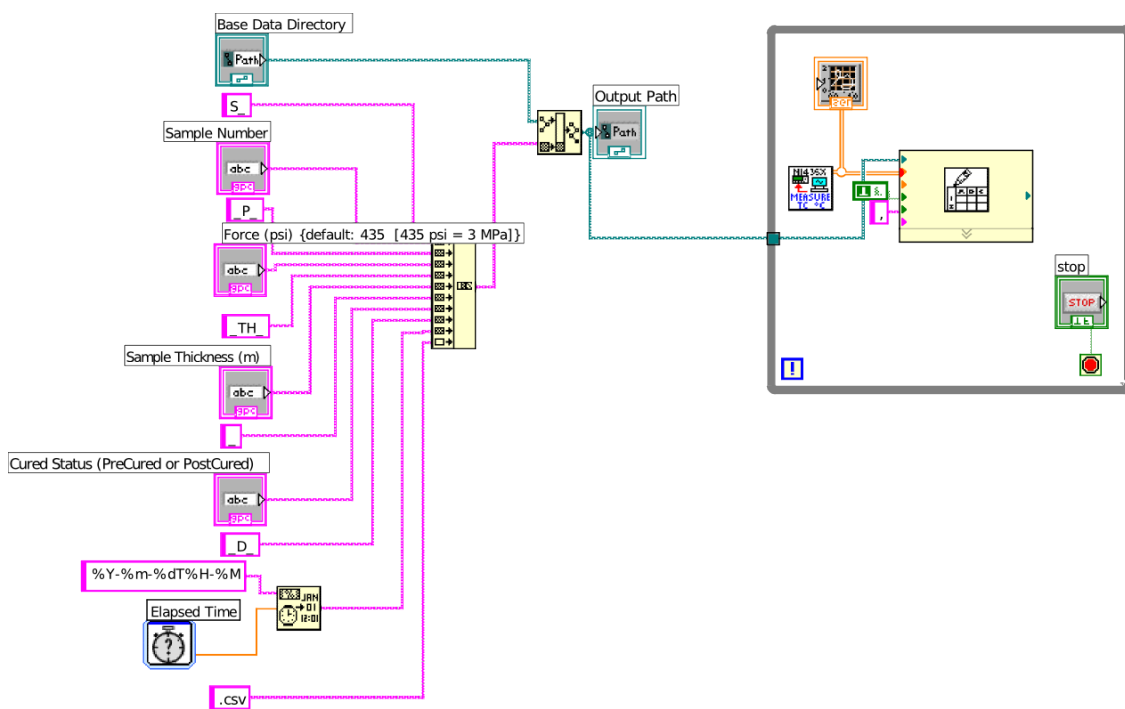
Figure D.2: LabView block diagram for comparative cut bar temperature measurement.

Figure D.3: LabView front panel for thermocouple measurement.

1 - Initialize the device to get a DAQ Session.
2 - Set up a Scan List based on the Channel String.
3 - Configure the Mode for the channels.
4 - Select the units of Temperature.
5 - Set Auto Zero On.
6 - Set Cold Junction Compensation.
7 - Set Ground Referencing to On.
8 - Set Open Thermocouple Detect to On.
9 - Set the upper and lower input limits on the signal range.
10 - Set the Powerline Frequency.

11 - Set the Reading Rate for the acquisition.
12 - Set the number of scans to be acquired.
13 - Start the Acquisition.
14 - While there is still data that needs to be read, or until an error occurs...
   a - Check how many scans are available to be read.
   b - Read that many scans.
15 - Stop the Acquisition.
16 - Close the DAQ Session.
17 - Report any errors to the Front Panel.

Figure D.4: LabView block diagram for thermocouple measurement.

Figure D.5: LabView front panel for comparative cut bar heat generation.
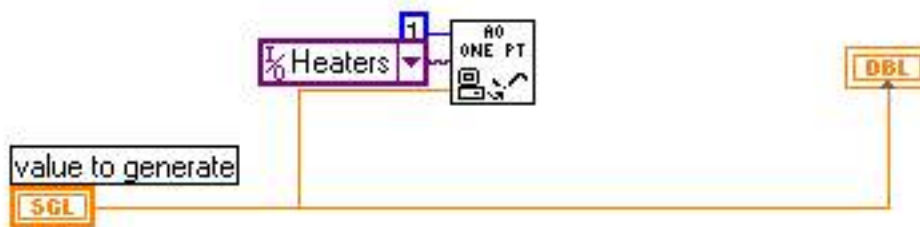
Figure D.6: LabView block diagram for comparative cut bar heat generation.
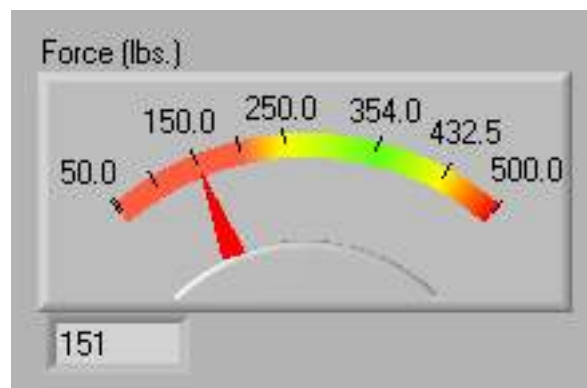
Figure D.7: LabView front panel for comparative cut bar load measurement.
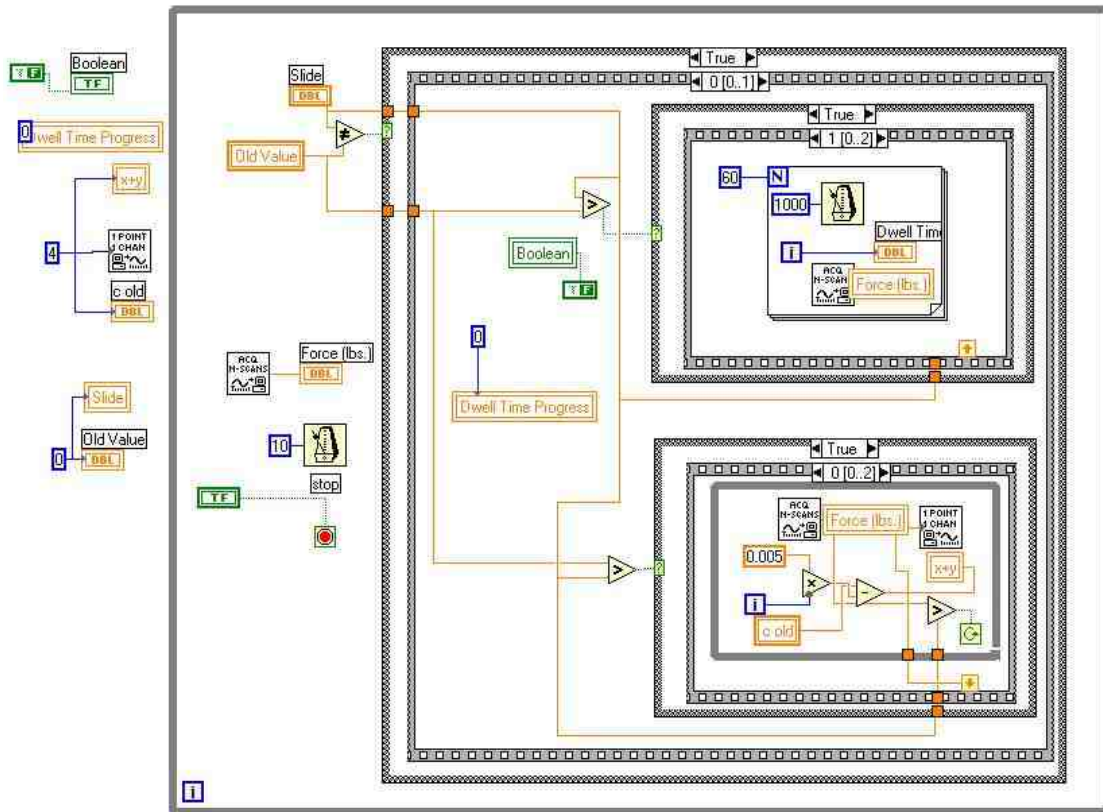
Figure D.8: LabView block diagram for comparative cut bar load measurement.

D.2.2 Data Reduction

CutBarThermalConductivityCalculation.py

```python
import sys
import SensorCalibration as sc
import ThermistorInterpolation as ti
import jfm as my
import numpy as np
import matplotlib.pylab as pyl
import os, time




class Thermocouple():
    """Yields an object, which when called gives the calibrated value of
     of the thermocouple"""
    def cal(self, MeasuredTemp):
        CalibratedTemp = np.polyval(self.coeffs, MeasuredTemp)
        return CalibratedTemp




class ConductivityMeasurement():
    '''Accepts a filename and returns an object containing the resulting
    values for the sample (thickness, test date, temperatures, contact
    resistance + conductive resistance, etc.)'''
    def __init__(self, filename, verbose=True, order_of_fit=1):
        # Parse filename
        if verbose :
```

```python
    print('parsing %s' % filename)
filename = filename.split('/')[-1]
parsed_filename = filename.split('_')
sample_number = my.safe_int_float(parsed_filename[1])
sample_force = int(parsed_filename[3])
sample_thickness = float(parsed_filename[5])
extra_info = parsed_filename[6]
test_date = time.strptime(parsed_filename[-1].split('.')[0], \
'%Y-%m-%dT%H-%M')


# Import the measured thermocouple readings
tc_readings = np.array(my.read_csv_file(filename))


# Apply Calibration Curve to the last 50 thermocouple readings
cal_tc_readings = np.array([[TC[1].cal(i[0]),TC[2].cal(i[1]),\
TC[3].cal(i[2]),TC[4].cal(i[3]),TC[5].cal(i[4]),TC[6].cal(i[5]),
TC[7].cal(i[6]),TC[8].cal(i[7]),TC[9].cal(i[8]),TC[10].cal(i[9])]\
 for i in tc_readings[:,-51:-1]])


# Take the average of calibrated temperature readings
averaged_tc_readings = map(np.mean, cal_tc_readings.transpose())


# Split the thermocouple readings into the readings for the top
# and bottom metering blocks
temps_bottom = averaged_tc_readings[0:5] # first five elements
temps_top = averaged_tc_readings[5:10] # next five elements
```

```python
# Apply a linear regression to the temperatures
locations_top = 0.01*np.arange(1,6) + sample_thickness/2
locations_bottom = -locations_top[::-1]
fit_bottom = my.Regression(locations_bottom, temps_bottom, \
order_of_fit)
fit_top = my.Regression(locations_top, temps_top, order_of_fit)


# Extrapolate to get the temperatures at the interfaces
interface_location_top = sample_thickness/2
interface_location_bottom = -interface_location_top
interface_temp_bottom = fit_bottom(interface_location_bottom)
interface_temp_top = fit_top(interface_location_top)


# Thermal conductivity of the sample
cross_sectional_area = 6.452 * 10**(-4) # m # 645.2 mm^2 = 1 in^2
k_metering_block = 133 # W/mK
tc_spacing = 0.01 # m # 10 mm spacing between thermocouples
q_bottom = k_metering_block * cross_sectional_area * -1 * \
fit_bottom.slope(interface_location_bottom)# Watts
q_flux_bottom = q_bottom/cross_sectional_area
q_top = k_metering_block * cross_sectional_area * -1 * \
fit_top.slope(interface_location_top) # Watts
q_flux_top = q_top/cross_sectional_area
q = np.mean([q_bottom, q_top])
q_flux = np.mean([q_flux_top,q_flux_bottom])
delta_T_sample = abs(interface_temp_bottom - interface_temp_top) \
# Degrees C # Temperature drop across sample
```

```python
thermal_impedance = delta_T_sample / q_flux

k_sample_total = sample_thickness / thermal_impedance

mean_temp_sample = np.mean([interface_temp_bottom, \
interface_temp_top])


# Define attributes
self.filename = filename

self.number = sample_number

self.thickness = sample_thickness

self.cross_sectional_area = cross_sectional_area

self.metering_block_cross_sectional_area = cross_sectional_area

self.interface_location_bottom = interface_location_bottom

self.interface_location_top = interface_location_top

self.extra_info = extra_info

self.test_date = test_date

self.force = sample_force

self.temps_bottom = temps_bottom

self.temps_top = temps_top

self.fit_bottom = fit_bottom

self.fit_top = fit_top

self.q_bottom = q_bottom

self.q_top = q_top

self.q = q

self.flux_bottom = q_flux_bottom

self.flux_top = q_flux_top

self.flux = q_flux

self.delta_T = delta_T_sample
```

```python
        self.mean_T = mean_temp_sample

        self.T_interface_top = interface_temp_top

        self.T_interface_bottom = interface_temp_bottom

        self.k_total = n(k_sample_total)

        self.tc_locations_top = locations_top

        self.tc_locations_bottom = locations_bottom

        self.thermal_impedance = thermal_impedance

        self.disp = 'S-' + str(self.number) + ' P-' + str(self.force) + \
        ' ' + self.extra_info + ' T-' + '%.2f' % self.mean_T


    def recalc(self):
        """Recalculate the thermal conductivity and thermal impedance
        """
        self.q_flux = self.q/self.cross_sectional_area

        self.thermal_impedance = self.delta_T / self.q_flux

        self.k_total = self.thickness / self.thermal_impedance


    def graph(self):
        # define plot sytles
        temperature_marker = 'k.'

        fit_line_style = '-k'

        sample_line_style = '--k'
        # Plot thermocouple readings
        pyl.plot(self.tc_locations_bottom, self.temps_bottom, \
        temperature_marker)

        pyl.plot(self.tc_locations_top, self.temps_top, temperature_marker)

        stepsize = 0.001
```

```python
        # Set x arrays for plotting fit lines
        x_bottom = np.arange(self.tc_locations_bottom[0], \
        self.interface_location_bottom + stepsize, stepsize)
        x_top = np.arange(self.interface_location_top, \
        self.tc_locations_top[-1] + stepsize, stepsize)
        # Plot fit lines
        pyl.plot(x_bottom, self.fit_bottom(x_bottom), fit_line_style)
        pyl.plot(x_top, self.fit_top(x_top), fit_line_style)
        # Plot sample temperature line
        pyl.plot([self.interface_location_bottom, \
        self.interface_location_top], [self.T_interface_bottom, \
        self.T_interface_top], sample_line_style)


def graph_sage(self, TC_color='black', TC_pointsize=20, \
fit_line_color='black', fit_line_style='-', extrap_line_color='black',\
extrap_line_style='--', sample_line_color='black', \
sample_line_style='--'):
        # Plot thermocouple readings
        TC_readings_bottom_plot = list_plot(zip(self.tc_locations_bottom, \
        self.temps_bottom), rgbcolor=TC_color, pointsize=20)
        TC_readings_top_plot = list_plot(zip(self.tc_locations_top, \
        self.temps_top), rgbcolor=TC_color, pointsize=TC_pointsize)


        # Plot fit lines
        fit_plot_bottom = plot(self.fit_bottom(x),(x,\
        self.tc_locations_bottom[0], self.tc_locations_bottom[-1]), \
        rgbcolor = fit_line_color, linestyle = fit_line_style)
```

```python
        fit_plot_top = plot(self.fit_top(x), (x, self.tc_locations_top[0], \
        self.tc_locations_top[-1]), rgbcolor = fit_line_color, \
        linestyle = fit_line_style)


        # Plot extrapolation to interface lines
        extrap_plot_bottom = plot(self.fit_bottom(x),(x, \
        self.tc_locations_bottom[-1], self.interface_location_bottom), \
        rgbcolor = extrap_line_color, linestyle = extrap_line_style)
        extrap_plot_top = plot(self.fit_top(x), (x, \
        self.interface_location_top, self.tc_locations_top[0]), rgbcolor \
        = extrap_line_color, linestyle = extrap_line_style)


        # Plot sample temperature line
        sample_plot = line([(self.interface_location_bottom, \
        self.T_interface_bottom), (self.interface_location_top, \
        self.T_interface_top)], rgbcolor = sample_line_color, \
        linestyle = sample_line_style)


        # combine plots
        return (TC_readings_bottom_plot + TC_readings_top_plot + \
        fit_plot_bottom + fit_plot_top + extrap_plot_bottom + \
        extrap_plot_top + sample_plot)


    def __str__(self):
        return self.disp


    def __repr__(self):
```

```python
        return '<' + self.disp + '>'


    def show(self):
        print('\nSample #: %s' % self.number)

        print('Filename: %s' % self.filename)

        print('Tested: %s' % time.strftime('%a %-1m/%-1d/%y at %-1I:%M %p',\

        self.test_date))

        print('Thickness: %f' % self.thickness)

        print('Temperature of bottom interface: %f%s' % \

        (self.T_interface_bottom, my.dgc))

        print('Temperature of top interface: %f%s' % (self.T_interface_top,\

        my.dgc))

        print('Mean Sample Temp: %f%s' % (self.mean_T, my.dgc))

        print('Thermal conductivity: k_sample + k_contact = %f W/mK' % \

        self.k_total)

        print('Heat flux at bottom interface: %f W/m^2' % self.flux_bottom)

        print('Heat flux at top interface: %f W/m^2' % self.flux_top)

        print('Orientation: ' + self.extra_info)



class Results(list):
    '''Organization class for conductivity measurements'''
    def __init__(self):
        self = []


    def __call__(self, n='all', temp='all', labelside='all', force=435):
        l = self[:]
```

```python
if n != 'all':

    if isinstance(n,tuple) or isinstance(n,list):

        l = [i for i in l if i.number in n]

    else :

        l = [i for i in l if i.number == n]


if force != 'all':

    if isinstance(force, tuple) or isinstance(force, list):

        l = [i for i in l if i.force in force]

    else :

        l = [i for i in l if i.force == force]

if temp != 'all':

    if temp == 'room' or temp == 25:

        l = [i for i in l if 20 < i.mean_T < 30]

    elif temp == 50:

        l = [i for i in l if 45 < i.mean_T < 55]

    elif temp == 75:

        l = [i for i in l if 70 < i.mean_T < 80]

    elif temp == 100:

        l = [i for i in l if 95 < i.mean_T < 105]

    else:

        print('The mean temperature of Sample %s is %.2f%s, \
        which does not fall into any of the specified categories' \
        % (i.number, i.mean_T, my.dgc))

if labelside != 'all':

    if labelside in ['cold', 'Cold', 'COLD', 'c', 'C', 'up', 'Up', \
        'UP', 'u', 'U']:
```

```python
            l = [i for i in l if i.extra_info == 'Label-Cold']
        elif labelside in ['hot', 'Hot', 'HOT', 'h', 'H', 'down', \
            'Down', 'd', 'D']:
            l = [i for i in l if i.extra_info == 'Label-Hot']
    return l



class kCalculation():
    """A k value calculated from the data collected
    """


    def __init__(self, samples, verbose=False):
        '''Find the least-squares solution for the thermal conductivity for
        the given samples'''
        samples = my.flatten(samples)
        A = []
        b = []
        for sample in samples:
            A.append([2, sample.thickness])
            b.append(sample.delta_T/sample.flux)
        Rc, k_inv = np.linalg.lstsq(A,b)[0]
        k = 1/k_inv
        self.value = k
        self.Rc = Rc
        self.k_inv = k_inv
        self.samples = samples
```

```python
def __add__(self, other):
    return self.value + other



def __mul__(self, other):
    return self.value * other



def __div__(self, other):
    return self.value / other



def __truediv__(self, other):
    return self.value / other



def __repr__(self):
    return str(n(self.value, digits=3))



def details(self):
    print('\n\tLeast-Squares solutions')
    print('Thermal Conductivity: k = %.2f W/mK' % self.value)
    print('Thermal Contact Resistance: Rc = %f m%sK/W' % (self.Rc, \
    my.sq))
    for sample in self.samples:
```

```python
            Rtot = sample.delta_T/sample.flux
            Rl = sample.thickness * self.k_inv
            print('\n\t%s' % sample)
            print('Total Thermal Resistance: Rtot = %f m%sK/W' % (Rtot, \
            my.sq))
            print('Thermal Interface Resistance (Contact) [each face]: \
            Rc = %f m%sK/W' % (self.Rc, my.sq))
            print('Sample Thermal Resistance (Conductive): Rl = L/k = \
            %f m%sK/W' % (Rl, my.sq))
            print('Contribution of Contact Resistance: Rc/Rtot = %f' % \
            (2*self.Rc/Rtot))
            print('Contribution of Conductive Resistance: Rl/Rtot = %f' \
            % (Rl/Rtot))
        print('')


def CalibrationCalculations(CalibrationCSVFile):
    '''Produce Thermocouple objects which contain the calibration curves
    for each of the thermocouples used'''
    ### Calibration Calculations ###
    # Import the calibration measurements from the .csv file
    CalibrationMeasurements = np.array(my.read_csv_file(CalibrationCSVFile))

    # Convert the first column resistance readings into temperatures
    TempStandard = map(ti.temp_from_thermistor, CalibrationMeasurements[:,0])

    # Create a dictionary to store the thermocouples in
```

```python
    TC = {}
    # Create an iterator for the number of thermocouples (note: the
    # thermocouples have stickers with letters -
    # A corresponds to 1, B to 2, ...)
    NofTCs = range(1, len(CalibrationMeasurements[0]))


    # Process each additional column after the first in the csv file as
    # thermcouples
    for i in NofTCs:
        # Instantiate a thermoucouple object
        TC[i]=Thermocouple()
        # define attibutes of the thermocouple
        TC[i].slope, TC[i].intercept, TC[i].rsq, TC[i].Sxy, TC[i].Sxx, \
        TC[i].xm, TC[i].u_precision, TC[i].u_scale, TC[i].u = \
        sc.Calibrate(CalibrationMeasurements[:,i], TempStandard)
        # store the slope and the intercept as the calibration coefficients:
        # this will be used to evaluate the TC[i].cal() method (note:
        # additional coefficents could be supplied here to get a quadratic,
        # cubic, ... calibration curve, however the sc.Calibrate function
        # currently only returns a linear fit because it uses
        # scipy.stats.linregress
        TC[i].coeffs = [TC[i].slope, TC[i].intercept]
    return TC



def BuildSampleList(sampleNumbers, temperature, extrainfo, force=400):
    '''Yields a list of sample objects meeting the given criteria'''
```

120

```python
    l = []
    for number in sampleNumbers:
        l.append(tests(n=number, temp=temperature, lableside=extrainfo,\
         force=force))
    return my.flatten(l)




def ProcessData(DataDir,CalibrationCSVFile, verbose=False):
    '''Process the data in DataDir using the thermocouple
    calibration data in CalibrationCSVFile'''

    StartDir = os.getcwd()
    CalibrationCalculations(CalibrationCSVFile)
    os.chdir(DataDir)
    files = [file for file in os.listdir(os.curdir) if (file !='.directory'\
     and '.swp' not in file)]
    files.sort()
    tests = Results()
    for i, file in enumerate(files):
        obj = ConductivityMeasurement(file, verbose=verbose)
        tests.append(obj)
    os.chdir(StartDir)
    if verbose: print(tests)
    return tests
```

jfm.py

```python
import csv
import numpy as np
import scipy.special # for the inverse student t function
import string
from sage.misc.latex import *
from sage.misc.functional import numerical_approx
import cPickle
import os
import sys
import cStringIO
import operator


def flatten(x):
    """flatten(sequence) -> list

    Returns a single, flat list which contains all elements retrieved
    from the sequence and all recursively contained sub-sequences
    (iterables).

    Examples:
    >>> [1, 2, [3,4], (5,6)]
    [1, 2, [3, 4], (5, 6)]
    >>> flatten([[[1,2,3], (42,None)], [4,5], [6], 7, MyVector(8,9,10)])
    [1, 2, 3, 42, None, 4, 5, 6, 7, 8, 9, 10]
    """
```

```python
    result = []
    for el in x:
        #if isinstance(el, (list, tuple)):
        if hasattr(el, "__iter__") and not isinstance(el, basestring):
            result.extend(flatten(el))
        else:
            result.append(el)
    return result




class Regression():
    """A regression object.  Call it with the syntax
    reg = Regression(x_values, y_values[, degree=1])
    degree=1 will produce a linear fit
    degree=2 will produce a quadratic fit
    and so on
    """


    def __init__(self, x_values, y_values, degree=1):
        self.coeffs = np.polyfit(x_values, y_values, degree)
        self.intercept = np.polyval(self.coeffs, 0)
        self.p = np.poly1d(self.coeffs)
        self.slope = np.polyder(self.p)
        yhat = [self.p(z) for z in x_values]
        ybar = sum(y_values)/len(y_values)
        ssreg = sum([(yihat-ybar)**2 for yihat in yhat])
```

```python
        sstot = sum([(yi-ybar)**2 for yi in y_values])
        self.rsq = ssreg/sstot


    def __call__(self, value):
        return np.polyval(self.coeffs, value)


    def __str__(self):
        return self.p.__str__()



def read_csv_file(filename):
    '''Reads a CSV file and returns it as a list of rows.
       Numbers will be coerced into either int or float type depending on
       the presence of a decimal'''


    data = []
    for row in csv.reader(open(filename)):
        data.append(row)
    floatdata = [map(safe_int_float,row) for row in data]
    return floatdata



def safe_int_float(string):
    '''convert a string to either an int or a float if appropriate, i.e.
       safe_int_float('a') >>> 'a'
       safe_int_float('1') >>> 1
       safe_int_float('1.') >>> 1.0
```

```python
        safe_int_float('3.14') >>> 3.14'''

    try:
        result = int(string)
    except ValueError:
        try:
            result = float(string)
        except ValueError:
            result = string
    return result



def tinv(nu, p):
    '''Student's t inverse cumulative distribution function

    t = tinv(nu, p) computes the inverse of Student's t cdf for degrees of
    freedom nu=n-1 and a confidence interval of p=1-conf_intv i.e. p=0.1
    for a 90% confidence interval'''

    # the negative sign is to correct for the format of the raw function
    return -scipy.special.stdtrit(nu, p)



### Constants ###
dg = u'\N{DEGREE SIGN}'
dgc = u'\N{DEGREE SIGN}'+'C'
```

```python
pm = u'\N{PLUS-MINUS SIGN}'

sq = u'\N{SUPERSCRIPT TWO}'

cu = u'\N{SUPERSCRIPT THREE}'

cdot = u'\N{MIDDLE DOT}'

mult = u'\N{MULTIPLICATION SIGN}'
```

SensorCalibration.py

```python
import scipy

import numpy as np

import jfm as my

from scipy import stats


class CalibrationCurve():
    '''An object class for storing information about a calibration curve'''


    def __init__(self, measured, standard, confidence_interval=0.95, \
    order=1):
        slope, intercept, r_value, p_value, std_err = stats.linregress(\
        measured,standard)
        rsq = r_value**2
        n = len(measured)
        nu = n-1
        calibrated=scipy.polyval([slope,intercept],measured)
        xm = np.mean(measured)
        Sxxsq = scipy.sum([(i - xm)**2 for i in measured])
        Sxx = scipy.sqrt(Sxxsq)
        Syx = scipy.sqrt(sum([(standard[i]-calibrated[i])**2 for i,v in \
```

```python
        enumerate(standard)])/(n-2))

        t_a_nu = st(nu,confidence_interval)

        U_offset = (t_a_nu*Syx) * scipy.sqrt(1/n + xm**2/Sxxsq)

        U_scale = (t_a_nu * Syx) / (Sxx)

        U = [U_offset, U_scale]

        self.slope = slope

        self.intercept = intercept

        self.p = np.poly1d([slope, intercept])

        self.rsq = rsq

        self.Syx = Syx

        self.Sxx = Sxx

        self.xm = xm

        self.u_offset = U_offset

        self.u_scale = U_scale

        self.u = U


    def __call__(self, value):

        return (np.polyval([self.slope, self.intercept], value), \

        np.polyval([self.u_scale, self.u_offset], value))


    def __str__(self):

        return 'f(x) = %f x + %f %s [%f x + %f]' % (self.slope, \

        self.intercept, my.pm, self.u_scale, self.u_offset)



def Calibrate(measured,standard,confidence_interval=0.95,order=1):

    '''Returns the calibration curve coefficients, R-squared valued,
```

Deviation from the standard (S_xy), and the calibrated uncertainty
from a list of measured values and a list of true values.
slope, intercept, Rsq, Syx, Sxx, xm, U_offset, U_scale, U =
Calibrate(meausred, standard, confidence interval = 0.95, order = 1)'''

```python
slope, intercept, r_value, p_value, std_err = \
stats.linregress(measured,standard)
rsq = r_value**2
n = len(measured)
nu = n-1
calibrated=scipy.polyval([slope,intercept],measured)
xm = np.mean(measured)
Sxxsq = scipy.sum([(i - xm)**2 for i in measured])
Sxx = scipy.sqrt(Sxxsq)
Syx = scipy.sqrt(sum([(standard[i]-calibrated[i])**2 for i,v in \
enumerate(standard)])/(n-2))
t_a_nu = my.tinv(nu,confidence_interval)
U_offset = (t_a_nu*Syx) * scipy.sqrt(1/n + xm**2/Sxxsq)
U_scale = (t_a_nu * Syx) / (Sxx)
U = [U_offset, U_scale]
return slope, intercept, rsq, Syx, Sxx, xm, U_offset, U_scale, U
```

D.3 In Situ Thermal Resistance Measurement of a PCB Attached to an Aluminum Substrate
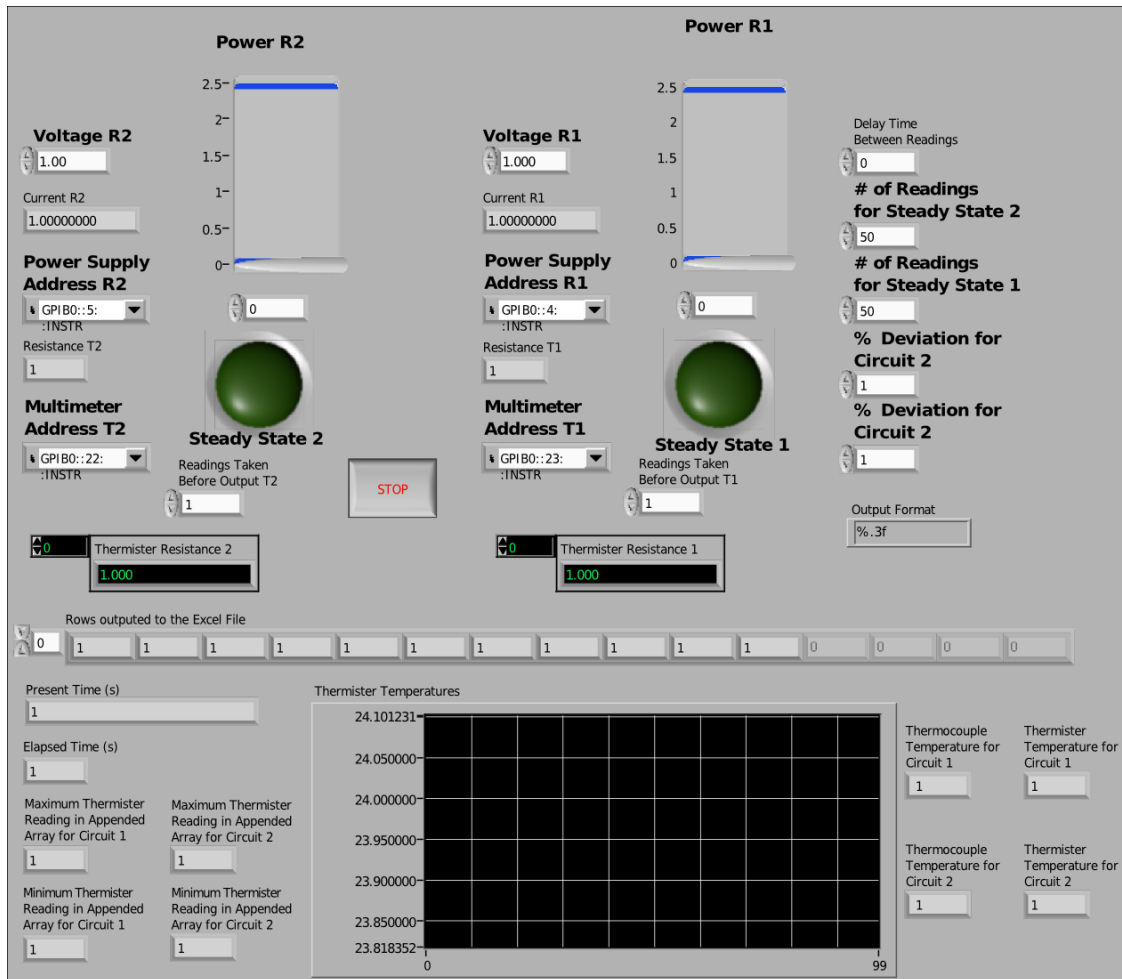
D.3.1 Data Acquisition

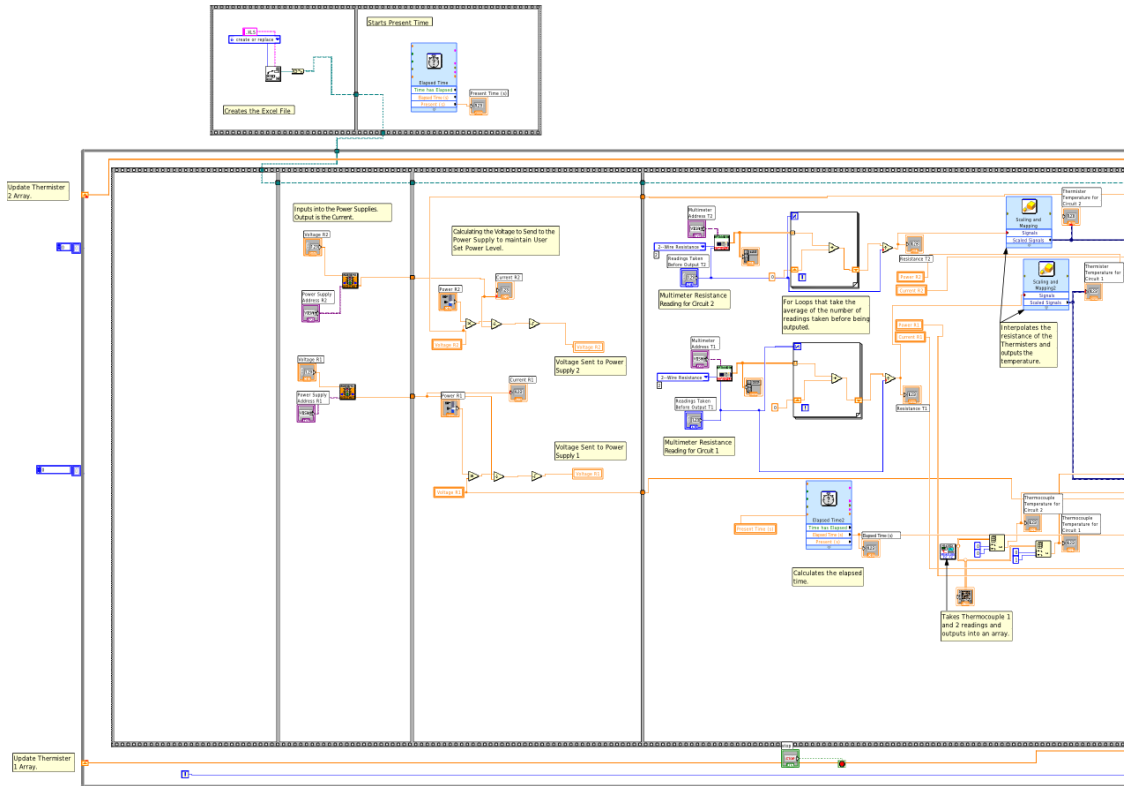**Figure D.9:** Front panel for junction resistance measurement data acquisition.

Figure D.10: Block diagram for junction resistance measurement data acquisition, Part 1 of 2.
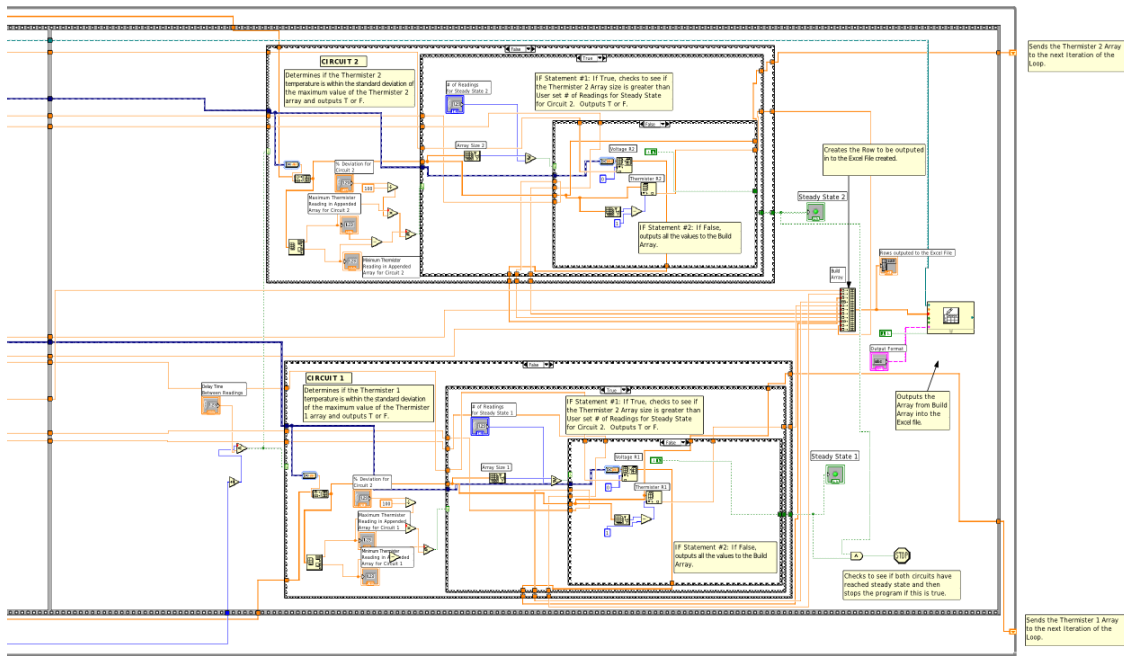
Figure D.11: Block diagram for junction resistance measurement data acquisition, Part 2 of 2.

D.3.2 Data-Reduction

JunctionResistanceCalculations.py

```python
import os, string, numpy, scipy.stats, re, pylab, matplotlib, pylab
import matplotlib.pyplot as plt
from matplotlib import rcParams


DefaultBaseDirectory='Path/To/Directory/'


class BoardList(dict):
    """List for storing Board objects"""
    def types(self):
        temp_list=[]
        for board in self.values():
            temp_list.append(board.type)
        return list(set(temp_list))


    def bytype(self,type='All'):
        Types=self.types()
        temp_list=[]
        for i in range(len(Types)):
            temp_list.append([])
            for board in self.values():
                if board.type == Types[i]:
                    temp_list[i].append(board)
            temp_list[i].sort()
        if type == 'All':
```

```python
            return sorted(temp_list)
        return sorted(temp_list[Types.index(type)])


    def all(self):
        return sorted(self.values())




class Board():
    """board object: has attributes of .cycles, .name, and .type"""
    def __init__(self, type, name):
        self.type=type
        self.name=name
        self.cycles=CycleList()


    def __str__(self): return self.name


    def __repr__(self): return '<'+self.name+'>'


    def __cmp__(self,other):
        if self.type != other.type:
            return cmp(self.type,other.type)
        if ('ALT' in self.name and 'ALT' in other.name) or \
          ('PSA' in self.name and 'PSA' in other.name):
            return cmp(int(re.search('(\d+)',self.name).group(1)),\
                int(re.search('(\d+)',other.name).group(1)))
        if '-' in self.name and '-' in other.name:
            return cmp(int(re.search('-(\d+)',self.name).group(1)),\
```

```python
                    int(re.search('-(\d+)',other.name).group(1)))


class CycleList(list):
    """list of cycles: is an attribute of a board object as .cycles:
    has attributes .clamped(), .unclamped(), .numbers, and .units"""
    def __init__(self):
        self=[]


    def __str__(self):
        l=''
        for cycle in sorted(self):
            l+=cycle.name+'\n'
        return l


    def __repr__(self):
        l=[]
        for cycle in sorted(self):
            l.append(cycle.name)
        return ', '.join(l)


    def numbers(self):
        l=[]
        for cycle in sorted(self):
            l.append(int(re.search('(\d+)(.+)',cycle.name).group(1)))
        return l
```

133

```python
    def units(self):
        return re.search('(\d+)(.+)',self[0].name).group(2).replace(' ','')


    def clamped(self):
        return [cycle for cycle in self if ' U' not in cycle.name]


    def unclamped(self):
        return [cycle for cycle in self if ' U' in cycle.name]



class Cycle():
    """cycle object: is a part of a CycleList() list:
    has attributes: .tr1 - Thermal resistance at location 1
    .tr2 - Thermal resistance at location 2
    .rsq1 - R squared value for the line fit used to determine the
            thermal resistance at location 1
    .rsq2 - R squared value for the line fit used to determine the
            thermal resistance at location 2
    .name - a string containing the name of the cycle derived from
            the name of the directory from which the Excel files were
            imported, i.e. 500 Cycles U
    .number - the number"""
    def __init__(self,cycle_number,tr_readings):
        self.tr1=tr_readings[0]
        self.tr2=tr_readings[1]
        self.rsq1=tr_readings[2]
        self.rsq2=tr_readings[3]
```

134

```python
        self.td1=tr_readings[4]

        self.td2=tr_readings[5]

        self.name=cycle_number


    def __str__(self): return self.name


    def __repr_(self): return '<'+self.name+'>'


    def __cmp__(self, other):

        return cmp(int(re.search('(\d+)',self.name).group(1)),\

                int(re.search('(\d+)',other.name).group(1)))


    def number(self):

        return int(re.search('(\d+)(.+)',self.name).group(1))



def ReadFromExcel(filename):

    """Import data from an Excel file"""

    # Open the file for reading

    file=open(filename)

    # Read the data from the file and store it into a variable called data

    # it is stored as a list of strings with each string contanining one

    # line from the original file

    data=file.readlines();

    # Close the file

    file.close()

    # Split the strings into individual elements so that the data will be
```

```python
        # a 2-d array rather than a 1-d list
    for i,v in enumerate(data):
        data[i]=string.split(data[i])
        for I,V in enumerate(data[i]):
            data[i][I]=float(data[i][I])
    return data




def ExtractTemperatureColumns(data):
    """Select the desired colums from the imported data"""
    # transpose the data for that each column is an element in the array
    datatrans=numpy.transpose(data)
    # return columns 5, 6, 10, and 11
    return numpy.array([datatrans[4],datatrans[5],datatrans[9],\
    datatrans[10]])




def FilterMeasurements(data):
    """Remove faulty or unnecessary readings from the list"""
    #Create a dummy list for putting data into
    new_array=[]
    #Check each value and exclude it if it is outside a reasonable range
    for v in data:
        if v>0 and v<100:
            new_array=numpy.append(new_array,v)
    return new_array[-20:]
```

```python
def AverageData(data):
    """Return the difference between the average reading of each
    thermistor/thermocouple pair"""
    # Average of (thermistor reading - thermocouple reading)
    try:
        TempDrop1=numpy.mean(FilterMeasurements(data[0])-\
        FilterMeasurements(data[1]))
    except ValueError:
        TempDrop1=-1
    try:
        TempDrop2=numpy.mean(FilterMeasurements(data[2])-\
        FilterMeasurements(data[3]))
    except ValueError:
        TempDrop2=-1
    return numpy.array([TempDrop1,TempDrop2])



def ProcessCycle(verbose=False):
    """Process the excel files in the current directory to get a thermal
    resistance for the current cycle"""
    TemperatureDrops = numpy.zeros((5,2))
    power = x = [0, 0.5, 1.0, 1.5, 2.0]
    res = lambda c,y,x: y-c*x
    for i,file in enumerate(['W00.XLS','W05.XLS','W10.XLS','W15.XLS',\
        'W20.XLS']):
```

```python
        data=ReadFromExcel(file)

        data=ExtractTemperatureColumns(data)

        TemperatureDrops[i]=(AverageData(data))
    if -1. in TemperatureDrops[:,0]:

        TR1 = ' '

        rsq1 = ' '
    else:

        y=TemperatureDrops[:,0]-TemperatureDrops[0,0]

        fit=scipy.optimize.leastsq(res, [6], args=(y,x))

        TR1 = fit[0]

        rsq1 = 1-sum([res(fit[0],y[i],x[i]) for i in range(1,5)])**2/\

        sum(y[1:-1])**2
    if -1. in TemperatureDrops[:,1]:

        TR2 = ' '

        rsq2 = ' '
    else:

        y=TemperatureDrops[:,1]-TemperatureDrops[0,1]

        fit=scipy.optimize.leastsq(res, [6], args=(y,x))

        TR2 = fit[0]

        rsq2 = 1-sum([res(fit[0],y[i],x[i]) for i in range(1,5)])**2/\

        sum(y[1:-1])**2
    return [TR1, TR2, rsq1, rsq2, TemperatureDrops[:,0], \

    TemperatureDrops[:,1]]




def CalculateClampedVsUnclamped(boards):

    """Calculates the absolute and percent differnece between the clamped
```

```python
        and unclamped reading for the non-overmolded boards"""
    for group in ['ALT FR4','PSA FR4','PSA FLEX']:
        for board in boards.bytype(group):
            board.trd1={}
            for index,cycle in enumerate(board.cycles.clamped()[2:]):
                if cycle.tr1 != ' ' and \
                board.cycles.unclamped()[index].tr1 != ' ':
                    diff=board.cycles.unclamped()[index].tr1-cycle.tr1
                    board.trd1[cycle.name]={'Difference':diff,\
                    'Percent Difference':diff/cycle.tr1}
            board.trd2={}
            for index,cycle in enumerate(board.cycles.clamped()[2:]):
                if cycle.tr2 != ' ' and \
                board.cycles.unclamped()[index].tr2 != ' ':
                    diff=board.cycles.unclamped()[index].tr2-cycle.tr2
                    board.trd2[cycle.name]={'Difference':diff,\
                    'Percent Difference':diff/cycle.tr2}


def ImportData(basedir=DefaultBaseDirectory,verbose=False):
    """Import the the data from excel files and categorize it by the
    location of the files following the pattern where the first
    subfolder is the type of the board, the second subfolder is the
    name of the board, the third subfolder is the number of cycles
    and the fourth subfolder contains the excel file with the
    meausrements"""
    # save the location of the current directory
```

```python
CurrentDirectory = os.getcwd()
# move into the base directory
os.chdir(basedir)
# then into the data directory
os.chdir('Data')
# Initialize a variable containing an empty board list, which
#is an oject of the class BoardList()
boards=BoardList()
# define a list a directories to ignore
dir_exclude_list=['CSV Files','Figures','November 08','TeX']
# iterate through a loop for directories not in  dir_exclude_list
for directory in os.listdir(os.getcwd()):
    if (directory in dir_exclude_list) or \
    (os.path.isdir(directory) == False):
        continue
    # assign the name of the current directory to be the type of board
    BoardType=directory
    # move into the directory for the current type
    os.chdir(directory)
    # debugging
    if verbose: print BoardType
    # iterate through for each subdirectory in the current directory
    for subdir in os.listdir(os.getcwd()):
        # assign the name of the current directory to be the name of
        # the board
        BoardName=subdir
        # create a new object of the type Board() and append it to the
```

```python
# variable boards
boards[BoardName]=Board(BoardType, BoardName)
# move into the directory for the current board
os.chdir(subdir)
# debugging
if verbose: print BoardName
# iterate through for each subdirectory
for subsubdir in sorted(os.listdir(os.getcwd())):
    # assign the name of the current directory to be the
    # name of the current cycle
    CycleNumber=subsubdir
    # debugging
    if verbose: print CycleNumber
    # move into the directory for the cycle
    os.chdir(subsubdir)
    # debugging
    if verbose: print os.getcwd()
    # append an object Cycle() to the attribute cycles
    # of the current board
    boards[BoardName].cycles.append(\
            Cycle(CycleNumber,ProcessCycle()))
    # move up a directory to process the next cycle
    os.chdir(os.pardir)
# sort the imported cycles
boards[BoardName].cycles.sort()
# move up a directory to process the next board
os.chdir(os.pardir)
```

```python
        # move up a directory to process the next board type
        os.chdir(os.pardir)
    # move back to the original directory
    os.chdir(CurrentDirectory)
    # clean up variables
    del(subdir, subsubdir, BoardType, BoardName)
    # fix any boards that were tested with the wires connected in the
    # wrong order
    for cycle in [boards['ALT8'].cycles[1],\
    boards['PSA-5 FLEX'].cycles[8]]:
        cycle.tr1, cycle.tr2 = cycle.tr2, cycle.tr1
    # Calculate Percent Differences in thermal resistances
    CalculateClampedVsUnclamped(boards)
    # return a list of boards with the thermal resistances
    # as attributes stored as a 2-D list in the location
    # board.cycles = [[tr1,tr2,rsq1,rsq2],[tr1,tr2,rsq1,rsq2],...]
    return boards



def CreateTables(boards,basedir=DefaultBaseDirectory,pub=False):
    """Apply the CreateTRsLatexTable() function for each type of board
    and save the resulting files to the appropriate location"""
    if pub:
        os.chdir(ipackdir)
        table_dir='Tables'
    else:
        os.chdir(basedir)
```

```python
        table_dir=os.path.join('Results','Tables')
    list_of_tables=[]
    if not os.path.exists(table_dir):
        os.makedirs(table_dir)
    os.chdir(table_dir)
    for board_group in boards.bytype():
        filename='%sThermalResistancesTable.tex' % board_group[0].type.replace(' ','')
        CreateTRsLatexTable(board_group, filename=filename)
        list_of_tables.append(filename)
    os.chdir(os.pardir)
    f=open('Tables.tex','w')
    for table in list_of_tables:
        f.writelines('\\input{Tables/%s}\n' % table)
    f.close()
    os.chdir(basedir)



def ExtractTRsForCSVFile(Boards):
    """Build a comma separated string for use in CreateCSVFiles()"""
    l=[]
    for board in Boards:
        l.append([board.name,'TR1'])
        for cycle in board.cycles.clamped():
            if cycle.tr1 == ' ': l[-1].append('    ')
            else: l[-1].append('%f' % cycle.tr1)
        for cycle in board.cycles.unclamped():
            if cycle.tr1 == ' ': l[-1].append('    ')
```

```python
            else: l[-1].append('%f' % cycle.tr1)
        l[-1]=','.join(l[-1])
        l.append([board.name,'TR2'])
        for cycle in board.cycles.clamped():
            if cycle.tr2 == ' ': l[-1].append('     ')
            else: l[-1].append('%f' % cycle.tr2)
        for cycle in board.cycles.unclamped():
            if cycle.tr2 == ' ': l[-1].append('     ')
            else: l[-1].append('%f' % cycle.tr2)
        l[-1]=','.join(l[-1])
    return ' \n'.join(l)



def CreateCSVFiles(boards,basedir=DefaultBaseDirectory):
    """Creates a CSV file with the processed thermal resistances"""
    OriginalDirectory=os.getcwd()
    os.chdir(basedir)
    csv_dir=os.path.join('Results','CSV Files')
    if not os.path.exists(csv_dir):
        os.makedirs(csv_dir)
    os.chdir(csv_dir)
    for board_group in boards.bytype():
        filename='%s.csv' % board_group[0].type
        f=open(filename,'w')
        f.write(ExtractTRsForCSVFile(board_group))
        f.close()
    f=open('AllBoards.csv','w')
```

```python
        f.write(ExtractTRsForCSVFile(boards.all()))

        f.close()

        os.chdir(OriginalDirectory)




def FindStats(Boards,Exclude='',verbose=False,ClampedThenUnclamped=False):
    """Returns two arrays.  The first array give the average resistance
    for each cycle and the second array gives the corresponding standard
    deviation.  The convention for this fucntion is to use the options:
    Exclude='Unclamped' - to get the values fo the clamped boards
    Exclude='Clamped' to get the values for the unclamped boards."""
    data=[]
    datacheck=True
    for board in Boards:
        templist=[]
        for cycle in board.cycles:
            if Exclude=='Unclamped' and ' U' in cycle.name: continue
            if Exclude=='Clamped' and ' U' not in cycle.name: continue
            elif cycle.tr1 == ' ': datacheck=False
            else: templist.append(cycle.tr1)
        if datacheck: data.append(templist)
        datacheck=True
        templist=[]
        for cycle in board.cycles:
            if Exclude=='Unclamped' and ' U' in cycle.name: continue
            if Exclude=='Clamped' and ' U' not in cycle.name: continue
            if cycle.tr2 == ' ': datacheck=False
```

```python
            else: templist.append(cycle.tr2)
        if datacheck: data.append(templist)
        datacheck=True
    data=numpy.array(data).transpose()


    average=[numpy.mean(data[i]) for i in range(len(data))]
    deviation=[numpy.std(data[i]) for i in range(len(data))]
    return average, deviation



def DelaminationData(Boards):
    """Display the number of boards for each degree of delamination for
    each cycle.  This is to be used in the interactive shell and is not
    currently incorporated into any other function definitions"""
    # Criteria for delamination
    full_delam = 0.5
    partial_delam =0.25
    delam_data={}
    for group in Boards.bytype():
        if ' OM' in group[0].type:
            continue
        delam_data[group[0].type]={}
        for index,cycle in enumerate(group[0].cycles.clamped()[2:]):
            number_of_full_delam=0
            number_of_partial_delam=0
            number_of_no_delam=0
            for board in group:
```

```python
            if board.cycles.clamped()[index+2].tr1 != ' ' and \
            board.cycles.unclamped()[index].tr1 != ' ' and \
            board.name != 'PSA-5 FLEX':
                pd=board.trd1[cycle.name]['Percent Difference']
                if pd >= full_delam: number_of_full_delam+=1
                elif pd >= partial_delam: number_of_partial_delam+=1
                else: number_of_no_delam+=1
            if board.cycles.clamped()[index+2].tr2 != ' ' and \
            board.cycles.unclamped()[index].tr2 != ' ':
                pd=board.trd2[cycle.name]['Percent Difference']
                if pd >= full_delam: number_of_full_delam+=1
                elif pd >= partial_delam: number_of_partial_delam+=1
                else: number_of_no_delam+=1
        delam_data[group[0].type][cycle.name]=(number_of_full_delam,\
        number_of_partial_delam,number_of_no_delam)
    return delam_data



if __name__ == '__main__':
    boards = ImportData()
    CreateCSVFiles(boards)
```